

General Disclaimer

One or more of the Following Statements may affect this Document

- This document has been reproduced from the best copy furnished by the organizational source. It is being released in the interest of making available as much information as possible.
- This document may contain data, which exceeds the sheet parameters. It was furnished in this condition by the organizational source and is the best copy available.
- This document may contain tone-on-tone or color graphs, charts and/or pictures, which have been reproduced in black and white.
- This document is paginated as submitted by the original source.
- Portions of this document are not fully legible due to the historical nature of some of the material. However, it is the best reproduction available from the original submission.

**APPLICATION OF FINITE ELEMENT TECHNIQUES IN PREDICTING
THE ACOUSTIC PROPERTIES OF TURBOFAN INLETS**

APPLICATION OF FINITE ELEMENT TECHNIQUES IN
PREDICTING THE ACOUSTIC PROPERTIES OF
TURBOFAN INLETS Interim Technical Report
(Georgia Inst. of Tech.) 194 p HC A09/MF
A01

N79-20831

Unclas
17275

CSSL 20A G3/71

by

R. K. Majjigi

R. K. Sigman

B. T. Zinn

GEORGIA INSTITUTE OF TECHNOLOGY
ATLANTA, GEORGIA 30332

prepared for

NATIONAL AERONAUTICS AND SPACE ADMINISTRATION

NASA Lewis Research Center
Grant NSG 3036



APPLICATION OF FINITE ELEMENT TECHNIQUES IN PREDICTING
THE ACOUSTIC PROPERTIES OF TURBOFAN INLETS

by

R. K. Majjigi
R. K. Sigman
B. T. Zinn

GEORGIA INSTITUTE OF TECHNOLOGY
ATLANTA, GEORGIA 30332

prepared for
NATIONAL AERONAUTICS AND SPACE ADMINISTRATION

NASA Lewis Research Center
Grant NSG 3036

TABLE OF CONTENTS

	Page
ACKNOWLEDGMENTS	ii
LIST OF ILLUSTRATIONS	vii
LIST OF TABLES	xiii
SUMMARY	xiv
Chapter	
I. INTRODUCTION	1
1.1 General	
1.2 Literature Review	
1.3 Objectives of Research	
II. FORMULATION OF THE PROBLEM	9
2.1 Governing Differential Equations	
2.2 Boundary Conditions of the Problem	
III. METHODS OF SOLUTION	20
3.1 The Inlet Steady Flow	
3.1.1 Analysis of the Incompressible Potential Flow	
3.1.2 Superposition of Solutions	
3.1.3 Compressibility Correction for Mean Flow	
3.2 Finite Element Solution of the Acoustic Equations	
3.2.1 Subdivision of the Solution Domain	
3.2.2 Selection of Interpolation Functions	
3.2.3 Establishing Elemental Relations	
3.2.4 Assembly of Element Equations to Obtain a System of Algebraic Equations	
3.2.5 Solution of the System of Equations	
3.2.6 Additional Calculations	
IV. RESULTS AND DISCUSSION OF RESULTS	42
4.1 Acoustic Calculations Using 3-Node Triangular Elements	
4.2 Comparison of Acoustic Calculations by Using Linear and Quadratic Triangular Elements	

TABLE OF CONTENTS (Continued)

	Page
4.3 Comparison Studies for Lined Wall Annular Cylinders	
4.4 Comparison Studies with the Integral Technique for the QCSEE Inlet	
4.5 "Compressible" Mean Flow Calculations for the QCSEE and Bellmouth Turbofan Inlets	
4.6 Acoustic Calculations for the Hard Walled QCSEE Inlet	
4.7 Sound Attenuation Studies for Zero Mean Flow Case for the QCSEE, Bellmouth and Cylindrical Inlets	
4.8 Sound Attenuation Studies for Non-zero Mean Flow Case for the QCSEE, Bellmouth and Cylindrical Inlets	
V. CONCLUSIONS AND RECOMMENDATIONS	110
5.1 Conclusions	
5.2 Recommendations for Future Research	
APPENDICES	116
A. PROOF OF EQUATION (60)	117
B. DEVELOPMENT OF ELEMENTAL RELATIONS	119
B.1 Application of Galerkin's Technique to a Finite Element	
B.2 Element Relations for an Internal Element	
B.2.1 Evaluation for a 3-Node Triangle	
B.2.2 Evaluation for a 6-Node Triangle	
B.3 Boundary Integral Evaluation for a Hard Wall	
B.3.1 Evaluation of Hard Wall Boundary Condition for a 3-Node Triangle	
B.3.2 Evaluation of Hard Wall Boundary Condition for a 6-Node Triangle	
B.4 Boundary Integral Evaluation for a Soft Wall	
B.4.1 Evaluation of Soft Wall Boundary Condition for a 3-Node Triangle (No mean flow case only)	
B.4.2 Evaluation of Soft Wall Boundary Condition for a 6-Node Triangle	
B.5 Boundary Integral Evaluation for Fan Plane Source Condition	
B.5.1 Evaluation of a Velocity Source Fan Plane Condition for a 3-Node Triangle	

TABLE OF CONTENTS (Continued)

	Page
B.5.2 Evaluation of a Velocity Source Fan Plane Condition for a 6-Node Triangle	
B.5.3 Evaluation of a Pressure Source Fan Plane Condition for a 3-Node Triangle	
B.5.4 Evaluation of a Pressure Source Fan Plane Condition for a 6-Node Triangle	
B.6 Boundary Integral Evaluation for Inlet Entrance Plane	
B.6.1 Evaluation of Entrance Plane Radiation Condition for a 3-Node Triangle	
B.6.2 Evaluation of Entrance Plane Radiation Condition for a 6-Node Triangle	
C. ACOUSTIC INTENSITY AND POWER CALCULATIONS	158
C.1 Derivation of Equation (64) for Acoustic Intensity	
C.2 Evaluation of Acoustic Power at the Inlet Boundaries and dB Calculations	
C.2.1 Acoustic Power Input into the Inlet at the Fan Plane	
C.2.2 Acoustic Power Output at the Inlet Entrance Plane	
C.2.3 Acoustic Power Absorbed at the Inlet Walls	
C.2.4 DB Calculations and the Principle of Conservation of Acoustic Energy	
D. GEOMETRICAL AND MEAN FLOW DATA FOR THE QCSEE AND BELLMOUTH INLETS	169
BIBLIOGRAPHY	176
VITA	179

LIST OF ILLUSTRATIONS

Figure	Page
1. a) The ACSEE Inlet Geometry b) The Bellmouth Inlet Geometry	6
2. Superposition of Incompressible Potential Flow Solutions for a Free Stream Velocity and Inlet Flow Rate	23
3. The QCSEE Inlet Triangulization into 3-Node Triangles . .	30
4. a) The QCSEE Inlet Triangulization into 6-Node Triangles b) The Bellmouth Inlet Triangulization into 6-Node Triangles	31
5. Linear and Quadratic Triangles	35
6. Condensed Storage Scheme Used in CDC Subroutine BLSWNP	39
7. Comparison of Acoustic Velocity Potential for Plane Wave Propagation in an Annular Cylinder ($M = 0.5$, $\omega = 2.0$)	44
8. Comparison of Acoustic Velocity Potential for Spinning Wave Propagation in an Annular Cylinder ($M = 0.5$, $\omega = 6.0$)	46
9. Triangulization of Annular Cylinder into 140 3-Node Triangles	48
10. Triangulization of Annular Cylinder into 140 6-Node Triangles	49
11. Comparison of Axial Acoustic Velocity Amplitude for Plane Wave Propagation in an Annular Cylinder as Predicted by Linear and Quadratic Elements ($\omega = 1.0$, Mach = 0.5)	50
12. Comparison of Acoustic Axial Velocity Phase for Plane Wave Propagation in an Annular Cylinder as Predicted by Linear and Quadratic Elements for $\omega = 1.0$; Mach = 0.5 (Symbols defined in Figure 11)	51

LIST OF ILLUSTRATIONS (Continued)

Figure	Page
13. Comparison of Axial Acoustic Velocity Amplitude for Plane Wave Propagation in an Annular Cylinder as Predicted by Linear and Quadratic Elements for $\omega = 5.0$; Mach = 0.5 (Symbols defined in Figure 11)	52
14. Comparison of Axial Acoustic Velocity Phase for Plane Wave Propagation in an Annular Cylinder as Predicted by Linear and Quadratic Elements for $\omega = 5.0$; Mach = 0.5 (Symbols defined in Figure 11)	53
15. Comparison of Axial Acoustic Velocity Amplitude for Plane Wave Propagation in an Annular Cylinder as Predicted by Linear and Quadratic Elements for $\omega = 10.0$; Mach = 0.5 (Symbols defined in Figure 11)	54
16. Comparison of Axial Acoustic Velocity Phase for Plane Wave Propagation in an Annular Cylinder as Predicted by Linear and Quadratic Elements for $\omega = 10.0$; Mach = 0.5 (Symbols defined in Figure 11)	55
17. Comparison of Axial Acoustic Velocity Amplitude for Plane Wave Propagation in an Annular Cylinder as Predicted by Linear and Quadratic Elements for $\omega = 15.0$; Mach = 0.5 (Symbols defined in Figure 11)	56
18. Comparison of Axial Acoustic Velocity Phase for Plane Wave Propagation in an Annular Cylinder as Predicted by Linear and Quadratic Elements for $\omega = 15.0$; Mach = 0.5 (Symbols defined in Figure 11)	57
19. Comparison of Axial Acoustic Velocity Amplitude for Plane Wave Propagation in an Annular Cylinder as Predicted by Linear and Quadratic Elements for $\omega = 20.0$; Mach = 0.5 (Symbols defined in Figure 11)	58
20. Comparison of Axial Acoustic Velocity Phase for Plane Wave Propagation in an Annular Cylinder as Predicted by Linear and Quadratic Elements for $\omega = 20.0$; Mach = 0.5 (Symbols defined in Figure 11)	59
21. Annular Cylinder Geometry Simulating Rectangular Duct	61
22. Comparison of Acoustic Pressure Magnitude Along the Upper Wall of the Rectangular Duct as Predicted by FEM Program and Reference 2. Hard Wall Solutions Shown in Circles	63

LIST OF ILLUSTRATIONS (Continued)

Figure	Page
23. Comparison of Acoustic Pressure Phase Along the Upper Wall as Predicted by FEM Program and Reference 2. Hard Wall Solutions Shown in Circles (Symbols defined in Figure 22).	64
24. Comparison of Acoustic Pressure Amplitude Along the Lower Wall as Predicted by FEM Program and Reference 2. Hard Wall Solutions Shown in Circles (Symbols defined in Figure 22).	65
25. Comparison of Acoustic Pressure Phase Along the Lower Wall as Predicted by FEM Program and Reference 2. Hard Wall Solutions Shown in Circles (Symbols defined in Figure 22)	66
26. Acoustic Power Absorbed by Each Element Located at the Lined Upper Wall	67
27. Acoustic Velocity Potential Distribution Along the Inlet Upper Wall ($\omega = 1.0$, No Flow, Hard Wall, Plane Wave Excitation)	70
28. Acoustic Velocity Potential Distribution Along the Inlet Upper Wall ($\omega = 2.0$, No Flow, Hard Wall, Plane Wave Excitation; Symbols defined in Figure 27)	71
29. Acoustic Velocity Potential Distribution Along the Inlet Upper Wall ($\omega = 5.0$, No Flow, Hard Wall, Plane Wave Excitation; Symbols defined in Figure 27)	72
30. Acoustic Velocity Potential Distribution Along the Inlet Upper Wall ($\omega = 10.0$, No Flow, Hard Wall Plane Wave Excitation; Symbols defined in Figure 27)	73
31. Acoustic Velocity Potential Distribution Along the Inlet Upper Wall ($\omega = 1.0$, No Flow, Soft Wall, Plane Wave Excitation; Symbols defined in Figure 27)	75
32. Acoustic Velocity Potential Distribution Along the Inlet Upper Wall ($\omega = 2.0$, No Flow, Soft Wall, Plane Wave Excitation; Symbols defined in Figure 27)	76
33. Acoustic Energy Absorbed by the Lined Inlet Upper Wall ($\omega = 1.0$, No Flow, Plane Wave Excitation)	77

LIST OF ILLUSTRATIONS (Continued)

Figure	Page
34. Acoustic Energy Absorbed by the Lined Inlet Upper Wall ($\omega = 2.0$, No Flow, Plane Wave Excitation)	78
35. Influence of Different Radiation Impedances on the Acoustic Velocity Potential Distribution Along the Inlet Upper Wall ($\omega = 1.0$, No Flow, Hard Wall, Plane Wave Excitation)	82
36. Influence of Different Radiation Impedance on the Acoustic Velocity Potential Distribution Along the Inlet Upper Wall ($\omega = 2.0$, No Flow, Hard Wall, Plane Wave Excitation; Symbols defined in Figure 35)	83
37. Influence of Different Radiation Impedance on the Acoustic Velocity Potential Distribution Along the Inlet Upper Wall ($\omega = 5.0$, No Flow, Hard Wall, Plane Wave Excitation; Symbols defined in Figure 35)	84
38. Influence of Different Radiation Impedances on the Acoustic Velocity Potential Distribution Along the Inlet Upper Wall ($\omega = 10.0$, No Flow, Hard Wall, Plane Wave Excitations; Symbols defined in Figure 35)	85
39. Radial Variation of "Compressible" Mean Flow Velocities at 3 Axial Locations for the QCSEE Inlet	89
40. Radial Variation of "Compressible" Mean Flow Velocities at 3 Axial Locations for the Bellmouth Inlet	90
41. Acoustic Pressure Distribution Along the Inlet Upper Wall ($\omega = 1.0$; Plane Wave Excitation)	92
42. Radial Variation of Acoustic Pressure at the Entrance Plane for $\omega = 1.0$ (Symbols defined in Figure 41)	92
43. Radial Variation of Acoustic Pressure at the Throat Plane for $\omega = 1.0$ (Symbols defined in Figure 41)	93
44. Radial Variation of Acoustic Pressure at the Inlet Exit Plane for $\omega = 1.0$ (Symbols defined in Figure 41)	93

LIST OF ILLUSTRATIONS (Continued)

Figure	Page
45. Acoustic Pressure Distribution Along the Inlet Upper Wall ($\omega = 2.0$, Plane Wave Excitation; Symbols defined in Figure 41)	94
46. Radial Variation of Acoustic Pressure at the Entrance Plane for $\omega = 2.0$ (Symbols defined in Figure 41)	94
47. Radial Variation of Acoustic Pressure at the Throat Plane for $\omega = 2.0$ (Symbols defined in Figure 41)	95
48. Radial Variation of Acoustic Pressure at the Exit Plane for $\omega = 2.0$ (Symbols defined in Figure 41)	95
49. Acoustic Pressure Distribution Along the Upper Wall of the Inlet for the Zero Mean Flow Case ($\omega = 1.0$; Plane Wave Excitation)	96
50. Acoustic Pressure Distribution Along the Upper Wall of the Inlet for the Zero Mean Flow Case ($\omega = 1.0$, Plane Wave Excitation; Symbols defined in Figure 49)	96
51. Radial Variation of Acoustic Pressure at the Entrance Plane for the Zero Mean Flow Case for $\omega = 1.0$ (Symbols defined in Figure 49)	98
52. Radial Variation of Acoustic Pressure at the Throat Plane for the Zero Mean Flow Case for $\omega = 1.0$ (Symbols defined in Figure 49)	98
53. Radial Variation of Acoustic Pressure at the Inlet Exit Plane for the Zero Mean Flow Case for $\omega = 1.0$ (Symbols defined in Figure 49)	99
54. Radial Variation of Acoustic Pressure at the Entrance Plane for the Zero Mean Flow Case for $\omega = 2.0$ (Symbols defined in Figure 49)	99
55. Radial Variation of Acoustic Pressure at the Throat Plane for the Zero Mean Flow Case for $\omega = 2.0$ (Symbols defined in Figure 49)	100
56. Radial Variation of Acoustic Pressure at the Inlet Exit Plane for the Zero Mean Flow Case for $\omega = 2.0$ (Symbols defined in Figure 49)	100

LIST OF ILLUSTRATIONS (Continued)

Figure	Page
57. Dependence of dB_{red} on Frequency for the QCSEE, Bellmouth and Cylindrical Inlets for the Zero Mean Flow Case	103
58. Dependence of dB_{red} on Frequency for the QCSEE and Cylindrical Inlets for Non-Zero Mean Flow Case	106
59. Dependence of dB_{red} on Frequency for the Bellmouth and Cylindrical Inlets for Non-Zero Mean Flow Case	108
B-1. Green's Theorem in a Plane Region, R Bounded by a Curve, C	120
B-2. Transformation of (r, z) Coordinate System to the Natural Coordinate System	120
B-3. Linear and Quadratic Elements on Inlet Wall	157
B-4. Linear and Quadratic Elements on Fan Plane	157
B-5. Linear and Quadratic Elements on Inlet Entrance Plane	157

LIST OF TABLES

Table	Page
1. "Exact" Radiation Impedances from the Integral Technique for the QCSEE Inlet with No Mean Flow	79
D-1. Geometrical and Mean Flow Data for the QCSEE Inlet ($M = 0.12$, $M_e = 0.52$; See Figure 4a)	170
D-2. Geometrical and Mean Flow Data for the Bellmouth Inlet ($M = 0.0$, $M_e = 0.52$; See Figure 4b)	173

SUMMARY

The thesis deals with the development of an analytical technique for predicting the acoustic performance of turbofan inlets carrying a subsonic axisymmetric steady flow. The Finite Element Method (FEM) in combination with the Method of Weighted Residuals has been chosen as the solution technique for predicting the acoustic properties of variable area, annular ducts with or without acoustic treatments along their walls.

An approximate solution for the steady inviscid flow field is obtained using an integral method for calculating the incompressible potential flow field in the inlet with a correction to account for compressibility effects.

The accuracy of the finite element technique in predicting the acoustic properties of annular ducts has been checked by comparison with available analytical solutions for the problems of plane and spinning wave propagation through a hard walled annular cylinder with a constant mean flow.

For a fixed number of triangular elements in the finite element scheme, the number of nodes per wavelength decreases as the frequency of oscillation increases, resulting in a loss in accuracy in the numerical results. Accuracy at higher frequency can be recovered by increasing the number of nodes per wavelength, either by increasing the number of linear elements (3-nodes per triangle) or by utilizing a more elaborate description of the dependent variable over each element as is

the case when quadratic elements (6-nodes per triangle) are used. It is clearly demonstrated for the case of plane wave propagation in a hardwalled annular cylinder containing a uniform steady flow that for an equal number of triangular elements, quadratic representation is superior to linear representation in handling high frequency wave propagation the reason being, the use of quadratic elements effectively doubles the number of nodes per wavelength as compared to an equal number of linear elements.

The accuracy of the developed finite element solution is again confirmed by comparing its predictions with those obtained by a finite difference solution approach. In this study, the results of the FEM for the case of sound propagation in an acoustically lined annular cylinder of a large radius of curvature and thin annular spacing carrying a uniform steady flow are compared with the comprehensive results of Baumeister for the equivalent case of a rectangular duct carrying a uniform flow. The duct attenuation and the acoustic pressure distributions obtained by both the methods are found to be generally in good agreement.

Since exact values of the impedance at the open end of a duct are generally not known, simple impedance boundary conditions such as "no reflection" impedance conditions are used to date in most cases. However, in the absence of a steady flow an integral solution approach developed by Bell, Meyer and Zinn provides the "exact" impedance condition at the open end of the duct. In order to compare the solution technique for the study of non-uniform ducts without steady flows, the finite element solutions were required to satisfy the impedance boundary

conditions obtained using the above mentioned integral solution approach and the resulting finite element solutions for the QCSEE (Quiet, Clear, Short-haul, Experimental, Engine) inlet are compared with those obtained for the same inlet, using the integral solution approach. The results obtained by the finite element program using the "exact" impedance condition are found to be in excellent agreement with the results of the integral solution approach for plane wave propagation in hard and soft walled QCSEE inlet carrying no mean flow. The wave structure within the inlet obtained by prescribing the simple "no reflection" impedance boundary condition is quite different from the one obtained by prescribing the "exact" impedance boundary condition for low frequencies of wave propagation. However, as frequency increases the two impedance boundary conditions approach one another and so do the corresponding wave structures. The propagation of high frequency plane waves in the inlet could be approximated as the wave propagation in a ray tube where the reflected component is negligible, in which case, the "no reflection" impedance condition indeed approaches the "exact" impedance condition and so also the corresponding wave structures.

Results are presented comparing low frequency plane wave propagation through the hard walled QCSEE inlet containing a one-dimensional steady flow with the same inlet containing a fully two-dimensional axisymmetric steady flow. It is shown that when one-dimensional steady flow is assumed to exist in the inlet, the plane wave propagates with relatively little distortion. However, propagation of a plane wave through the fully two-dimensional flow field in the inlet produces severe distortions due to the excitation of higher order modes.

To estimate the sensitivity of inlet curvature, center body and mean flow gradients on duct attenuation, acoustic calculations for soft walled QCSEE inlet, a straight cylinder and a Bellmouth inlet of the same overall dimensions are performed for various frequencies for the cases of zero mean flow and fully two-dimensional axisymmetric mean flow. The liner impedance values chosen are the same for each inlet at a particular frequency and they correspond to the near optimum impedance values for a plane pressure wave input into an infinitely long circular duct with zero mean flow. At high frequencies focusing of the sound wave toward the duct axis occurs for both zero mean flow and non-zero mean flow cases and hence the duct attenuation falls rapidly with increase in frequency for all the three inlets. Attenuation of low frequency plane waves is found to be more sensitive to inlet curvature, center body and mean flow gradients (for the non-zero mean flow case) compared to that of high frequency plane waves. The approximate method proposed by Rice to obtain the near optimum liner impedance values for the flow case is found to be reasonable for high frequency plane waves but leads to a rapid drift in the optimum values for the low frequency plane waves resulting in a considerable reduction of duct attenuation.

CHAPTER I

INTRODUCTION

1.1 General

As evidenced by the recent surge in commercial aviation mainly due to Federal deregulation of price control on air travel by the US Civil Aeronautics Board (C.A.B.), the aircraft industry has come up with a new generation of aircrafts to meet the record high demands of domestic and international air travel. The new series Boeing 767 and 757 aircrafts, the modified Lockheed L 1011 aircraft and the shorter version of French Airbus A300B aircraft will be put into airline service in early 1980s to satisfy the growing needs of air transportation. With the increase in air traffic and consequent congestion in airport operations, it has become increasingly apparent to government, industry and other research and development organizations that major efforts must be undertaken to improve the general community environment affected by the commercial and also military air transportation. The recent legislation of the Federal Act FAR 36 (1978) calls for very stringent measures to be taken by aircraft industries to reduce the overall noise levels of their aircraft. Since the aircraft engines are the major contributors to the overall aircraft noise, one has to develop a capability to accurately predict the noise levels due to various components of the aircraft engines, which in turn will enable the engine designer to develop a viable design capable of meeting the new lower noise levels

without adversely affecting the performance of the power plant.

Aircraft generated noise sources can be divided into two groups; namely the externally generated noise produced by the jet exhaust, and the internally generated noise that is primarily due to the rotating turbomachinery blades and the combustion process. The utilization of energy efficient, high bypass ratio turbofan engines in the present day civil and military aircraft reduce the jet velocity and hence jet noise compared to earlier low bypass turbofan or turbojet engines. The pure tone turbofan noise emitted by these engines now becomes the major source of noise pollution. Sound absorbing liners have been designed and utilized in the engine inlets to reduce the emitted turbofan noise mainly on the basis of costly trial and error development programs. Hence, the need for an efficient analytical technique which can predict the acoustic properties of complex shaped inlet ducts with sound absorbing liners and carrying a multidimensional mean flow for a variety of practical noise source inputs is more apparent now than ever before. The development of such an analytical technique utilizing the Finite Element Method (to be denoted henceforth by FEM) is the object of this work.

1.2 Literature Review

An extensive survey of the acoustics of aircraft inlets has been presented by Nayfeh, Kaiser, and Telionis¹ including a comprehensive bibliography. Of particular interest are the use of numerical methods such as finite differences² and integral techniques³ in the study of acoustic propagation in variable area hard walled ducts without mean

flow. Due to the additional complications created by the presence of a steady flow, most studies of sound propagation in annular ducts with varying cross sectional area containing a mean flow employ one or more simplifying assumptions such as one-dimensional mean flow,⁴ quasi-one dimensional mean flow,⁵ or slowly varying cross sectional area.⁶ In many instances, however, practical considerations call for the use of relatively short ducts having large transverse and streamwise velocity gradients. Under such conditions, the predictions of existing theoretical approaches in which the mean flow is assumed to be one-dimensional or nearly one-dimensional is open to question. Thus, there is a need for an analytical method that can determine the acoustics of duct systems involving multidimensional flows.

The relative merits of the various numerical techniques are evaluated in this section. The application of the method of finite differences by Baumeister,² to solve the wave propagation problem is restricted to the simple geometry of a rectangular duct carrying a uniform steady flow. The finite difference method employs a uniform rectangular grid structure which can not adequately represent complex duct geometries encountered in aircraft inlet design. Bell, Meyer and Zinn³ have developed an integral approach using Green's functions to solve the Helmholtz equation for an arbitrarily shaped body. In this method, the dimensionality of the problem is reduced by one (e.g. a three dimensional problem is reduced to a two dimensional surface integral equation, an axi-symmetric problem is reduced to a line integral equation, etc. The integral solution technique is, however, limited to dealing with acoustic problems involving either no or constant mean flow. The Galerkin, which is a special application of the method of weighted residuals, was

applied by Unruh and Eversman⁷ to solve the wave equation in a duct. In this method the solution is sought in terms of a complete set of orthogonal basis functions which individually satisfy the natural boundary conditions and collectively satisfy the forced boundary conditions of the problem. The unknown coefficients of the basis functions are solved for by requiring the resulting residues to be orthogonal to each of the basis functions. This yields a system of linear algebraic equations for the coefficients which can be solved by standard matrix methods. The disadvantage of the method is that a new set of basis functions has to be determined by solving the corresponding eigenvalue problem for each frequency. For ducts with complex geometries and acoustic liner configurations the evaluation of the basis functions is quite complicated and time consuming. Hence, a parametric study of ducts for a range of frequencies and liner configurations can not be efficiently conducted by employing this method. The method of asymptotic expansions⁶ has been used to study the problem of wave propagation in ducts which slightly deviate from the simple geometry of a cylinder or a rectangle and the resulting mean flow also slightly deviates from a one dimensional flow. This method obviously can not be used if the duct has large variations in shape resulting in a multi dimensional mean flow.

The finite element method (to be denoted by FEM) which has its roots in the field of structural mechanics has been gaining popularity in other fields of mechanics because of its ability to deal with complex 'real life' geometrical shapes and to handle mixed boundary conditions. The application of the FEM to the solution of Helmholtz's equation⁸ in a waveguide indicates the versatility of this method in treating various two and three dimensional problems subject to mixed boundary conditions. In the finite element method the region of interest is subdivided into

a number of elements of simple shapes (e.g. triangles for two dimensional problems and tetrahedrons for three dimensional problems) of variable sizes which can be arranged to represent complex shapes. This flexibility to utilize a variable mesh distribution of the elements for an efficient yet adequate representation of the geometry makes the FEM a powerful numerical tool. The FEM is generally thought of in connection with variational problems. However, since a variational form of the problem of duct acoustics has not been established, the governing differential equations are converted to integral equations by the Galerkin process.

1.3 Objectives of Research

The research work described in this work was initiated for the purpose of predicting the acoustic properties of practical turbofan inlets carrying high subsonic Mach number mean flows. The inlet configurations chosen for study are the Quiet, Clean, Short-haul Experimental Engine (to be henceforth denoted as QCSEE) inlet⁹ and the Bellmouth inlet¹⁰ (see Figures 1a and 1b). The QCSEE inlet was designed jointly by General Electric Co., Douglas Aircraft Company and NASA Lewis Research Center for the purpose of developing the technology for a turbofan engine intended for application to short take-off and landing (STOL) aircraft. The Bellmouth inlet has been used extensively at NASA Lewis Research Center as a standard reference base to compare experimentally the acoustic performance of realistic aircraft inlets because of its simple geometry. The Bellmouth inlet acoustic studies are conducted for static cases, the mean flow being created by suction

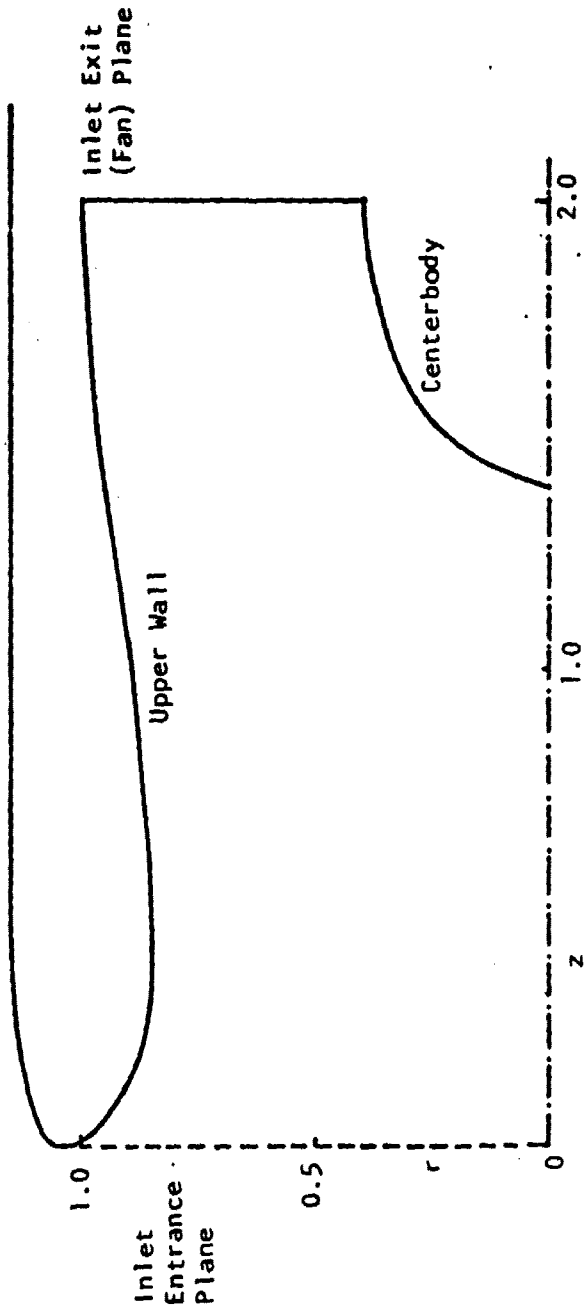


Figure 1a. The QCSEE Inlet Geometry

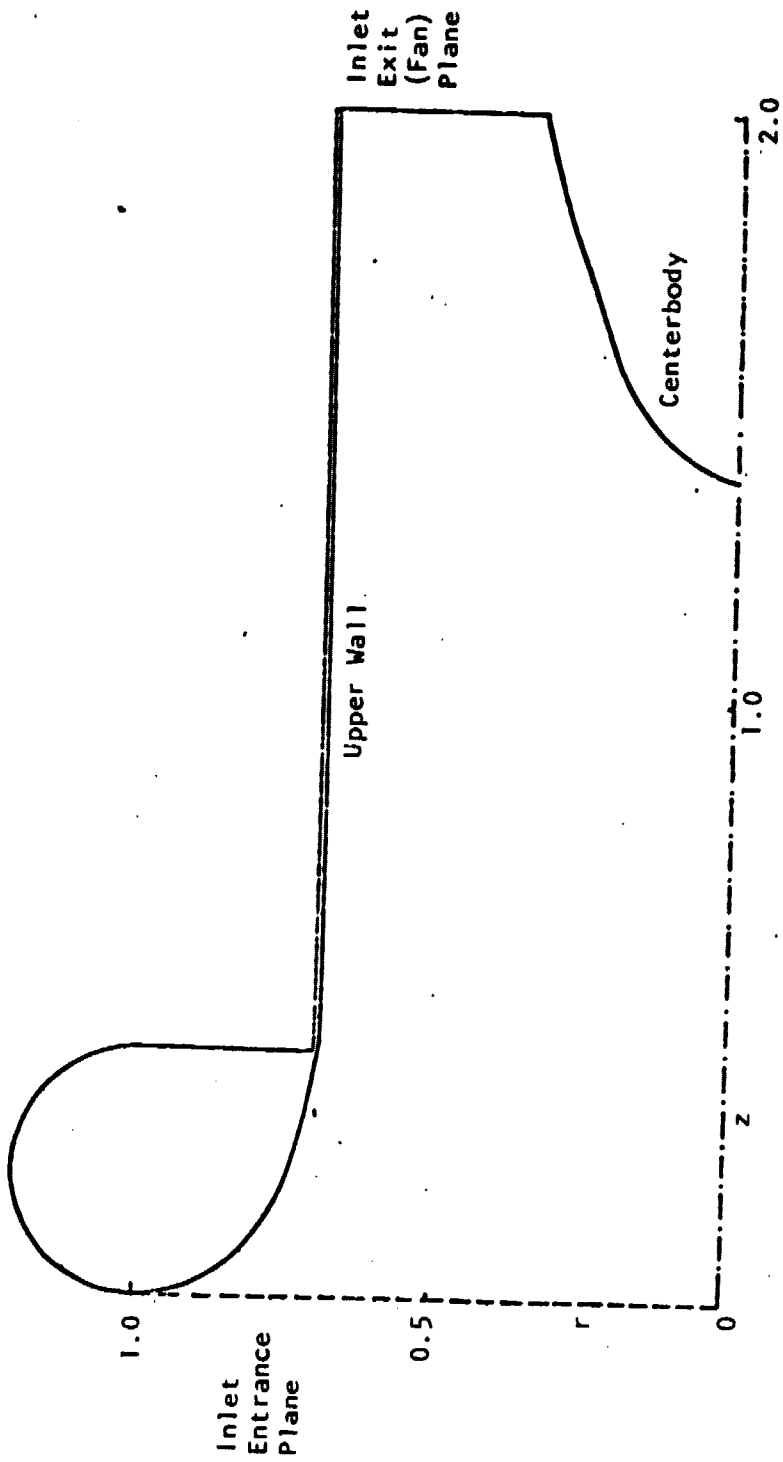


Figure 1b. The Bellmouth Inlet Geometry.

at the fan plane of the inlet (see Figure 1b).

To achieve the objectives of this research work, it is necessary to develop solution techniques that are capable of predicting the acoustic properties of variable area, annular ducts with or without acoustic treatments along their walls, subjected to a variety of practical sound excitation conditions. Such a solution technique should be capable of properly accounting for the reflection processes at the inlet entrance plane, the space dependence of the noise source at the fan plane (see Figure 1), the odd shape geometry of the ducts under consideration, the multidimensionality of the steady flow and the mixed boundary conditions (e.g., partial lining) at the duct walls. The above requirements obviously preclude the development of an analytical solution for the duct under consideration and one must resort to the development of an efficient numerical solution approach. It will be shown in this work that the application of the Finite Element Method (FEM) (see Reference 11 for a general discussion of this method), in conjunction with the Method of Weighted Residuals can indeed provide the needed solutions.

CHAPTER 11

FORMULATION OF THE PROBLEM

2.1 Differential Equations

To develop the needed solution technique, the problem of acoustic wave propagation through either one of the duct configurations shown in Figure 1 will be considered. The duct carries a two dimensional, axisymmetric mean flow which is assumed to be inviscid, non heat conducting and irrotational. Body forces are neglected. To derive the needed nondimensional conservation equations, velocities, lengths and time are respectively normalized with respect to the ambient speed of sound c_0^* , a characteristic duct diameter d_r^* , and d_r^*/c_0^* . The density ρ and pressure p are respectively normalized with the ambient density ρ_0^* and $\rho_0^* c_0^{*2}$. The velocity potential ϕ is normalized with respect to $c_0^* d_r^*$ and the frequency with respect to c_0^*/d_r^* . Under these conditions, it can be shown¹² that the behavior of the flow in the duct is described by the following nonlinear partial differential equation for the flow potential ϕ :

$$\frac{\partial^2 \phi}{\partial t^2} + \frac{\partial}{\partial t} (\nabla \phi \cdot \nabla \phi) + \frac{1}{2} \nabla \phi \cdot \nabla (\nabla \phi \cdot \nabla \phi) = c^2 \nabla^2 \phi \quad (1)$$

where

$$c^2 = 1 - (\gamma - 1) \left[\frac{\partial \phi}{\partial t} + \frac{1}{2} \nabla \phi \cdot \nabla \phi \right]$$

and γ is the ratio of specific heats. Rewriting Eq. (1) in a cylindrical

coordinate system (i.e., r, θ, z) with the z -axis coinciding with the turbofan inlet axis yields:

$$\begin{aligned}
 & c^2 \left[\phi_{rr} + \frac{\phi_r}{r} + \frac{\phi_{\theta\theta}}{r^2} + \phi_{zz} \right] - \phi_{tt} \\
 &= 2 \phi_r \phi_{rt} + \frac{2\phi_\theta \phi_{\theta t}}{r^2} + 2 \phi_z \phi_{zt} + \phi_r^2 \phi_{rr} \\
 &+ \frac{\phi_\theta^2 \phi_{\theta\theta}}{r^4} + \phi_z^2 \phi_{zz} + \frac{2\phi_r \phi_\theta \phi_{r\theta}}{r^2} + 2\phi_r \phi_z \phi_{rz} \\
 &+ \frac{2\phi_z \phi_\theta \phi_{z\theta}}{r^2} - \frac{\phi_r \phi_\theta^2}{r^3} \tag{2}
 \end{aligned}$$

where the subscripts indicate partial differentiation with respect to the subscripted variables.

To obtain the needed acoustic solutions, the flow potential is rewritten as the sum of a steady-axi-symmetric mean flow potential $\bar{\phi}(r, z)$ and an acoustic potential $\phi'(r, \theta, z, t)$; that is

$$\phi(r, \theta, z, t) = \bar{\phi}(r, z) + \phi'(r, \theta, z, t) \tag{3}$$

Because of the rotational nature of the fan and compressor,¹³ they tend to generate sound that is characterized by spinning acoustic modes. In order to account for spinning modes, the acoustic potential is assumed to have the following form

$$\phi(r, \theta, z, t) = \phi(r, z) e^{-i(\omega t - m\theta)} \tag{4}$$

where $\phi(r, z)$ is a complex quantity; that is

$$\phi = \bar{\phi} + i \hat{\phi} \tag{5}$$

Substituting Eq. (3) into Eq. (2), neglecting the nonlinear products of the acoustic quantities and separating the resulting equation into its real and imaginary parts leads to the derivation of the following two linear, coupled, partial differential equations for $\tilde{\phi}$ and $\hat{\phi}$:

$$\begin{aligned}
& [\bar{c}^2 - \bar{\phi}_r^2] \tilde{\phi}_{rr} + [\bar{c}^2 - \bar{\phi}_z^2] \tilde{\phi}_{zz} - 2\bar{\phi}_r \bar{\phi}_z \tilde{\phi}_{rz} \\
& + [-(\gamma+1)\bar{\phi}_{rr} \bar{\phi}_r - 2\bar{\phi}_{rz} \bar{\phi}_z + \frac{\bar{c}^2}{r} - (\gamma-1)\frac{\bar{\phi}_r^2}{r} - (\gamma-1)\bar{\phi}_r \bar{\phi}_{zz}] \tilde{\phi}_r \\
& + [-(\gamma+1)\bar{\phi}_{zz} \bar{\phi}_z - 2\bar{\phi}_{rz} \bar{\phi}_r - (\gamma-1)\bar{\phi}_{rr} \bar{\phi}_z - (\gamma-1)\frac{\bar{\phi}_z \bar{\phi}_r}{r}] \tilde{\phi}_z \\
& + [\omega^2 - m^2 \frac{\bar{c}^2}{r^2}] \tilde{\phi} - 2\omega \bar{\phi}_r \hat{\phi}_r - 2\omega \bar{\phi}_z \hat{\phi}_z \\
& - \omega(\gamma-1) [\bar{\phi}_{rr} + \frac{\bar{\phi}_r}{r} + \bar{\phi}_{zz}] \hat{\phi} = 0
\end{aligned} \tag{6}$$

and

$$\begin{aligned}
& (\bar{c}^2 - \bar{\phi}_r^2) \hat{\phi}_{rr} + (\bar{c}^2 - \bar{\phi}_z^2) \hat{\phi}_{zz} - 2\bar{\phi}_z \bar{\phi}_r \hat{\phi}_{rz} \\
& + [-(\gamma+1)\bar{\phi}_{rr} \bar{\phi}_r - 2\bar{\phi}_{rz} \bar{\phi}_z + \frac{\bar{c}^2}{r} - (\gamma-1)\frac{\bar{\phi}_r^2}{r} - (\gamma-1)\bar{\phi}_r \bar{\phi}_{zz}] \hat{\phi}_r \\
& + [-(\gamma+1)\bar{\phi}_{zz} \bar{\phi}_z - 2\bar{\phi}_{rz} \bar{\phi}_r - (\gamma-1)\bar{\phi}_{rr} \bar{\phi}_z - (\gamma-1)\frac{\bar{\phi}_z \bar{\phi}_r}{r}] \hat{\phi}_z \\
& + [\omega^2 - m^2 \frac{\bar{c}^2}{r^2}] \hat{\phi} + 2\omega \bar{\phi}_r \tilde{\phi}_r + 2\omega \bar{\phi}_z \tilde{\phi}_z \\
& + \omega(\gamma-1) [\bar{\phi}_{rr} + \frac{\bar{\phi}_r}{r} + \bar{\phi}_{zz}] \tilde{\phi} = 0
\end{aligned} \tag{7}$$

where

$$\bar{c}^2 = 1 - \frac{(\gamma-1)}{2} [\bar{\phi}_r^2 + \bar{\phi}_z^2]$$

It should be pointed out that in the development of Eqs. (6) and (7) the following expression for the sound velocity perturbation $(c^2)'$ has been used:

$$(c^2)' = -(\gamma-1)[-i\omega\phi' + \bar{\phi}_z\phi_z' + \bar{\phi}_r\phi_r']$$

Since the steady flow is axisymmetric, the linearized θ -momentum equation can be integrated to give a relationship between the pressure and, velocity potential:

$$p' = -\bar{\rho}(-i\omega\phi' + \bar{\phi}_z\phi_z' + \bar{\phi}_r\phi_r') \quad (8)$$

2.2 Boundary Conditions

Before proceeding to obtain the needed solutions, the geometry and boundary conditions for the problem under consideration must be established. The geometry of typical turbofan inlets are shown in Figure 1 where due to the geometry of the inlets, only a single meridional plane is shown. The boundary of the inlets may be divided into three distinct sections, each described by a different boundary condition. The inlet exit plane represents the interface between the inlet and the remainder of the engine; it is referred to as the inlet exit plane as it is the location where the steady flow leaves the inlet. This plane also represents the location at which the fan-compressor noise is introduced into the inlet. In view of the earlier mentioned spinning nature of the sound excitation at the inlet exit plane, the boundary condition describing the normal acoustic velocity, ϕ_z' , at this plane can be expressed in the following form

$$\phi_{z_{\text{exit}}}^{\prime} = f(r)e^{-i(\omega t - m\theta)}; \quad f(r) = \tilde{f}(r) + i\hat{f}(r) \quad (9)$$

where the complex quantity $f(r)$ describes the radial dependence of the

source. Using Eq. (5), Eq. (9) can be rewritten as follows

$$\tilde{\phi}_{z_{\text{exit}}} = \tilde{f}(r) \quad (10)$$

$$\hat{\phi}_{z_{\text{exit}}} = \hat{f}(r) \quad (11)$$

The sound excitation at the inlet exit plane could also be prescribed in terms of a spinning pressure wave expressed as follows

$$p'_{\text{exit}} = g(r)e^{-i(\omega t - m\theta)}; \quad g(r) = \tilde{g}(r) + i\hat{g}(r) \quad (12)$$

where $g(r)$ represents the radial variation of the pressure source.

Suppressing the t and θ dependence in Eq. (12) and separating into real and imaginary parts yields

$$\tilde{p}_{\text{exit}} = \tilde{g}(r) \quad (13)$$

$$\hat{p}_{\text{exit}} = \hat{g}(r) \quad (14)$$

For the study of plane velocity wave propagation (i.e., $m=0$) the condition $f(r) = \text{a constant}$ applies and similarly for a plane pressure wave propagation the condition $g(r) = \text{a constant}$ applies. For a more general excitation, an appropriate combination of higher order spinning modes, (i.e., Bessel functions¹³) must be used to describe the sound source.

At a hard wall of the duct boundary, the appropriate boundary condition is

$$\phi'_n = 0 \quad (15)$$

Equation (15) expresses the fact that fluid can not penetrate the wall.

To absorb the emitted turbomachinery noise in the front and aft ends of jet engines, various types of sound absorbing liners have been developed by the aircraft industry. For example, point reacting liners which are essentially a series of sharply tuned Helmholtz resonators and bulk reacting liners which provide a broad band noise reduction by virtue of their porous lining have been developed. Though the point reacting liners are effective absorbers of sound over a narrow range of frequencies, they are better suited to sustain the operating conditions of a jet engine compared to the bulk reacting liners. To estimate the liner performance, the appropriate boundary conditions need to be applied at the interface of a point reacting liner. A good deal of controversy exists in the literature about the correct boundary condition to be applied across the liner in the presence of a grazing flow, as to whether particle displacement or particle velocity normal to the liner is continuous. Matched asymptotic expansion studies by Eversman and Beckemeyer⁴ and Tester¹⁵ indicate that in the limit of zero boundary layer thickness, the results using the shear flow model approach the no shear model employing the condition of particle displacement continuity. Nayfeh et al.¹⁶ confirmed the conclusions of References 14 and 15 numerically.

A physically meaningful explanation of the continuity of particle displacement is as follows. Consider an interface between two fluids being in relative motion. When a sound wave is incident on this interface from one of the mediums, it generates ripples on the interface and also creates a reflected wave in the original medium and a transmitted

wave in the other medium. The interface is a stream surface common to the flows in the two media. The boundary conditions at the interface are:

- (a) The pressure must be equal on both sides, and
- (b) The stream surface slopes must be equal on both sides. If $S(\underline{r}, t)$ is the equation of the interface which deforms with respect to time, the statement corresponding to condition (b) is

$$\frac{DS}{Dt} = 0 \quad (16)$$

where $\frac{D(\quad)}{Dt}$ is the substantial time derivative or time derivative following the fluid particle. Equation (16) states that the adjacent fluid particles on either side move along the interface which indeed is the statement of particle displacement continuity. For the case of a relative motion across the interface, continuity of particle displacement does not imply continuity of acoustic particle velocity, since acoustic particle velocity is the time derivative of particle displacement following the fluid particle, it receives contributions from the convective terms which are different on either side of the interface.

Hence the appropriate boundary conditions across the liner interface are:

$$p' = p'_p \quad (17)$$

$$\xi' = \xi'_p \quad (18)$$

where ξ' is the acoustic particle displacement and subscript p refers to the liner side. The equivalent condition to Eq. (18) in the continuum

is Eq. (16) which states that any particle on the interface $S(\underline{r}, t)$ remains on it for all times, i.e.,

$$\text{and } \left. \begin{aligned} \frac{\partial S}{\partial t} + (\underline{v} \cdot \nabla) S &= 0 \\ \frac{\partial S}{\partial t} + (\underline{v}_p \cdot \nabla) S &= 0 \end{aligned} \right\} \text{ at } S = 0 \quad (19)$$

For the special case $S(\underline{r}, t) = n - \xi(s)e^{-i\omega t}$ where n is outward normal coordinate and s is the coordinate along the boundary of the wall, Eqs. (19) become

$$\frac{\partial S}{\partial t} + (\bar{\phi}_s + \phi'_s) \frac{\partial S}{\partial s} + (\bar{\phi}_n + \phi'_n) \frac{\partial S}{\partial n} + (\bar{\phi}_\theta + \phi'_\theta) \frac{\partial S}{\partial \theta} = 0 \quad (20)$$

$$\frac{\partial S}{\partial t} + (\bar{\phi}_s + \phi'_s)_p \frac{\partial S}{\partial s} + (\bar{\phi}_n + \phi'_n)_p \frac{\partial S}{\partial n} + (\bar{\phi}_\theta + \phi'_\theta)_p \frac{\partial S}{\partial \theta} = 0$$

Since the normal and azimuthal components of the mean flow are zero and the mean flow is assumed to be identically zero on the liner side, the above equations yield

$$i\omega\xi(s)e^{-i\omega t} - \bar{\phi}_s \frac{d\xi(s)}{ds} e^{-i\omega t} - \phi'_n = 0 \quad (21)$$

$$i\omega\xi_p(s)e^{-i\omega t} + \phi'_{n_p} = 0$$

The specific acoustic impedance of the liner is defined by

$$Z_\ell = \frac{1}{\bar{c} \rho \omega} \frac{p'_p}{\phi'_{n_p}} \quad (22)$$

where $\bar{\rho}_\omega$ and \bar{c}_ω respectively describe the values of density and sound speed at the wall. Substituting Eqs. (17), (18), and (22) into Eqs. (21) yields

$$\phi_n' = \frac{p'}{\bar{\rho}_\omega \bar{c}_\omega Z_\ell} + i \frac{\bar{\phi}_s}{\omega} \frac{\partial}{\partial s} \left(\frac{p'}{\bar{\rho}_\omega \bar{c}_\omega Z_\ell} \right) \quad (23)$$

It is assumed that $\bar{\rho}_\omega \bar{c}_\omega Z_\ell$ is a piecewise constant function of s . Hence Eq. (23) becomes

$$\bar{\rho}_\omega \bar{c}_\omega Z_\ell \phi_n' = p' + i \frac{\bar{\phi}_s}{\omega} \frac{\partial p'}{\partial s} \quad (24)$$

As seen above, the condition of particle displacement continuity and that of particle velocity continuity are identical if there is no relative motion between the two fluids on either side of the liner (i.e., $\bar{\phi}_s \equiv 0$).

For a general liner impedance $\bar{\rho}_\omega \bar{c}_\omega Z_\ell = \theta_\ell + ix_\ell$, Eq. (24) can be rewritten by equating real and imaginary parts separately as

$$\theta \tilde{\phi}_n - x \hat{\phi}_n = \tilde{p} - \frac{\bar{\phi}_s}{\omega} \frac{\partial \hat{p}}{\partial s} \quad (25)$$

$$x \tilde{\phi}_n + \theta \hat{\phi}_n = \hat{p} + \frac{\bar{\phi}_s}{\omega} \frac{\partial \tilde{p}}{\partial s} \quad (26)$$

Decomposing velocities along and normal to the wall and noting that the normal component of the mean flow velocity is zero at the wall, Eq.

(8) after separating into real and imaginary parts becomes

$$\tilde{p} = -\bar{\rho} [\omega \hat{\phi} + \bar{\phi}_s \tilde{\phi}_s] \quad (27)$$

$$\hat{p} = -\bar{\rho} [-\omega \tilde{\phi} + \bar{\phi}_s \hat{\phi}_s] \quad (28)$$

Substituting Eqs. (27) and (28) into Eqs. (25) and (26) yields the following desired lined wall boundary condition in terms of the velocity potential and its derivatives only:

$$\begin{aligned} \theta \bar{\phi}_n - x \hat{\phi}_n = & -\bar{\rho} [\omega \hat{\phi} + \bar{\phi}_s \tilde{\phi}_s] + \bar{\rho} \frac{\bar{\phi}_s}{\omega} [-\omega \tilde{\phi}_s + \bar{\phi}_{ss} \hat{\phi}_s + \bar{\phi}_s \hat{\phi}_{ss}] \\ & + \left(\frac{2}{\gamma-1} \right) \frac{\bar{\rho}}{c} \frac{\partial \bar{c}}{\partial s} \frac{\bar{\phi}_s}{\omega} [-\omega \tilde{\phi} + \bar{\phi}_s \hat{\phi}_s] \end{aligned} \quad (29)$$

and

$$\begin{aligned} x \tilde{\phi}_n + \theta \hat{\phi}_n = & -\bar{\rho} [-\omega \tilde{\phi} + \bar{\phi}_s \hat{\phi}_s] - \bar{\rho} \frac{\bar{\phi}_s}{\omega} [\omega \hat{\phi}_s + \bar{\phi}_{ss} \tilde{\phi}_s + \bar{\phi}_s \tilde{\phi}_{ss}] \\ & - \left(\frac{2}{\gamma-1} \right) \frac{\bar{\rho}}{c} \frac{\partial \bar{c}}{\partial s} \frac{\bar{\phi}_s}{\omega} [\omega \hat{\phi} + \bar{\phi}_s \tilde{\phi}_s] \end{aligned} \quad (30)$$

Due to the complex nature of the reflection process at the inlet entrance plane, the precise form of the boundary condition at this location is currently not known. Rice¹⁷ has argued that except for modes near cut off frequencies the assumption of no reflection of "internal" duct waves at the inlet entrance plane is a reasonable one. As the primary objective of the present analysis is the development of the needed solution technique, the inlet entrance plane boundary condition in the present study is specified in the following form

$$p' = -\bar{\rho} \bar{c} Z_e \phi_z' \quad (31)$$

where $\bar{\rho}$ and \bar{c} are the local steady flow density and sound speed at the entrance plane and Z_e is the local impedance. The analytical solution for the propagation of a single acoustic mode, with cut-off frequency β , in a cylindrical or annular duct with constant mean flow Mach

number M is known. This solution provides the following impedance condition for transmission without reflection:

$$Z_e = \frac{\omega + \bar{\phi}_z \sqrt{\omega^2 - \beta^2 (1 - \bar{\phi}_z^2)}}{\bar{\phi}_z \omega + \sqrt{\omega^2 - \beta^2 (1 - \bar{\phi}_z^2)}} \quad (32)$$

and values of β are available in Reference 13. For plane waves, the cut-off frequency, β , equals zero and Eq. (32) reduces to the more familiar result

$$Z_e = 1$$

Since in the inlet case the steady flow velocity is not uniform at the inlet entrance plane, there will be a partial reflection of the principle mode. Furthermore, any additional modes excited by duct cross sectional area variations and steady flow velocity gradients will be also partially reflected.

A general radially varying radiation impedance condition at the inlet entrance plane can be described by

$$Z_e(r) = \theta_e(r) + ix_e(r) \quad (33)$$

Application of Eqs. (8) and (33) to Eq. (31) yields the following, equivalent boundary conditions:

$$\bar{\phi}_z (\bar{c} \theta_e - \bar{\phi}_z) - \bar{c} x_e \hat{\phi}_z = \omega \hat{\phi} + \bar{\phi}_r \tilde{\phi}_r \quad (34)$$

$$\hat{\phi}_z \bar{c} x_e + \hat{\phi}_z (\bar{c} \theta_e - \bar{\phi}_z) = -\omega \tilde{\phi} + \bar{\phi}_r \hat{\phi}_r \quad (35)$$

CHAPTER III

METHODS OF SOLUTION

3.1 The Inlet Steady Flow

3.1.1 Analysis of the Incompressible Potential Flow

Analytical solutions for the nonlinear equations describing the steady compressible flow in axisymmetric, axially nonuniform passages are not generally available and complex numerical solution approaches must be employed to obtain the desired flow description. Since the main objective of the current study is the description of the acoustic flow field, for which the steady flow is needed as an input, an approximate solution was used to obtain the needed steady inlet flow description. The approximate steady flow computation consists of a potential flow solution with a correction accounting for compressibility effects. An integral solution technique was used to compute the inlet potential flow utilizing a computer program developed earlier at Georgia Tech,¹⁸ and Lieblein's correction¹⁹ was utilized to account for compressibility effects.

The incompressible potential flow is governed by Laplace's equation and is subject to boundary conditions specifying the magnitude of the velocity normal to the inlet. The component of velocity normal to the solid surfaces of the inlet must be zero. A finite velocity distribution may be prescribed at the inlet fan plane as the forcing boundary condition for this boundary value problem. The governing equations in

a doubly connected region, R bounded by the inlet surface, B and a spherical surface of infinite radius, B' are

$$\nabla^2 \phi = 0 \quad \text{in } R \quad (36)$$

$$\nabla \phi \cdot \hat{n}|_B = F - \underline{v}_\infty \cdot \hat{n}|_B \quad (37)$$

and

$$|\nabla \phi|_{B'} = 0 \quad (38)$$

where ϕ is the velocity potential created because of the inlet, \hat{n} is unit normal vector pointing away from region R and F is the prescribed velocity normal to the inlet surface B .

The method developed by Smith et al.²⁰ to solve the linear incompressible potential flow problem for bodies of arbitrary shape consists of transforming the differential equation (36) subject to the boundary conditions (37) and (38) into a linear surface integral equation. In this method, the flow field created due to the inlet is thought of as due to a continuous distribution of sources and sinks on the inlet surface. Hence, the potential at a point p due to the source distribution on the inlet is

$$\phi(p) = \int_B \frac{\sigma(p')}{r(p,p')} dB \quad (39)$$

where $\sigma(p')$ is the unknown source strength distribution on the inlet surface, B and $r(p,p')$ is the distance between points p and p' . It can be easily verified that the velocity potential given by Eq. (39) satisfies Eqs. (36) and (38) for a finite value of $\sigma(p')$. The source

distribution $\sigma(p')$ is determined by requiring it to satisfy Eq. (37) which leads to the formulation of the following surface integral equation^{18,21} for σ

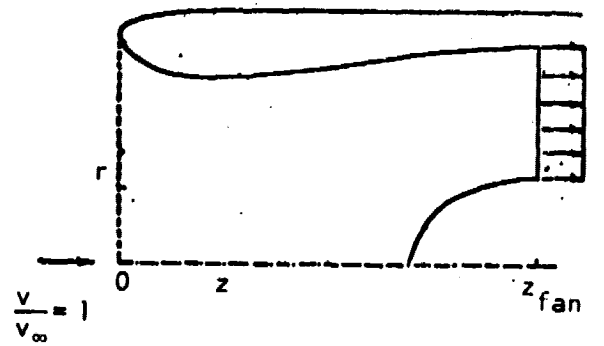
$$2\pi\sigma(p) - \int_B \sigma(p') \nabla \left[\frac{1}{r(p,p')} \right] \cdot \hat{n} \, dB = F(p) - \underline{v}_\infty \cdot \hat{n} \Big|_p \quad (40)$$

The first term in Eq. (40) is the velocity normal to the inlet induced at p by the source at p' . The second term is the normal velocity component at a point p due to the source distribution over the remainder of the inlet surface.

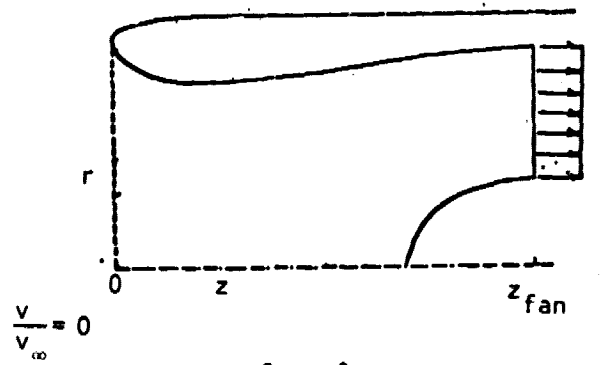
For flows past axisymmetric or two dimensional bodies Eq. (40) reduces to a line integral equation in a single plane. Furthermore, a numerical solution to the line integral equation is sought by assuming that the inlet surface is made up of many small straight line segments and that the source strength σ is constant over each segment. The above discretization procedure leads to a set of linear simultaneous algebraic equations for source strengths over each segment which can be solved by standard matrix routines. The velocities on and off the inlet surface are calculated from the computed source distribution (see Reference 18 for a detailed mathematical development).

3.1.2 Superposition of Solutions

Since the Laplace equation (36) is linear, the principle of superposition can be utilized to obtain solutions for various free stream velocities and inlet flow rates from the following two basic solutions (see Figure 2):



Case 1



Case 2

Figure 2. Superposition of Incompressible Potential Flow Solutions for a Free Stream Velocity and Inlet Flow Rate.

Let the computed velocities for Case 1 be denoted by $(\frac{V}{V_\infty})_1$ and for Case 2 by $(\frac{V}{V_F})_2$, since V_F is the reference velocity for Case 2. The principle of superposition for these two cases yields

$$\frac{V}{V_\infty} = A\left(\frac{V}{V_\infty}\right)_1 + B\left(\frac{V_F}{V_\infty}\right)\left(\frac{V}{V_F}\right)_2 \quad (41)$$

The constants A and B are obtained by using the boundary values of $\frac{V}{V_\infty}$ at $Z = -\infty$ and $Z = Z_F$.

That is,

$$\lim_{Z \rightarrow -\infty} \frac{V}{V_\infty} = 1 = A \times 1 + B \cdot \left(\frac{V_F}{V_\infty}\right) \times 0 = A \quad (42)$$

Since $(\frac{V}{V_F})_2$ tends to zero as $Z \rightarrow -\infty$ as the velocity created at $Z = -\infty$ due to a suction at the fan is zero. And at Z_F ,

$$\left.\frac{V}{V_\infty}\right|_{Z_F} = 1 \times 1 + B\left(\frac{V_F}{V_\infty}\right) \times 1 = \frac{V_F}{V_\infty}$$

or

$$B = 1 - \frac{V_\infty}{V_F} \quad (43)$$

Since from Case 1 $(\frac{V}{V_\infty})_1$ at Z_F is $\frac{V_F}{V_\infty}$. Substituting Eqs. (42) and (43) into Eq. (41) one obtains

$$\frac{V}{V_\infty} = \left(\frac{V}{V_\infty}\right)_1 + \left(\frac{V_F}{V_\infty} - 1\right)\left(\frac{V}{V_F}\right)_2 \quad (44)$$

The ratio of the two reference velocities $\frac{V_F}{V_\infty}$ is determined by the prescribed free stream velocity and the mass flow rate through the fan.

3.1.3 Compressibility Correction for Mean Flow

Next, since the inlet will be operating at high subsonic Mach numbers during takeoff or landing configurations, the incompressible solution obtained earlier needs to be corrected to account for compressibility effects using the semi-empirical equation proposed by Lieblin and Stockman.¹⁹ The justification for such an ad hoc approach to arrive at a compressible mean flow description within the inlet is that obtaining solutions to the exact nonlinear compressible potential flow equation in a complex duct shape is beyond the scope of the present study.

The empirical equation developed in Reference 19 to obtain "compressible" velocity, V_c from incompressible velocity, V_i at a point is

$$V_c = V_i \left(\frac{\rho_i}{\rho_c} \right)^{V_i/\bar{V}_i} \quad (45)$$

where \bar{V}_i is the area weighted average incompressible velocity across the duct at a given station, ρ_i is the incompressible density which is also equal to the stagnation density and $\bar{\rho}_c$ is the average compressible density across the flow passage. If the duct were a circular cylinder, the exponent V_i/\bar{V}_i equals unity and Eq. (45) is a statement of continuity. However, because of area variations in an aircraft inlet V_i/\bar{V}_i does not equal unity and it expresses the influence of geometry on the "compressible" velocity distribution.

The unknowns V_c and $\bar{\rho}_c$ in Eq. (45) are related through the isentropic gas dynamic relations as follows. Principle of mass conservation at an axial station requires that

$$\rho_i \bar{V}_i = \bar{\rho}_c \bar{V}_c \quad (46)$$

Dividing Eq. (46) by the critical velocity V_c^* and using the gas dynamic relations⁽²³⁾ one obtains

$$\frac{\bar{V}_i}{V_c^*} = \frac{\bar{\rho}_c}{\rho_i} \left[\frac{\gamma+1}{\gamma-1} \left\{ 1 - \left(\frac{\bar{\rho}_c}{\rho_i} \right)^{\gamma-1} \right\} \right]^{1/2} \quad (47)$$

The ratio $\frac{\bar{V}_i}{V_c^*}$ can be related to the free stream Mach number by making use of the isentropic gas dynamic relations again and one can show that

$$\frac{\bar{V}_i}{V_c^*} = \frac{\bar{V}_i}{V_\infty} \times \sqrt{\frac{\gamma+1}{2}} \times \frac{M_\infty}{\sqrt{1 + \frac{\gamma-1}{2} M_\infty^2}} \quad (48)$$

Denoting for simplicity $\frac{\bar{V}_i}{V_c^*}$ as α and $\frac{\bar{\rho}_c}{\rho_i}$ as β equation (47) reduces to

the following nonlinear algebraic equation for β :

$$\beta^2 - \beta^{\gamma+1} - \left(\frac{\gamma-1}{\gamma+1} \right) \alpha^2 = 0 \quad (49)$$

Equation (49) is solved by the classical Newton-Ralphson scheme as follows:

Setting

$$F(\beta) = \beta^2 - \beta^{\gamma+1} - \left(\frac{\gamma-1}{\gamma+1} \right) \alpha^2$$

one obtains

$$F' = \frac{dF}{d\beta} = 2\beta - (\gamma+1)\beta^{\gamma}$$

The iteration scheme is

$$\beta_{n+1} = \beta_n - \frac{F(\beta_n)}{F'(\beta_n)}, \quad n=0,1,2,\dots \quad (50)$$

A reasonable guess for the initial value, β_0 is 0.9 and the iteration scheme converges very rapidly to a physically meaningful value. Knowing β the compressible velocity is calculated by using Eq. (45)

3.2 Finite Element Solution of the Acoustic Equations

Due to its apparent advantages, the application of the FEM in the solution of a variety of engineering problems has been rapidly growing in recent years. A detailed discussion of the FEM can be found in Reference 11. Due to its suitability for handling problems involving complex geometries and mixed boundary conditions the FEM is used in the present investigation in the solution of the inlet wave equations.

Any numerical procedure developed to solve a problem in the realm of continuum mechanics essentially converts the problem with an infinite number of degrees of freedom to one with a finite number of degrees of freedom. The solutions so obtained are expected to approach the exact solutions as the number of degrees of freedom is increased. In the finite element method the continuum region under consideration is subdivided into a number of elements and the variation of the field variable within each element is prescribed in terms of its value at a number of preassigned points in each element (i.e., nodes) and a set of known interpolating functions. Once the values of the field variables at the nodes are determined, the behavior of the field variables within each

element and hence in the overall continuum is known. Thus, the problem of determining the field variables at an infinite number of points is reduced to one of finding their values at a finite number of nodes.

To obtain the needed solutions, Eqs. (6) and (7) which describe the wave propagation in the inlet have been transformed into integral equations utilizing the Galerkin Method. The resulting integral equations were then solved using the FEM. The solution involves the following six operations:

3.2.1 Subdivision of the solution domain: In the finite element method the commonly employed element shapes for discretizing the domain of interest are triangles, rectangles or isoparametric triangles (i.e., triangles with curved edges) for two dimensional or axisymmetric problems and tetrahedrons, cuboids or isoparametric tetrahedrons for three dimensional problems. The choice of the element shapes in solving a particular problem is determined by the geometry of the domain of interest and the level of complexity that can be employed. For two dimensional problems, straight edged triangular elements are by far the most commonly used elements because of the relative ease in closely approximating complex shaped domains as compared to rectangular elements and the lower level of complexity in the finite element methodology as compared to the isoparametric triangles. Hence, straight edged triangular elements with three or six nodes have been chosen in the present study for subdividing the inlet duct. A computer code has been developed which subdivides a duct into triangles with three nodes and catalogues the geometric nodal locations, nodal numbers and element numbers. The assembly

of nodes and triangles is such that each element number corresponds to three nodal numbers and each nodal number is associated with a fixed number of elements whose number may vary between two and six depending upon the node location (see Figure 3). For the six node elements, the vertices and the midside points of the triangle are normally chosen as the nodes. In such a case, the node and element numbers are catalogued so that each element number corresponds to six nodal numbers and each nodal number is associated with a fixed number of elements varying between one and six (see Figure 4).

3.2.2 Selection of Interpolation Functions: Polynomials are the popular interpolating functions because of their desirable mathematical properties of completeness and ease in mathematical manipulation. The variation of the field variable (acoustic potential in this case) within a three node triangle can be expressed in terms of a linear Lagrangian polynomial in two dimensions. Hence, three node triangles are also known as linear triangles. A quadratic representation of the acoustic potential ϕ can be obtained using six node triangles since a quadratic Lagrangian polynomial in two dimensions has six coefficients.

A linear transformation from the global Cartesian system to a local "area coordinate system" for each element has been found to simplify the mathematical operations involving triangular elements considerably. In this transformation, a triad set of coordinates for each element, $(L_i^{(e)}, L_j^{(e)}, L_k^{(e)})$ out of which only two are linearly independent replaces the diad set of coordinates, (r, z) through the following relationships:

ORIGINAL PAGE IS
OF POOR QUALITY

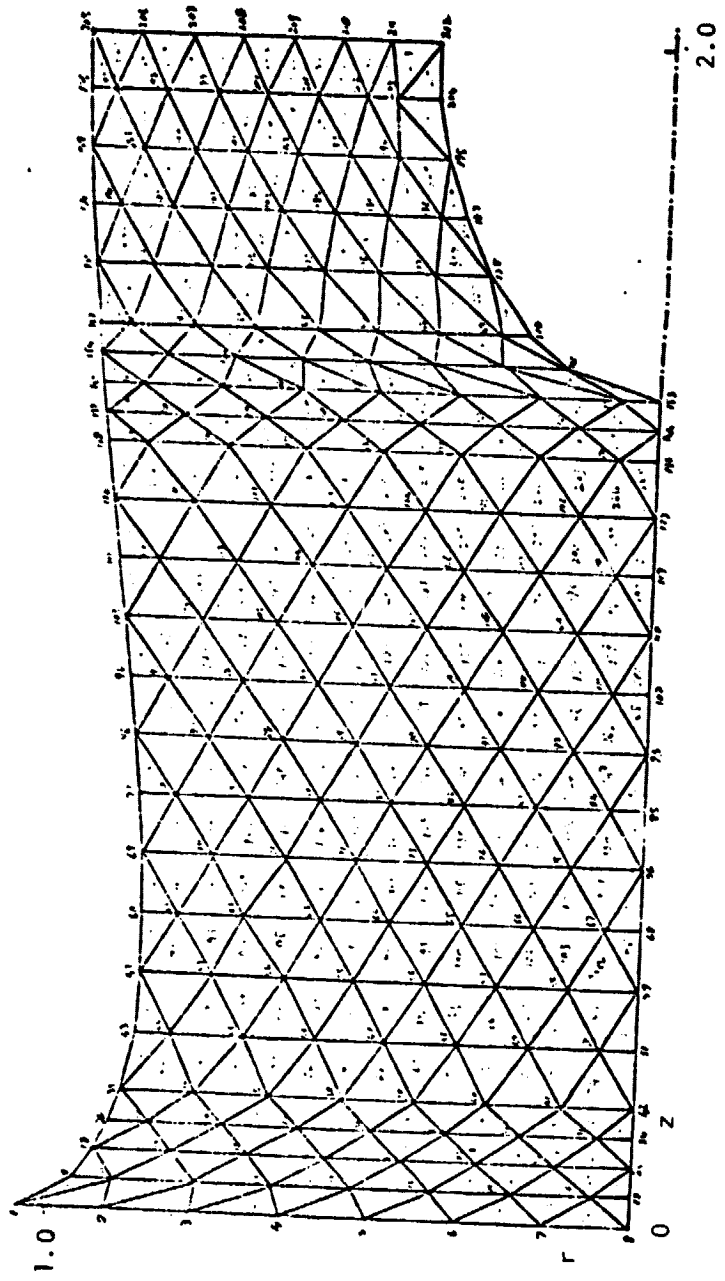


Figure 3. The QCSEE Inlet Triangulization into 3-Node Triangles

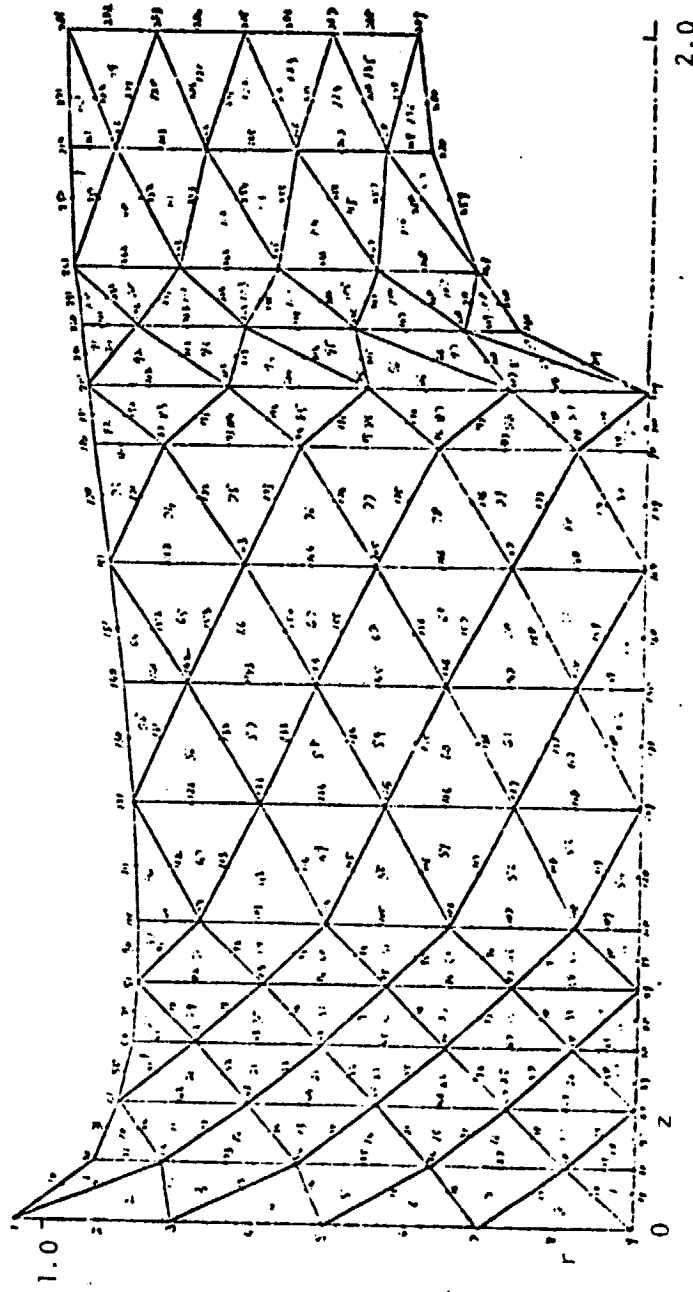


Figure 4a. The QCSEE Inlet Triangulization into 6-Node Triangles.

ORIGINAL PAGE IS
OF POOR QUALITY

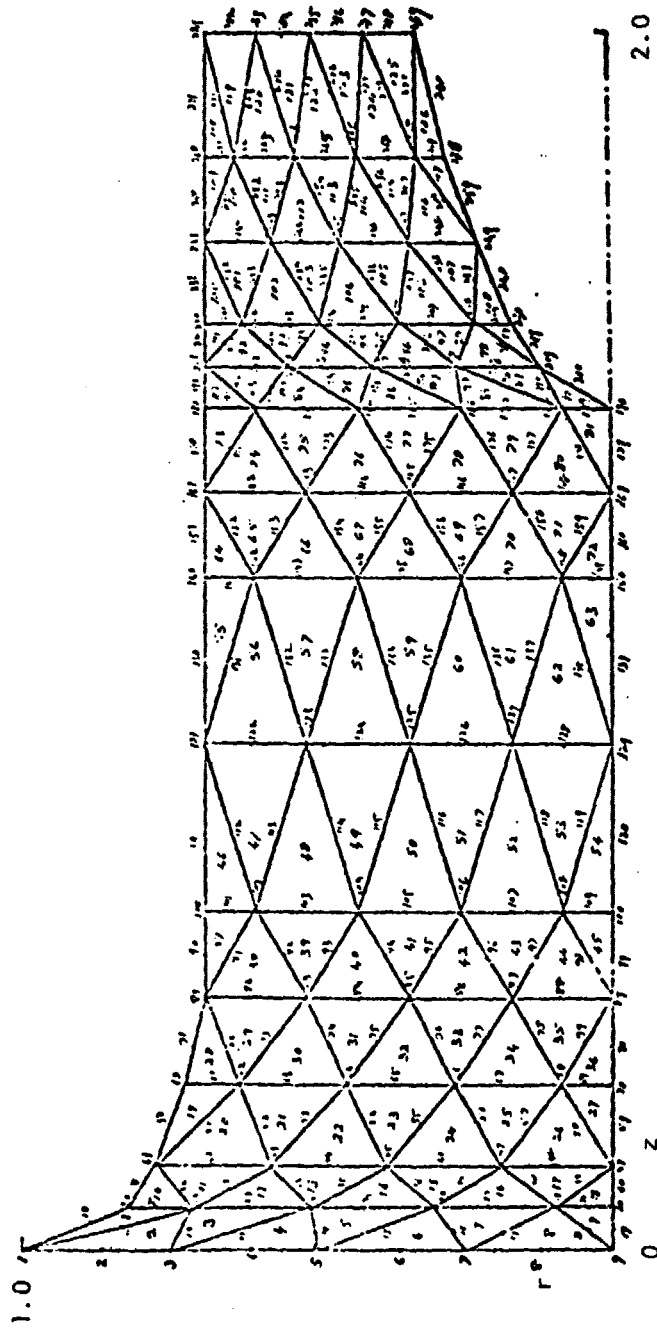


Figure 4b. The Bellmouth Inlet Triangulization into 6-Node Triangles.

$$\begin{aligned}
 L_i^e z_i + L_j^e z_j + L_k^e z_k &= z \\
 L_i^e r_i + L_j^e r_j + L_k^e r_k &= r \\
 L_i^e + L_j^e + L_k^e &= 1
 \end{aligned}
 \tag{51}$$

Solving Eqs. (51) for L_i^e , L_j^e and L_k^e ,

$$\begin{aligned}
 L_i^e &= (a_i + b_i z + c_i r) / 2\Delta \\
 L_j^e &= (a_j + b_j z + c_j r) / 2\Delta \\
 L_k^e &= (a_k + b_k z + c_k r) / 2\Delta
 \end{aligned}
 \tag{52}$$

where

$$\Delta = \frac{1}{2} \det \begin{vmatrix} 1 & z_i & r_i \\ 1 & z_j & r_j \\ 1 & z_k & r_k \end{vmatrix} = \text{Area of } e^{\text{th}} \text{ triangle}$$

and

$$\begin{aligned}
 a_i &= z_j r_k - z_k r_j; & a_j &= z_k r_i - z_i r_k; & a_k &= z_i r_j - z_j r_i \\
 b_i &= r_j - r_k; & b_j &= r_k - r_i; & b_k &= r_i - r_j \\
 c_i &= z_k - z_j; & c_j &= z_i - z_k; & c_k &= z_j - z_i
 \end{aligned}$$

For a triangle with three nodes at the vertices, the interpolating functions are simply the area coordinates. Thus the acoustic potential over the e^{th} element varies linearly and is given by

$$\tilde{\phi}(r, z) = L_i^e(r, z)\tilde{\phi}_i + L_j^e(r, z)\tilde{\phi}_j + L_k^e(r, z)\tilde{\phi}_k \quad (53)$$

$$\hat{\phi}(r, z) = L_i^e(r, z)\hat{\phi}_i + L_j^e(r, z)\hat{\phi}_j + L_k^e(r, z)\hat{\phi}_k \quad (54)$$

A quadratic variation for the acoustic potential over the element is achieved by choosing triangles with six nodes, three being corner nodes and the remaining three being mid-side nodes (see Figure 5) and is described by the following relationships:

$$\begin{aligned} \tilde{\phi}(r, z) = & N_i^e(r, z)\tilde{\phi}_i + N_j^e(r, z)\tilde{\phi}_j + N_k^e(r, z)\tilde{\phi}_k + N_\ell^e(r, z)\tilde{\phi}_\ell \\ & + N_m^e(r, z)\tilde{\phi}_m + N_n^e(r, z)\tilde{\phi}_n \end{aligned} \quad (55)$$

$$\begin{aligned} \hat{\phi}(r, z) = & N_i^e(r, z)\hat{\phi}_i + N_j^e(r, z)\hat{\phi}_j + N_k^e(r, z)\hat{\phi}_k + N_\ell^e(r, z)\hat{\phi}_\ell \\ & + N_m^e(r, z)\hat{\phi}_m + N_n^e(r, z)\hat{\phi}_n \end{aligned} \quad (56)$$

where the quadratic interpolating functions are related to the area coordinates L_i^e , L_j^e , and L_k^e by the following:

For Corner nodes,

$$\begin{aligned} N_i^e &= 2(L_i^e)^2 - L_i^e \\ N_j^e &= 2(L_j^e)^2 - L_j^e \\ N_k^e &= 2(L_k^e)^2 - L_k^e \end{aligned} \quad (57)$$

For mid-side nodes

$$\begin{aligned} N_\ell^e &= 4L_i^eL_j^e \\ N_m^e &= 4L_j^eL_k^e \\ N_n^e &= 4L_k^eL_i^e \end{aligned} \quad (58)$$

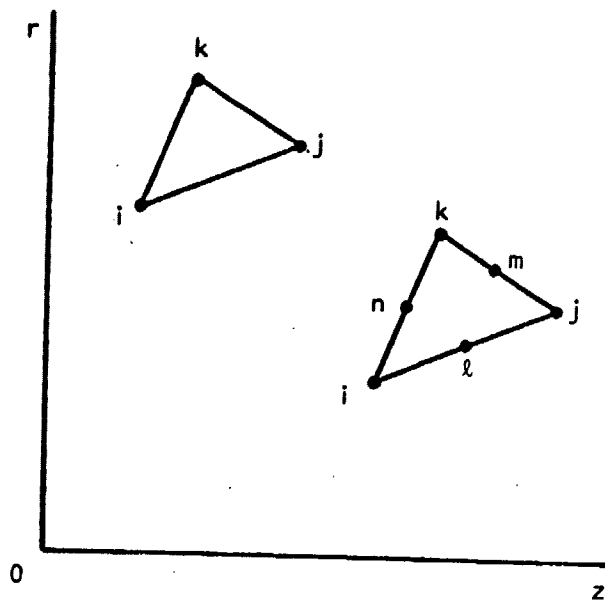


Figure 5. Linear and Quadratic Triangles.

3.2.3 Establishing Elemental Relations: The Galerkin method is applied to the governing differential equations and boundary conditions to develop the matrix equations that express the properties of individual elements in terms of the unknown nodal values. Denoting either of the partial differential equations, 6 and 7, by the operator $L(\phi')$, application of the Galerkin and FEM methods¹¹ yields the following relationships:

$$\sum_{e=1}^E \iiint_{\Delta(e)} N_m^e L(\phi') dv^{(e)} = 0 \quad m=1,2,\dots,N \quad (59)$$

where the integration is performed over each element. In Eq. (59) N is the total number of nodes in the problem under consideration and E is the number of elements. It should be noted that N_m^e is zero for all elements not having the nodal point, m , as a vertex. Equation (59) provides $2N$ equations for the $2N$ unknown nodal values.

In evaluating Eq. (59) over each element the following integral involving the area coordinates and arbitrary exponents a, b , and c is needed:

$$\iiint_{\Delta(e)} (L_i^e)^a (L_j^e)^b (L_k^e)^c drdz = \frac{a!b!c!}{(a+b+c+2)!} \times 2\Delta^{(e)} \quad (60)$$

(see Appendix A for the proof of Eq. (60)).

There exists¹¹ a mathematical restriction in the choice of interpolating functions stating that the values of ϕ' and its partial derivatives up to the highest order appearing in Eq. (59) must have

representation as the element size shrinks to zero. If linear interpolating functions are chosen, the second order partial derivatives of ϕ' will be identically zero. To avoid this, all terms in Eq. (59) containing second order partial derivatives of ϕ' can be reduced to terms containing first order derivatives of ϕ' using Green's theorem for a plane geometry²⁴ (also known as integration by parts). The boundary conditions, given in the previous chapter, are introduced into the boundary integrals that are obtained as a result of the above-mentioned integration by parts. However, for an inlet lined with point-reacting liners carrying a steady mean flow the boundary conditions at the lined wall, as given by Eqs. (29) and (30), involve second derivatives of ϕ' . Hence, linear interpolating functions cannot be used since the terms containing second derivatives of ϕ will be identically equal to zero. In such a case, one has to choose quadratic or higher order representation of ϕ' over each triangle. In the present study, quadratic interpolating functions have been used to handle the lined wall boundary conditions. A point to note is that if there is no mean flow in the duct, the lined wall boundary conditions do not contain any second order derivatives of ϕ' and again one does not need a quadratic representation for ϕ to treat the no mean flow case. After the choice of interpolating functions is made, five different elemental relations are developed depending upon the location of the triangles under consideration; that is: (1) triangles interior to the flow region; (2) triangles adjacent to a hard wall; (3) triangles adjacent to a lined wall; (4) triangles adjacent to the fan plane; and (5) triangles adjacent to the entrance

plane (see Appendix B for the mathematical development).

3.2.4 Assembly of Element Equations to Obtain a System of Algebraic Equations: Based on the ordering system defined in the first step, the individual element equations are combined into a matrix equation describing the properties of the potential ϕ' in the domain under study. Since each node is only affected by adjacent elements, the resulting matrix is banded.

3.2.5 Solution of the System of Equations: Considerable amount of information is currently available about the solution of large, banded matrices. In the present study, CDC subroutine BLSWNP is used for calculations.²⁵ The BLSWNP subroutine has been developed to solve efficiently a system of linear algebraic equations with a banded coefficient matrix. Let k_1 and k_2 be the bandwidth of the lower and upper triangles of the $N \times N$ banded matrix, excluding the main diagonal. All the elements outside this bandwidth are equal to zero. In the BLSWNP Subroutine only the nonzero elements (i.e. at most $N \times (k_1 + k_2 + 1)$) are stored such that the columns of the condensed matrix are the diagonals of the banded matrix and rows are stored as rows of the banded matrix (see Figure 6). Such a condensed storage scheme reduces the computer memory requirements. Further, the solution of the system of equations is obtained in two sequential steps as described below.

To solve the banded system of equations,

$$[k] \{x\} = \{b\} \quad (61)$$

decompose the problem into

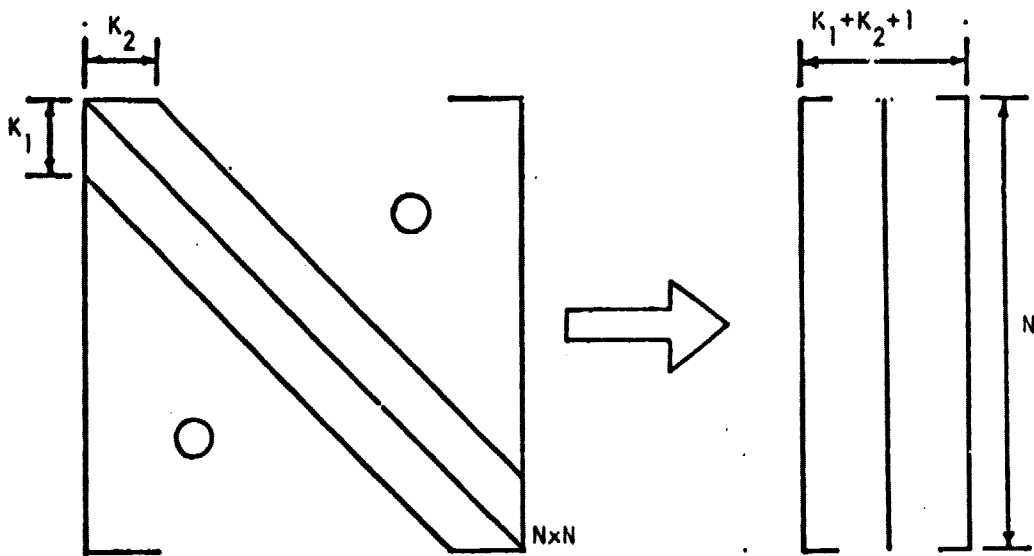


Figure 6. Condensed Storage Scheme Used in CDC Subroutine BLSWNP.

$$[L] \{y\} = \{b\} \quad (62)$$

and

$$[U] \{x\} = \{y\} \quad (63)$$

where [L] and [U] are lower and upper triangular matrices derived from [K] and {y} is an intermediate solution vector. Since solution of triangular matrices can be obtained without pivoting, the above scheme is computationally quite efficient.

3.2.6 Additional Calculations: Once the velocity potential is obtained at the nodes, additional variables such as the axial and radial velocities and acoustic pressures can be calculated at any point in the domain, by utilizing the computed solutions of ϕ' together with Eqs. (53) and (54) for a three node element case or with Eqs. (55) and (56) for a six node element as the case may be.

The results obtained can be checked for the recovery of the boundary conditions and conservation of acoustic energy. The time averaged acoustic intensity in the a^{th} direction for an irrotational, uniform-entropy flow to second order in acoustic quantities is given by the following expression²⁶ (also see Appendix C for the derivation)

$$\begin{aligned} \langle \underline{I}' \rangle \cdot \underline{a} = & \langle p' \nabla \phi' \rangle \cdot \underline{a} + \frac{\nabla \bar{\phi} \cdot \underline{a}}{\bar{\rho} \bar{c}^2} \langle p'^2 \rangle + \frac{(\nabla \bar{\phi} \cdot \underline{a}) \nabla \bar{\phi}}{\bar{c}^2} \cdot \langle p' \nabla \phi' \rangle \\ & + \bar{\rho} (\nabla \bar{\phi} \cdot \langle \nabla \phi' \nabla \phi' \rangle) \cdot \underline{a} \end{aligned} \quad (64)$$

where \underline{I} is the acoustic intensity vector, \underline{a} is unit vector in the direction along which acoustic intensity is needed, and $\langle \rangle$ describes

time average over a long period of time. The time average energy flow across a surface S is then

$$\langle E \rangle = \int_S \langle \underline{I}' \rangle \cdot \hat{n} dS \quad (65)$$

where \hat{n} is the unit outward normal to surface S .

In the present study, the time average acoustic energy flows at the entrance to the duct, at the exit plane of the duct and at the duct walls have been computed using Eqs. (64) and (65) (see Appendix C for a detailed finite element evaluation procedure). The effectiveness of a liner in absorbing the sound is expressed by the decibel reduction defined by

$$\text{dB}_{\text{reduction}} = 10 \log_{10} \left| \frac{\langle E \rangle_{\text{input}}}{\langle E \rangle_{\text{output}}} \right| \quad (66)$$

As a check on the accuracy of the developed solution, the difference between the energy flow into the duct and out of the duct should equal the energy absorbed by the lined walls; i.e., acoustic energy should be conserved.

CHAPTER IV

RESULTS AND DISCUSSION OF RESULTS

4.1 Acoustic Calculations Using 3-Node Triangular Elements

To check the accuracy of the developed FEM computer program, solutions for the problems of plane and spinning wave propagation through a hard walled annular duct with constant mean flow have been obtained for comparison with available analytical solutions. For this case, Eqs. (6) and (7) reduce to the following form:

$$\tilde{\phi}_{rr} + \frac{\tilde{\phi}_r}{r} + (1-M^2)\tilde{\phi}_{zz} + \left(\omega^2 - \frac{m^2}{r^2}\right)\tilde{\phi} - 2M\omega\hat{\phi}_z = 0 \quad (67)$$

$$\hat{\phi}_{rr} + \frac{\hat{\phi}_r}{r} + (1-M^2)\hat{\phi}_{zz} + \left(\omega^2 - \frac{m^2}{r^2}\right)\hat{\phi} + 2M\omega\tilde{\phi}_z = 0 \quad (68)$$

where ω is the frequency (non-dimensionalized by the outer annulus diameter and the sound speed), m is the spinning mode number and M is the constant mean flow Mach number.

The hard wall boundary conditions are described by the following expressions:

$$\left. \begin{array}{l} \tilde{\phi}_r = 0 \\ \hat{\phi}_r = 0 \end{array} \right\} \text{at } \left\{ \begin{array}{l} r = \sigma \text{ (inner wall)} \\ r = 1 \text{ (outer wall)} \end{array} \right. \quad (69)$$

and the sound source boundary condition at the exit plane (i.e., $z = L$) is given by

$$\tilde{\phi}_z = -f(r) ; \hat{\phi}_z = 0 \quad (70)$$

Assuming no reflection at the duct entrance plane, where $z = 0$, the following boundary condition applies:

$$\tilde{p} = -Z\tilde{\phi}_z ; \hat{p} = -Z\hat{\phi}_z \quad (71)$$

The needed expressions for the impedance Z and $f(r)$ are given below.

The exact solution to this problem is given by

$$\tilde{\phi} = -\frac{f(r)}{k} \sin[k(z-L)] \quad (72)$$

$$\hat{\phi} = -\frac{f(r)}{k} \cos[k(z-L)] \quad (73)$$

For the plane wave case (i.e., $m = 0$), the various quantities in Eqs. (70) through (73) take on the following form:

$$f(r) = 1 ; Z = 1 ; k = \frac{\omega}{1-M} \quad (74)$$

The real and imaginary components of the velocity potential as calculated by the FEM for an annular cylinder with $\sigma = 0.5$ and $L = 1$ are compared with the exact values computed using Eqs. (72) and (73) in Figure 7 for the case of $M = 0.5$ and $\omega = 2.0$. A good agreement between the FEM and analytical solutions is shown; good agreement has also been obtained when the predictions for the acoustic velocities and pressures were compared.

The expressions describing the propagation of a spinning wave with lobe number m and radial mode μ are:

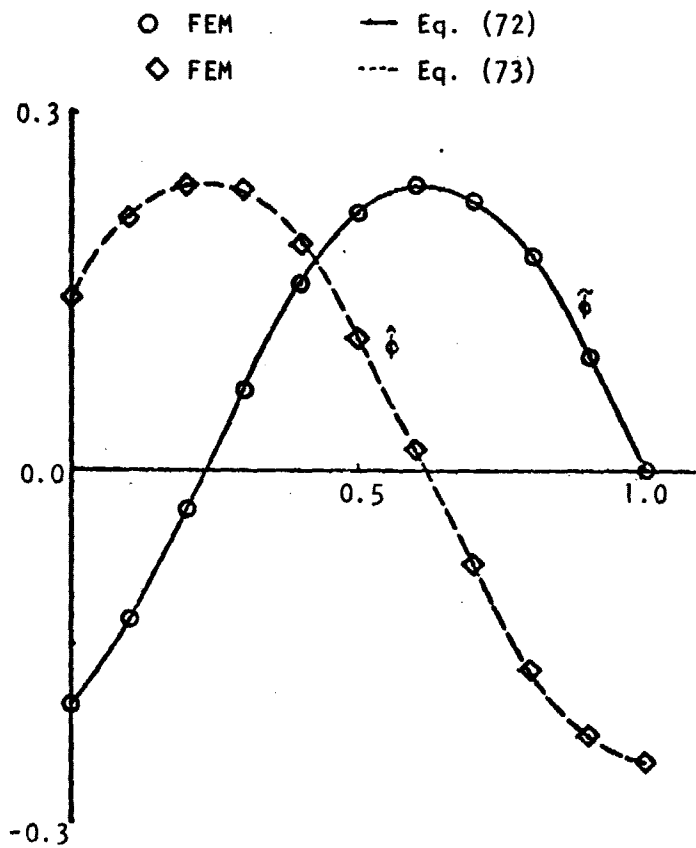


Figure 7. Comparison of Acoustic Velocity Potential for Plane Wave Propagation in an Annular Cylinder ($M = .5$, $\omega = 2.0$).

$$f(r) = E_{m\mu}^{(\sigma)}(\beta r)$$

$$Z = \frac{\omega + M\sqrt{\omega^2 - \beta^2(1 - M^2)}}{\omega M + \sqrt{\omega^2 - \beta^2(1 - M^2)}} \quad (75)$$

and

$$k = \frac{M\omega + \sqrt{\omega^2 - \beta^2(1 - M^2)}}{1 - M^2}$$

where $E_{m\mu}^{(\sigma)}$ and $\beta (=k_{m\mu}^{(\sigma)})$ in Reference 13) are tabulated in Reference 13.

Results of FEM calculations for the velocity potential in the previously described annular duct with $m = 4$, $\mu = 0$, $\omega = 6$ and $M = .5$ are presented in Figure 8. The analytical solutions, given by Eqs. (72) and (73) are also shown in Figure 8 and good agreement between the two solutions is noted. Similar comparisons for other acoustic variables such as acoustic velocity and pressure have also shown good agreement.

For the FEM calculations shown above, the duct was subdivided into 220 3-node triangles with 136 nodes. For a Mach number of 0.5 good agreement between FEM calculations and the exact solutions was obtained for values of ω up to 10. At this point, ($\omega = 10$, $M = 0.5$) there are about 13 nodes per wave length parallel to the annular cylinder axis. Clearly, the accuracy lost at higher frequencies can be recovered by a finer element subdivision or a more elaborate description of the dependent variable ϕ within each element (e.g., quadratic representation of ϕ in each triangle).

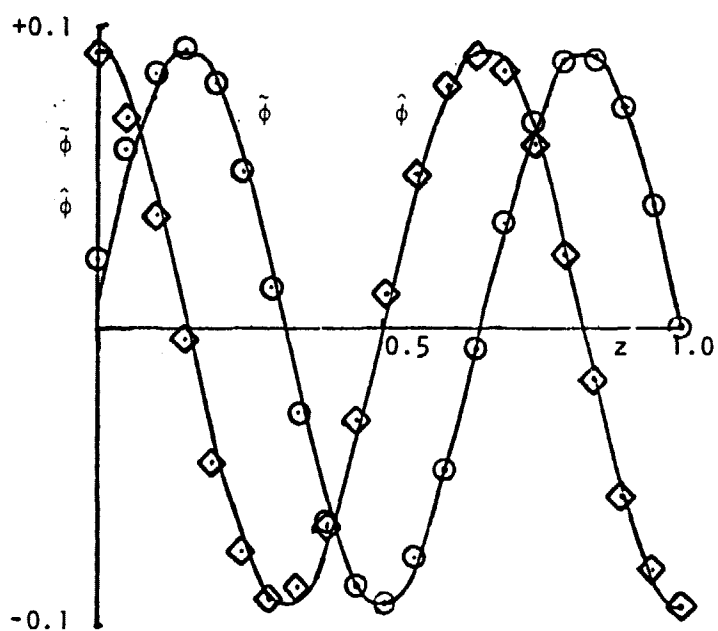


Figure 8. Comparison of Acoustic Velocity Potential for Spinning Wave Propagation in an Annular Cylinder ($M = .5$, $\omega = 6.0$).

4.2 Comparison of Acoustic Calculations by Using Linear and Quadratic Triangular Elements

The problem of plane wave propagation in the annular cylinder carrying a uniform steady flow considered above is chosen to compare the accuracy obtained by using linear and quadratic elements for various frequencies. For the case of linear elements, the cylinder is divided into 140 3-node triangles with the total number of nodes being 94 (see Figure 9) while for the case of quadratic elements, it is divided into 140 6-node triangles with a total of 327 nodes (see Figure 10), 94 out of which are the corner nodes and the remaining 233 nodes are the mid-side nodes.

FEM calculations have been performed for 5 angular frequencies (viz., $\omega = 1, 5, 10, 15,$ and 20) using linear and quadratic elements. The amplitude and phase of the axial acoustic velocity obtained by FEM programs are shown in Figures 11 through 20 along with the exact solutions derived from Eqs. (72) and (73). For the case of $\omega = 1$ and $\omega = 5$, the results obtained by both the FEM programs agree with the exact solution to within 1 to 2%. For the case of $\omega = 10$, quadratic elements give results accurate to 4% while as linear elements give results accurate up to 9%. The predictions by linear elements for $\omega = 15$ and 20 are about 30% off the exact solution and they do not even show the proper trend. However, quadratic elements yield results which are at worst 7% off for $\omega = 15$ and 12% off the exact solutions for $\omega = 20$. Moreover, even at $\omega = 20$ the results of quadratic elements indicate the proper trend (e.g., the acoustic axial velocity amplitude remains reasonably constant). These results unequivocally prove that quadratic representation

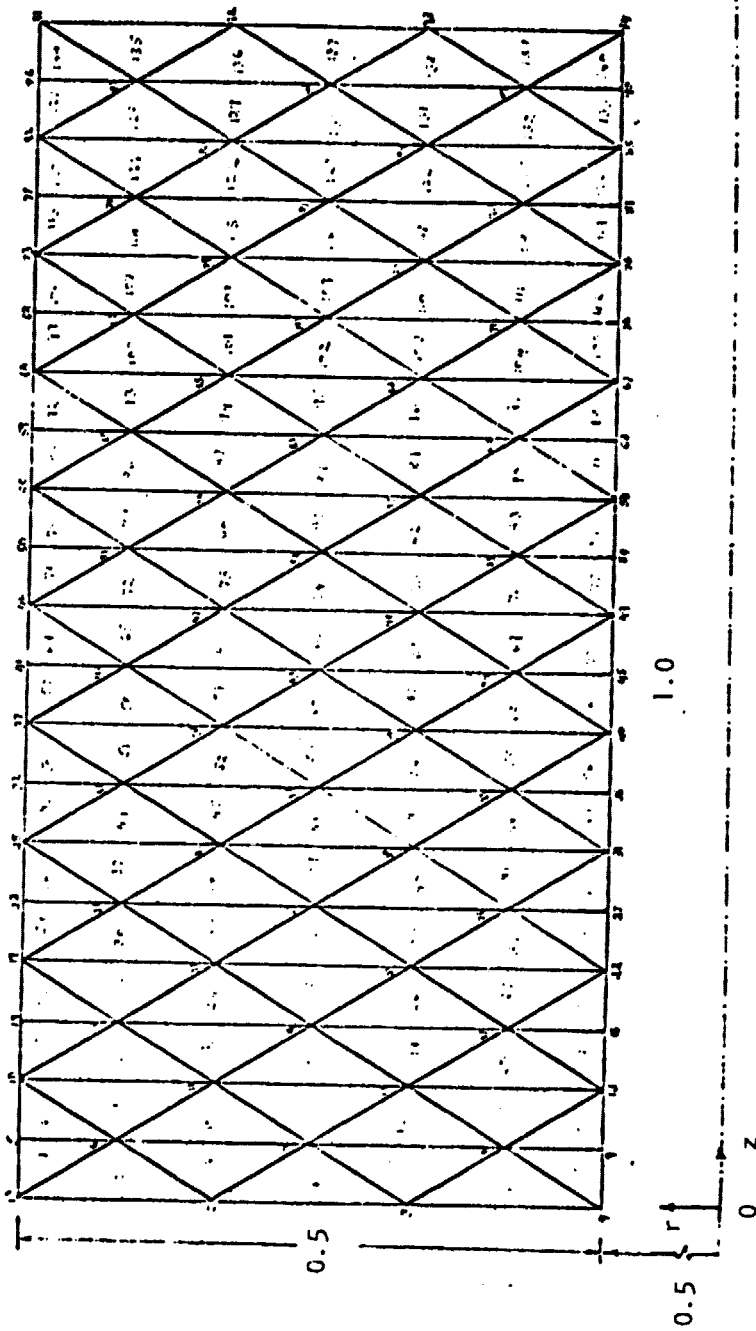


Figure 9. Triangulization of Annular Cylinder into 140 3-Node Triangles.

ORIGINAL PAGE IS
OF POOR QUALITY

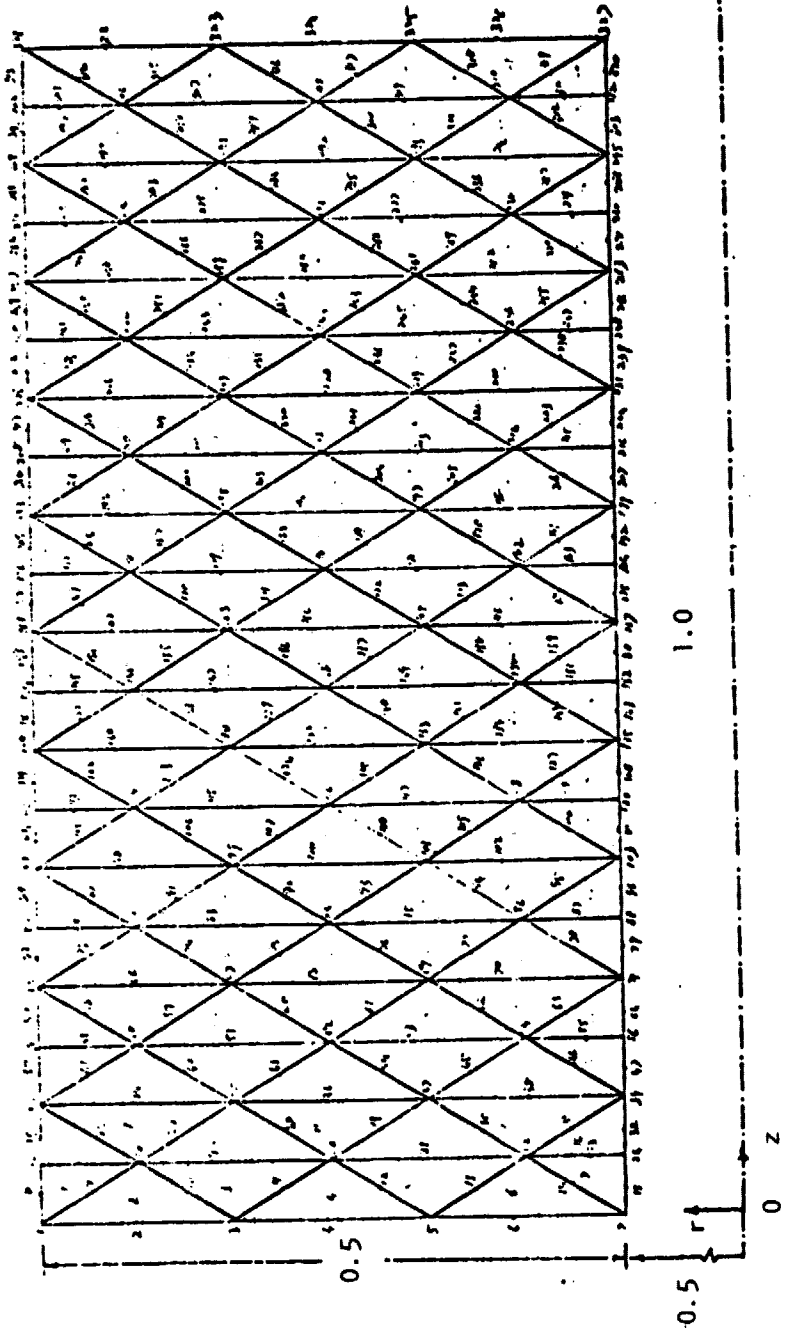


Figure 10. Triangulation of Annular Cylinder into 140 6-Node Triangles.

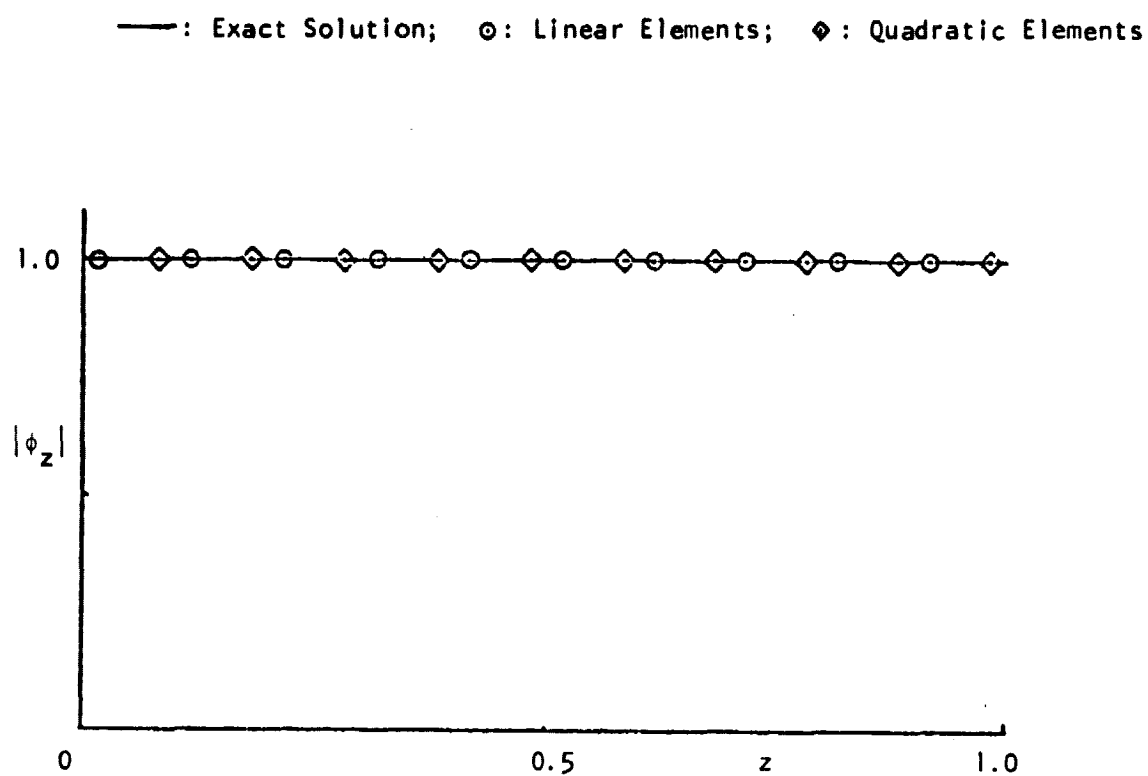


Figure 11. Comparison of Axial Acoustic Velocity Amplitude for Plane Wave Propagation in an Annular Cylinder as Predicted by Linear and Quadratic Elements ($\omega = 1.0$, Mach = 0.5)

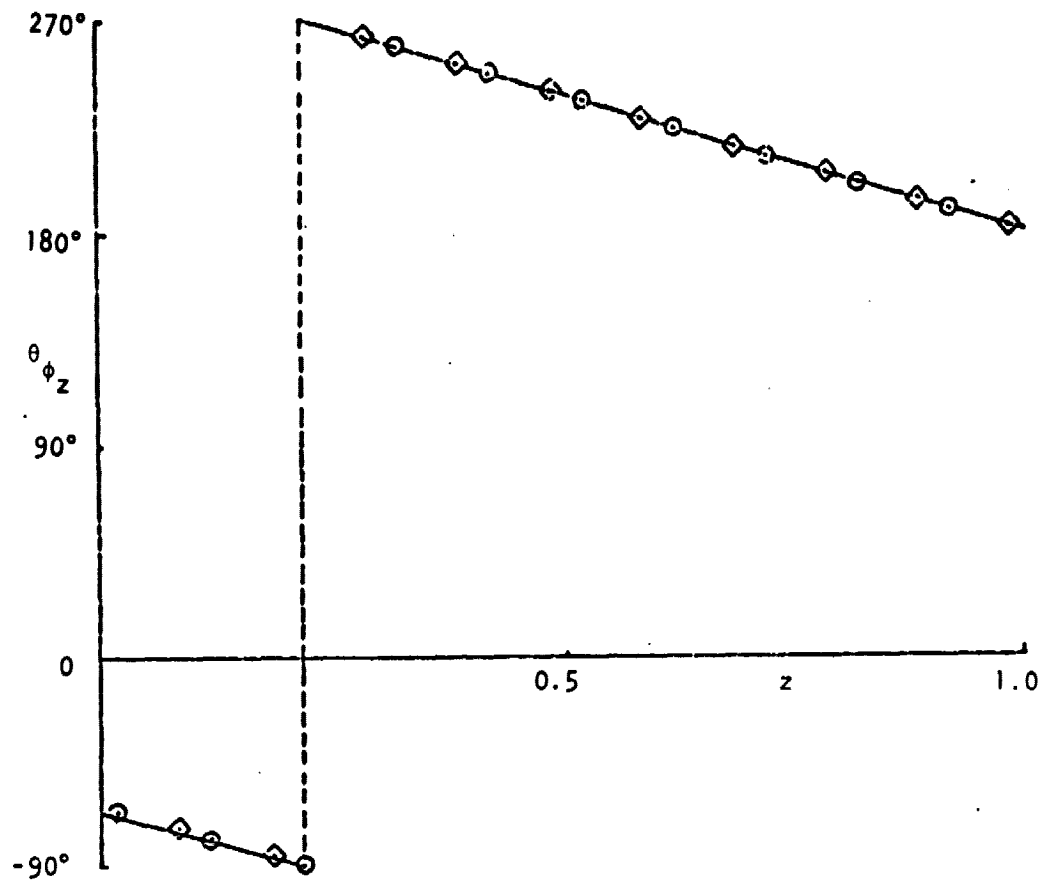


Figure 12. Comparison of Acoustic Axial Velocity Phase for Plane Wave Propagation in an Annular Cylinder as Predicted by Linear and Quadratic Elements for $\omega = 1.0$; Mach = 0.5 (Symbols defined in Figure 11).

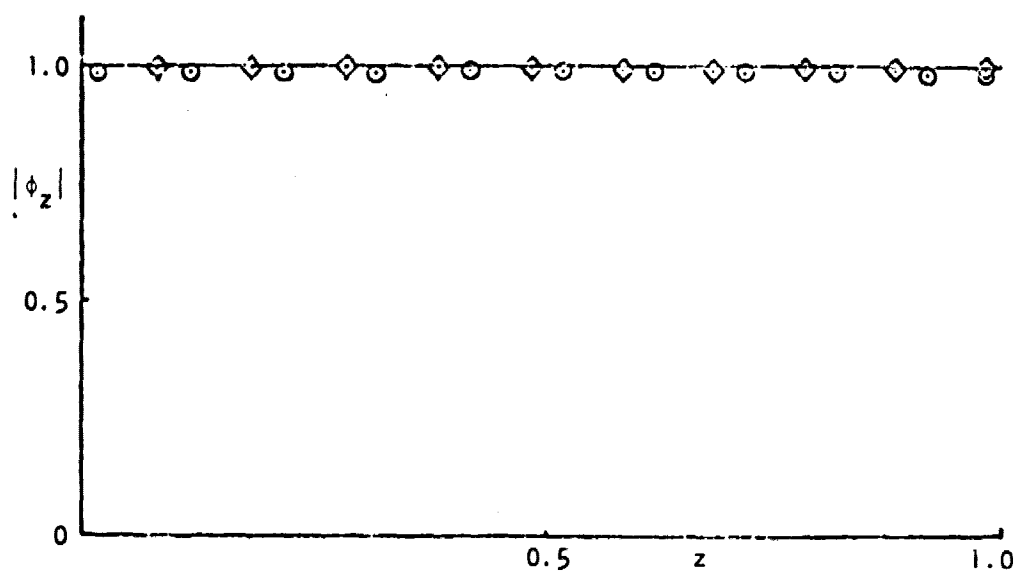


Figure 13. Comparison of Axial Acoustic Velocity Amplitude for Plane Wave Propagation in an Annular Cylinder as Predicted by Linear and Quadratic Elements for $\omega = 5.0$; Mach = 0.5 (Symbols defined in Figure 11).

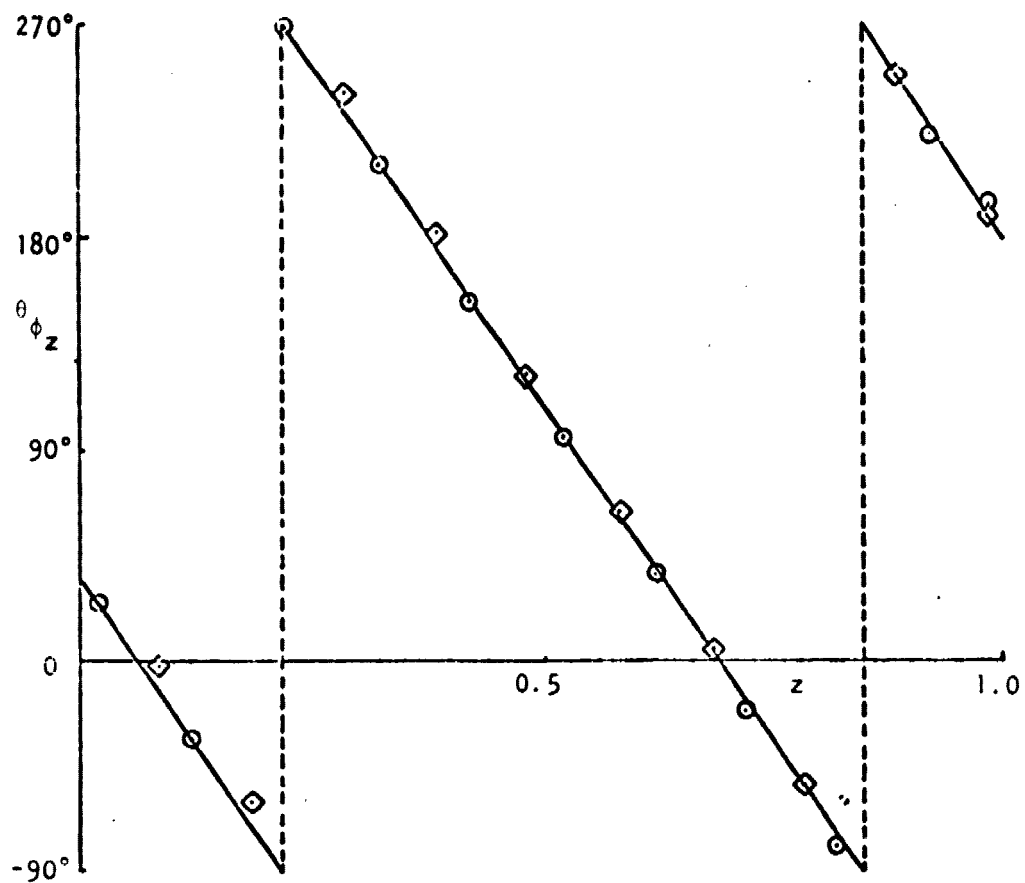


Figure 14. Comparison of Axial Acoustic Velocity Phase for Plane Wave Propagation in an Annular Cylinder as Predicted by Linear and Quadratic Elements for $\omega = 5.0$; Mach = 0.5 (Symbols defined in Figure 11).

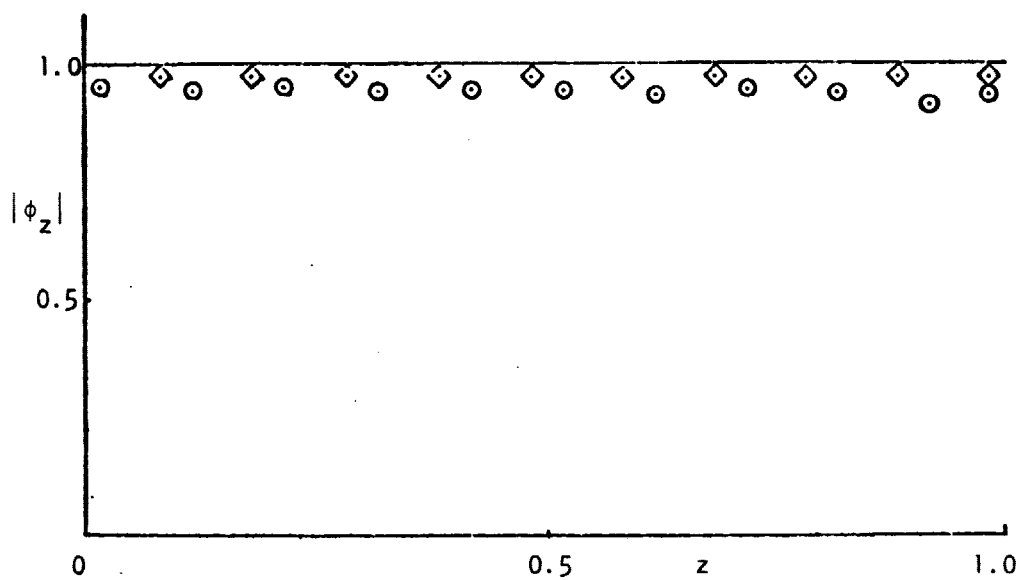


Figure 15. Comparison of Axial Acoustic Velocity Amplitude for Plane Wave Propagation in an Annular Cylinder as Predicted by Linear and Quadratic Elements for $\omega = 10.0$ and Mach = 0.5 (Symbols defined in Figure 11).

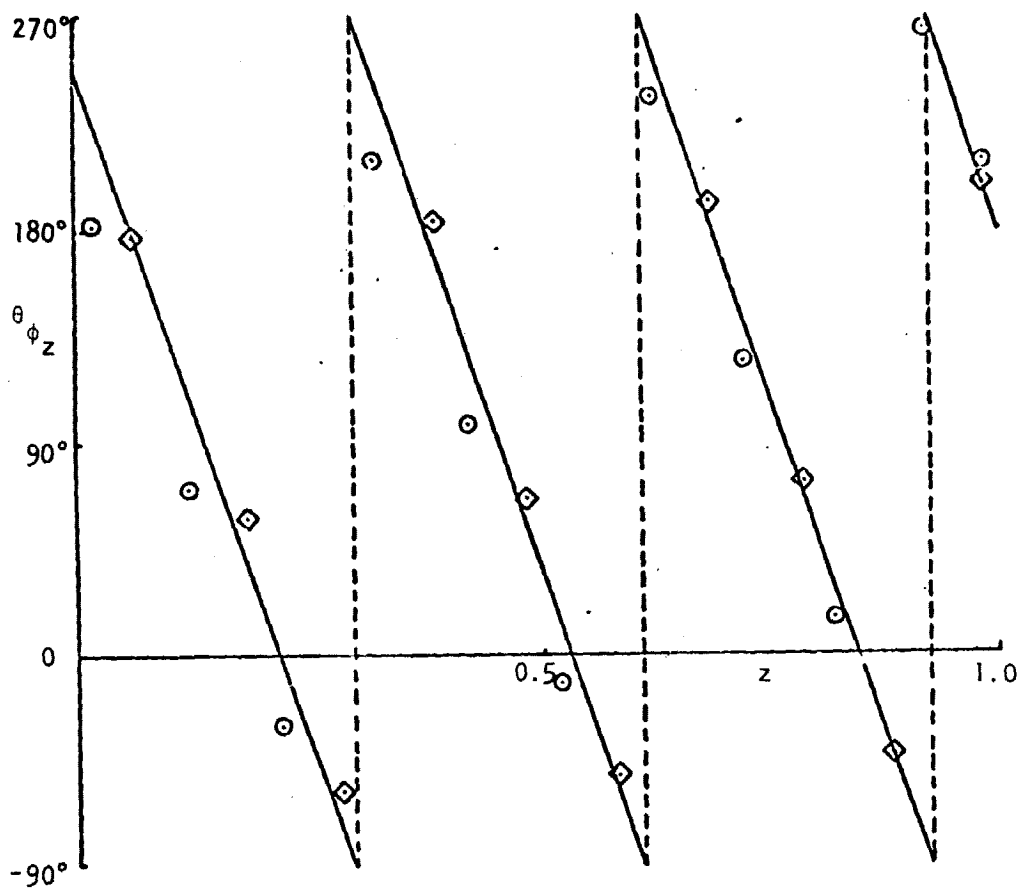


Figure 16. Comparison of Axial Acoustic Velocity Phase for Plane Wave Propagation in an Annular Cylinder as Predicted by Linear and Quadratic Elements for $\omega = 10.0$ and $\text{Mach} = 0.5$ (Symbols defined in Figure 11).

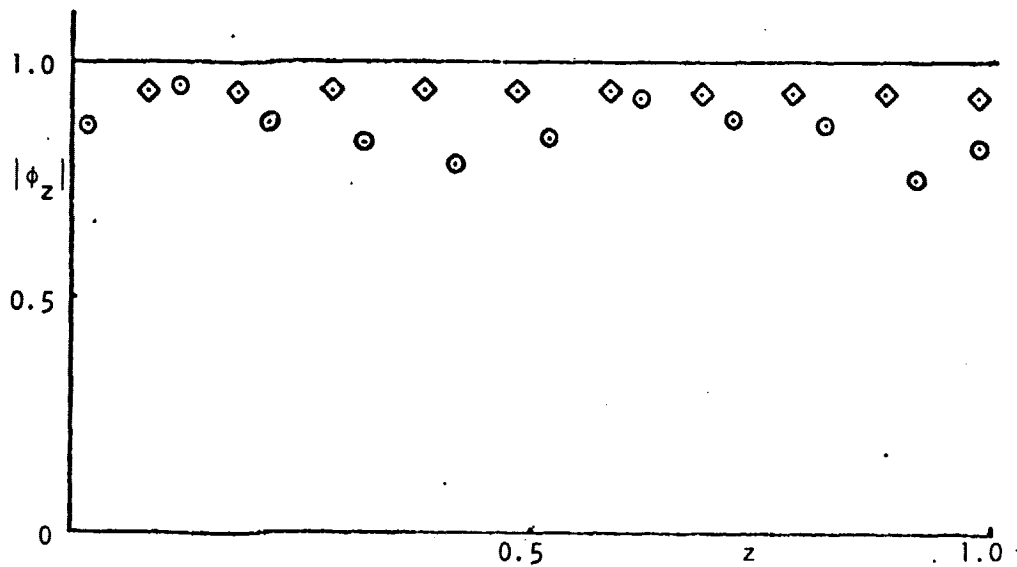


Figure 17. Comparison of Axial Acoustic Velocity Amplitude for Plane Wave Propagation in an Annular Cylinder as Predicted by Linear and Quadratic Elements for $\omega = 15.0$ and $\text{Mach} = 0.5$ (Symbols defined in Figure 11).

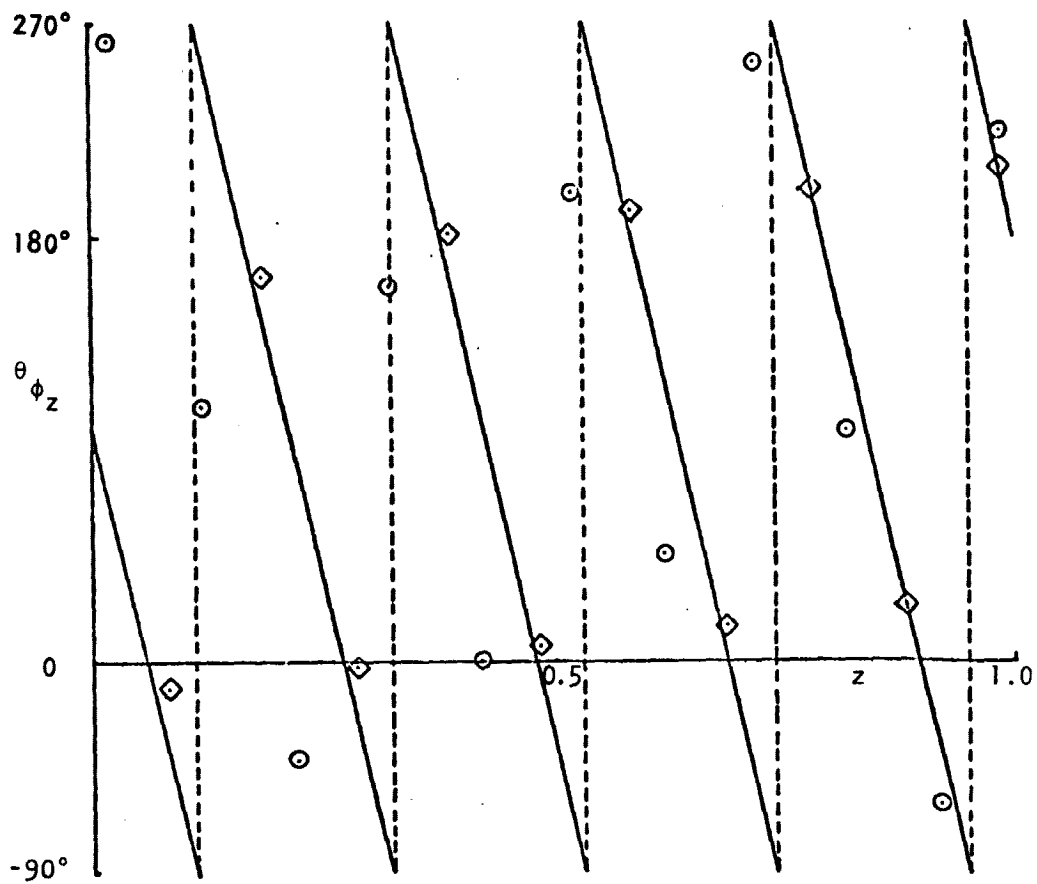


Figure 18. Comparison of Axial Acoustic Velocity Phase for Plane Wave Propagation in an Annular Cylinder as Predicted by Linear and Quadratic Elements for $\omega = 15.0$ and Mach = 0.5 (Symbols defined in Figure 11).

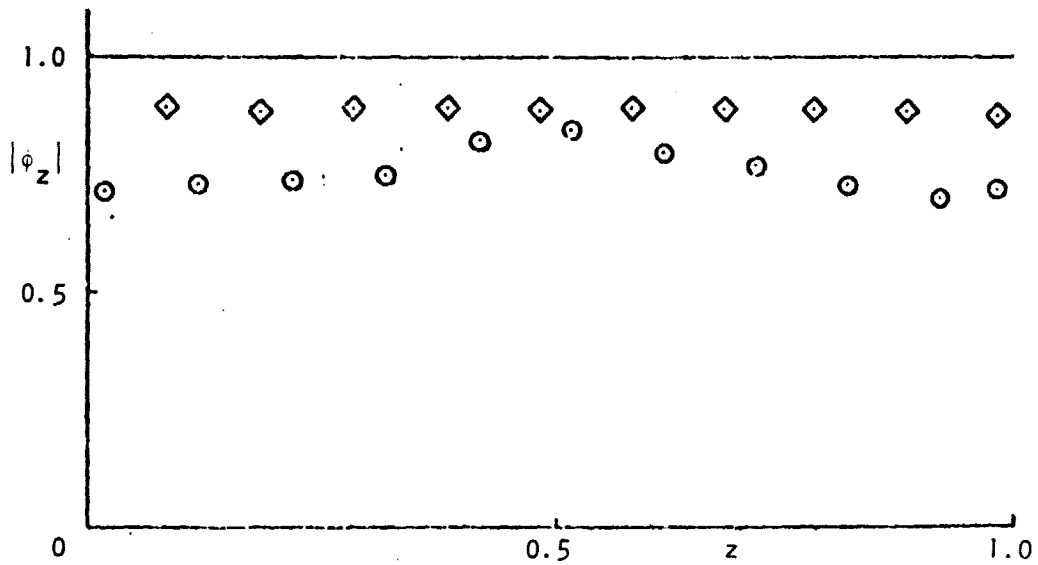


Figure 19. Comparison of Axial Acoustic Velocity Amplitude for Plane Wave Propagation in an Annular Cylinder as Predicted by Linear and Quadratic Elements for $\omega = 20.0$ and Mach = 0.5 (Symbols defined in Figure 11).

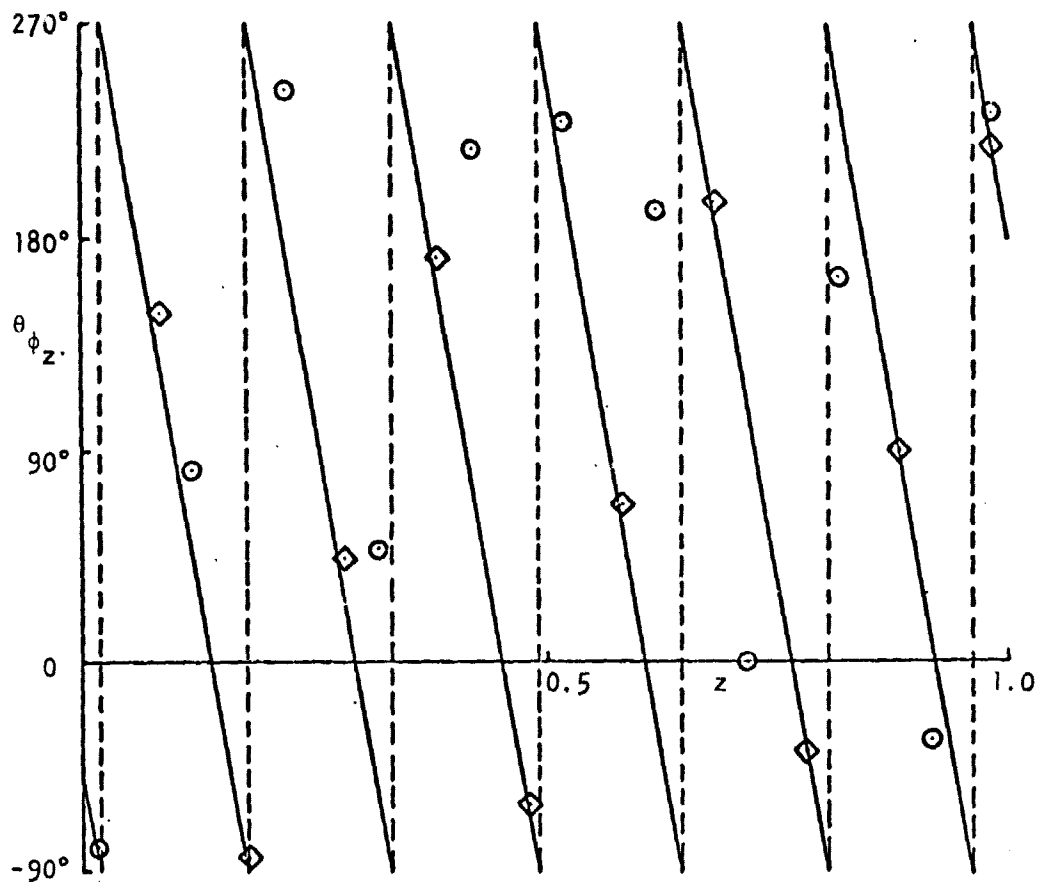


Figure 20. Comparison of Axial Acoustic Velocity Phase for Plane Wave Propagation in an Annular Cylinder as Predicted by Linear and Quadratic Elements for $\omega = 20.0$ and Mach = 0.5 (Symbols defined in Figure 11).

of ϕ over each element yields much better results compared to linear representation for higher frequencies, for a fixed number of elements.

4.3 Comparison Studies for Lined Wall Annular Cylinders

In order to evaluate the accuracy of the finite element method and to de-bug the computer codes, the case of sound propagation in an annular cylinder with uniform steady flow and lined walls has been investigated.

Because a comprehensive set of results including radial and axial profiles of acoustic variables along with the $\text{dB}_{\text{reduction}}$ for the case of a cylindrical duct is not available, comparison was made with the results of Baumeister² for the case of a rectangular duct carrying a uniform steady flow. A rectangular duct is a good approximation to the annular cylinder if the radius of curvature of the cylinder is large and if the radius ratio is sufficiently close to 1.²⁷ The investigated problem is example #3 in Appendix F of Reference 2. The geometry and associated parameters are shown in Figure 21. The radius of the annular cylinder was increased from 100 to 1000 to check the convergence of the dB_{red} to a constant value. The dB_{red} obtained is 4.726 which is close to the 5.6 value obtained by Baumeister. Baumeister has solved the same problem by using the generalized wave envelope transformation.²⁸ A new variable, ψ , defined as

$$\psi(r, z) = e^{\delta z} \phi'(r, z) \quad (76)$$

where δ is a free constant, is substituted into Eqs. (67), (68), (70) and (71) to obtain a new set of partial differential equations and

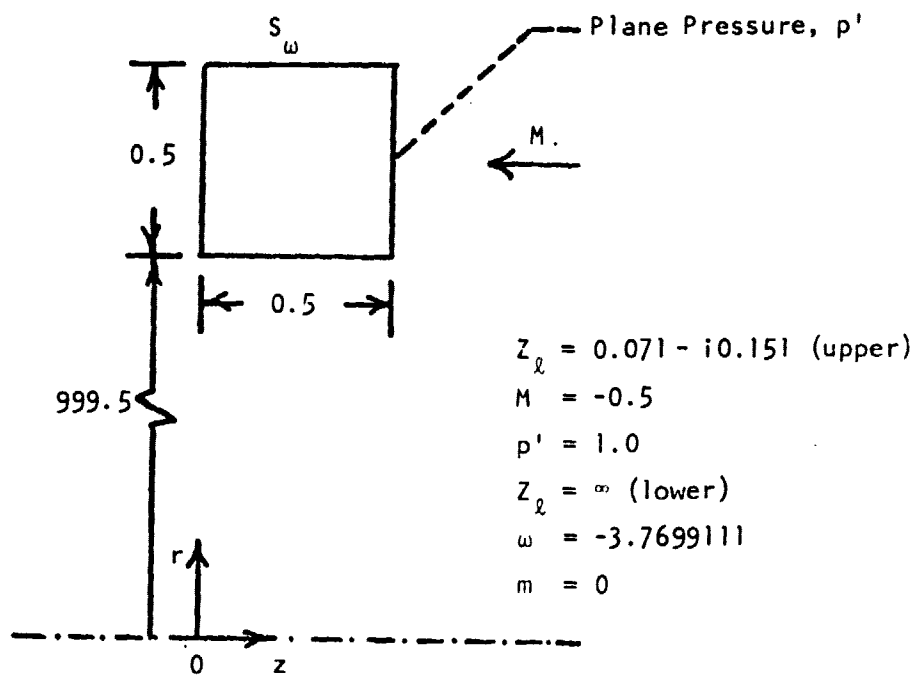


Figure 21. Annular Cylinder Geometry Simulating Rectangular Duct.

boundary conditions for the variable ψ . Having chosen δ to be equal to the appropriate wave number, Baumeister has obtained a dB_{red} of 4.072. The dB_{red} obtained by the FEM program lies in between the two values obtained in Reference 2. Figures 22 through 25 indicate the variation of acoustic pressure (i.e., magnitude and phase) as predicted by the FEM program and Reference 2. Also plotted are the corresponding hard wall duct solutions for the same flow conditions, for the purpose of indicating the effect of the liner in reducing the pressure amplitude. With the exception of the results in Figure 22, the agreement between the two sets of computations is good. Since the liner is known to attenuate the sound wave, one would expect a reduction in acoustic pressure magnitude as one moves from the fan plane towards the entrance plane of the duct. While the FEM results agree with this intuitive argument, the results of Reference 2 indicate an opposite trend. A possible explanation for this is as follows. The finite difference grid used in Reference 2 employs 100 points to model the region of interest while as the finite element model employed 327 points to model the same region. Hence, one could anticipate a better agreement between the two solution schemes if the finite difference grid is made finer. Figure 26 shows the variation of acoustic power absorbed by the lined upper wall. The total acoustic energy absorbed by the liner should equal the difference between the acoustic energy at the entrance and exit planes. This acoustic energy balance has been checked and acoustic energy is conserved with an error of 8%. The prescribed radiation impedance condition at the exit plane and the pressure boundary condition

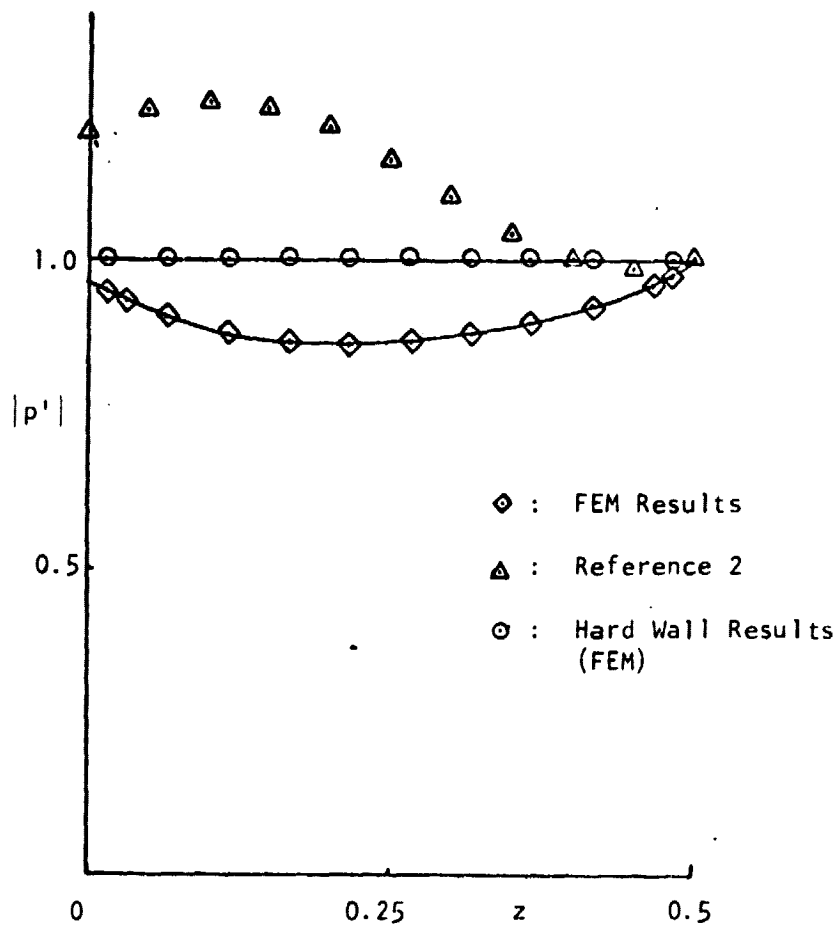


Figure 22. Comparison of Acoustic Pressure Magnitude Along the Upper Wall of the Rectangular Duct as Predicted by FEM Program and Reference 2. Hard Wall Solutions Shown in Circles.

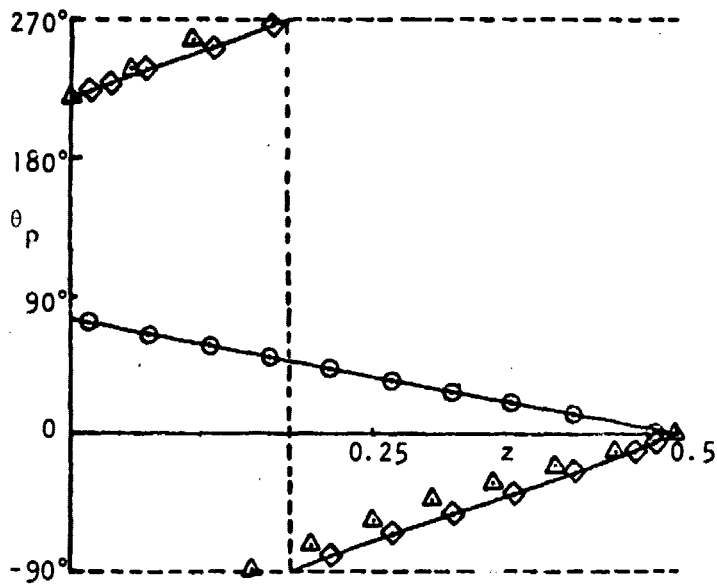


Figure 23. Comparison of Acoustic Pressure Phase Along the Upper Wall as Predicted by FEM Program and Reference 2. Hard wall Solution shown in Circles. (Symbols defined in Figure 22.)

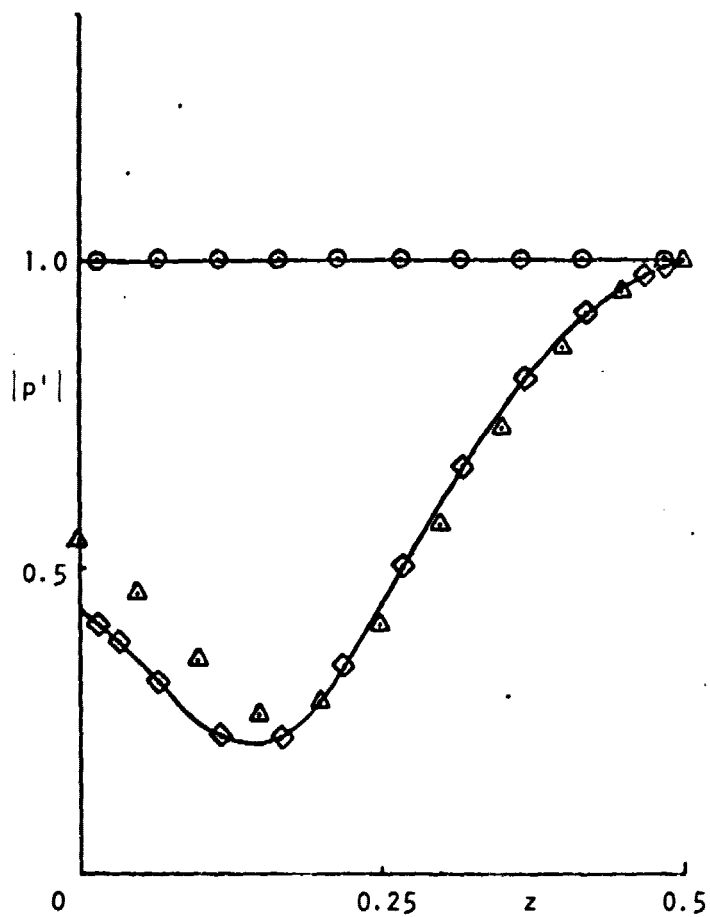


Figure 24. Comparison of Acoustic Pressure Amplitude Along the Lower Wall as Predicted by FEM Program and Reference 2. Hard wall solution shown in circles. (Symbols defined in Figure 22.)

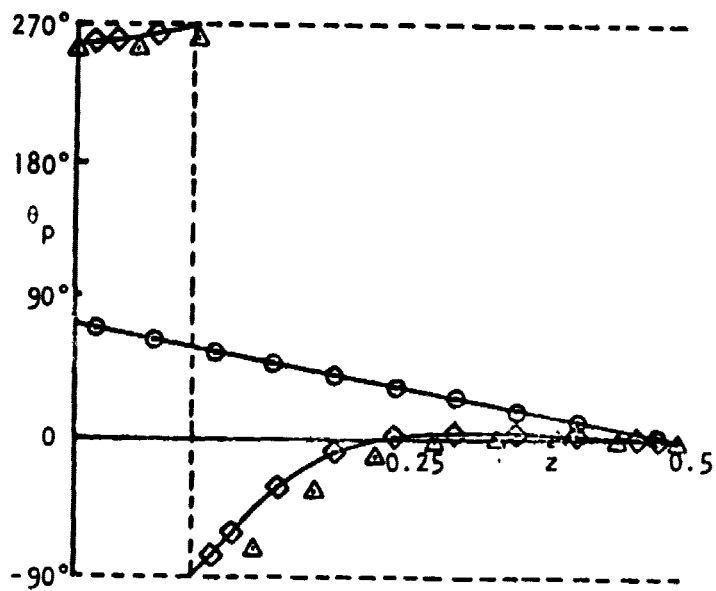


Figure 25. Comparison of Acoustic Pressure Phase Along the Lower Wall as Predicted by FEM Program and Reference 2. Hard wall Solutions shown in circles. (Symbols defined in Figure 22.)

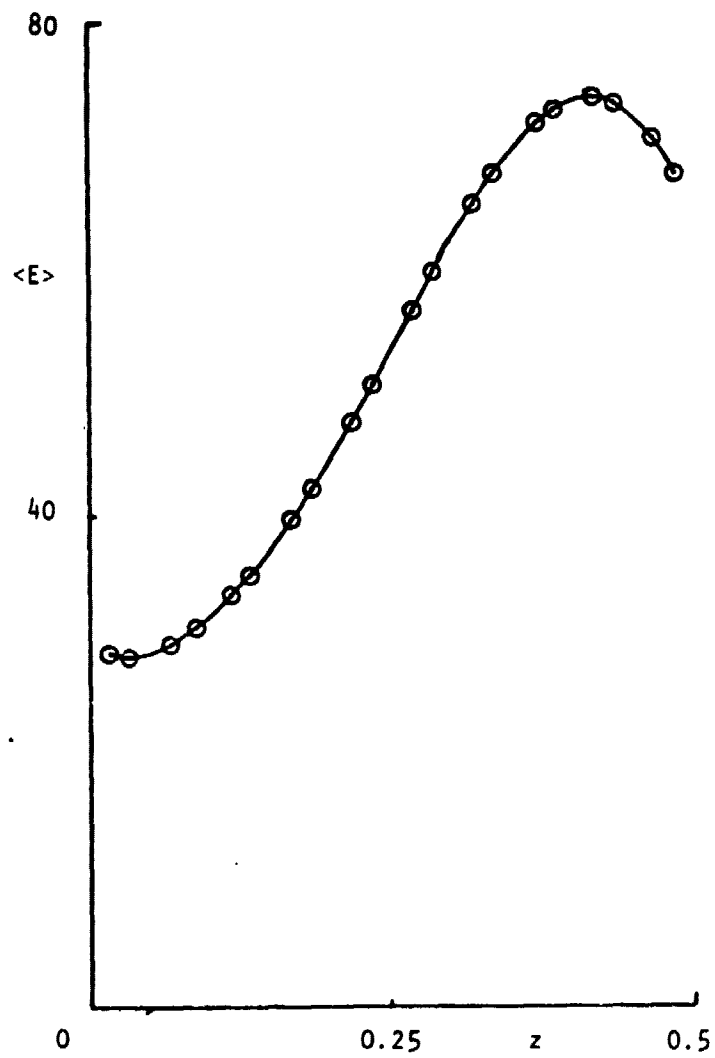


Figure 26. Acoustic Power Absorbed by Each Element Located at the Lined Upper Wall.

at the entrance plane are recovered with a maximum error of 6%. Errors obtained in other computed soft wall cases are smaller than the above-mentioned 6 and 8 percent. Computations for hard walled annular ducts produce acoustic energy conservation with an error of $10^{-5}\%$ and the radiation impedance condition and the pressure boundary condition are recovered with $10^{-4}\%$ error.

4.4 Comparison Studies with the Integral Technique for the QCSEE Inlet

The problem of prescribing the correct radiation impedance condition at the entrance plane of an inlet carrying a variable mean flow has not yet been solved. However, for the case of no mean flow, Bell, Meyer and Zinn³ have solved the problem of wave propagation in an inlet using the Green's function approach in the interior of the inlet and also in the far field. With the knowledge of the solution in the interior and the exterior regions of the inlet a radially varying radiation impedance Z_e can be calculated at the entrance plane of the inlet. The calculated Z_e was incorporated in the FEM program that was specialized to handle the no mean flow case and the solutions obtained by the FEM program and the integral approach for various frequencies and for both hard and soft walled QCSEE inlet one compared in this section.

For the case of no mean flow (i.e., $\bar{\phi}_r = \bar{\phi}_z \equiv 0$) Eq. (8) reduces to

$$p' = i\omega\phi'$$

since, $\bar{\rho} = 1$ as the density of air in the inlet equals the ambient air density. Thus, the acoustic pressure is directly proportional to the

acoustic velocity potential and comparisons have been made with the acoustic potential rather than the acoustic pressure.

As described in Section 3.2.3, in the absence of mean flow one does not need a quadratic representation for the acoustic potential ϕ to handle the lined wall boundary condition. Hence, the comparison studies described in this section have been performed using the 3-node triangulization scheme of the QCSEE inlet (see Figure 3). In both the FEM and integral approaches the sound excitation at the fan plane is prescribed as a plane velocity wave of unit amplitude and a phase angle of 180° . Table 1 shows the distribution of Z_e at the nodes located at the entrance plane of the hard walled QCSEE inlet as calculated by the integral approach for the plane wave propagation of angular frequencies $\omega = 1, 2, 5$ and 10 . The above radiation impedances were incorporated in the FEM program and the acoustic velocity potentials obtained by both the FEM and the integral approach are plotted in Figures 27, 28, 29 and 30 for plane wave propagation of angular frequencies $\omega = 1, 2, 5$ and 10 respectively. One observes that the agreement between the two results is excellent and particularly so at the low frequencies of $\omega = 1$ and 2 . Though the results obtained by both methods are slightly different for $\omega = 5$ and 10 , they indicate similar trends in their behavior. The integral approach used only 50 source points on the inlet surface whereas the FEM used 212 nodal points to map the domain of interest. A better agreement between the two methods at higher frequencies can be obtained if more source points are utilized in the integral approach to represent the inlet surface.

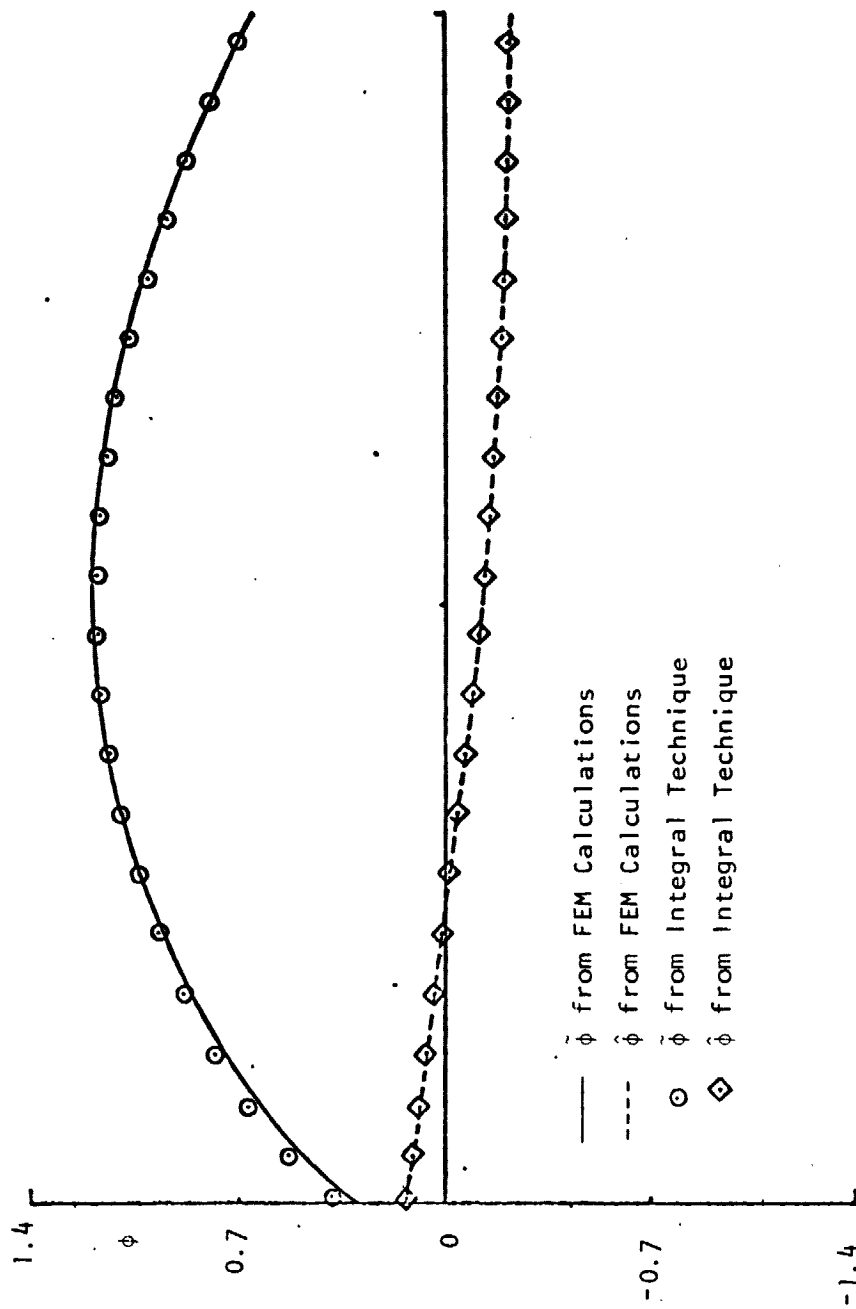


Figure 27. Acoustic Velocity Potential Distribution along the Inlet Upper Wall
 ($\omega = 1.0$, No Flow, Hard Wall, Plane Wave Excitation).

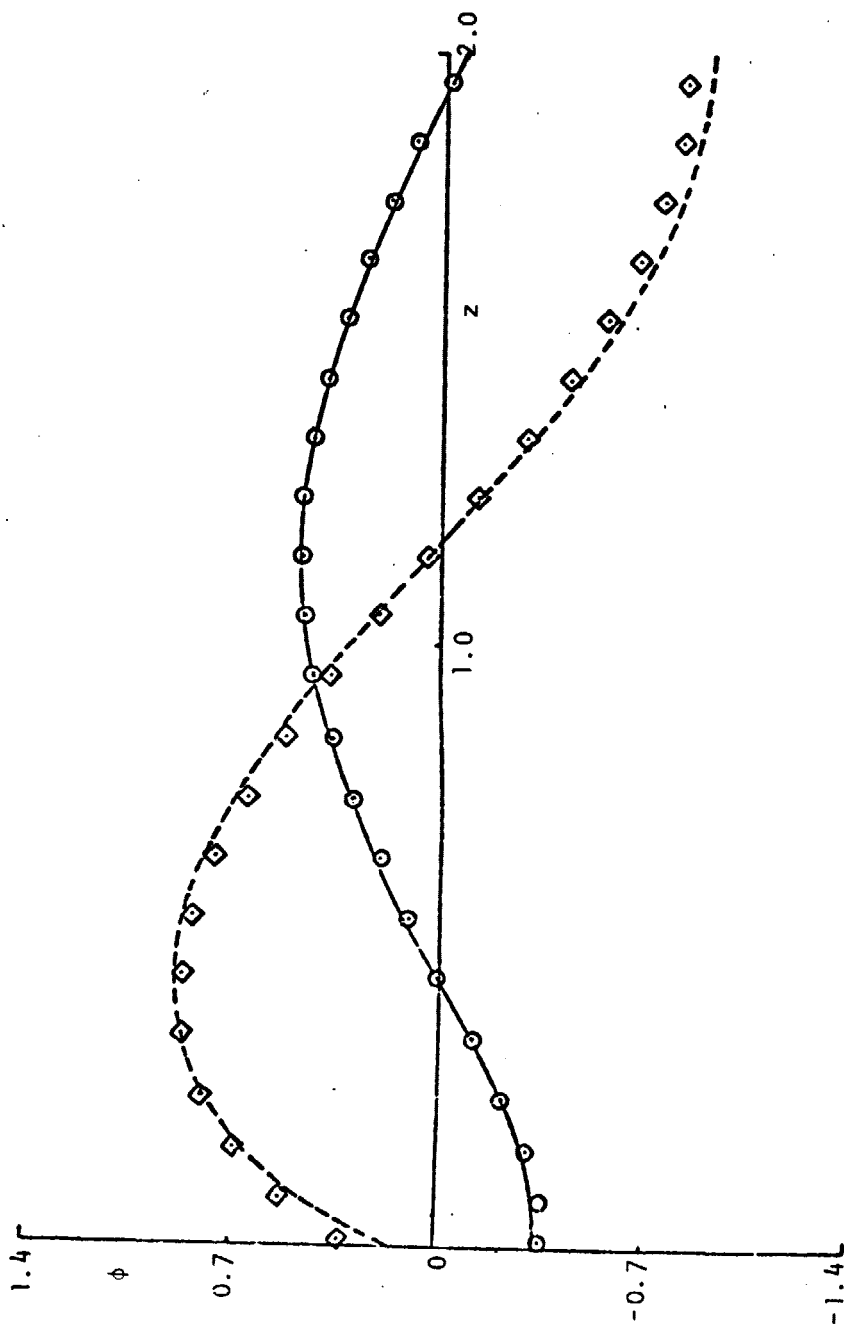


Figure 28. Acoustic Velocity Potential Distribution along the Inlet Upper Wall
 $(\omega = 2.0$, No Flow, Hard Wall, Plane Wave Excitation; Symbols defined in Figure 27).

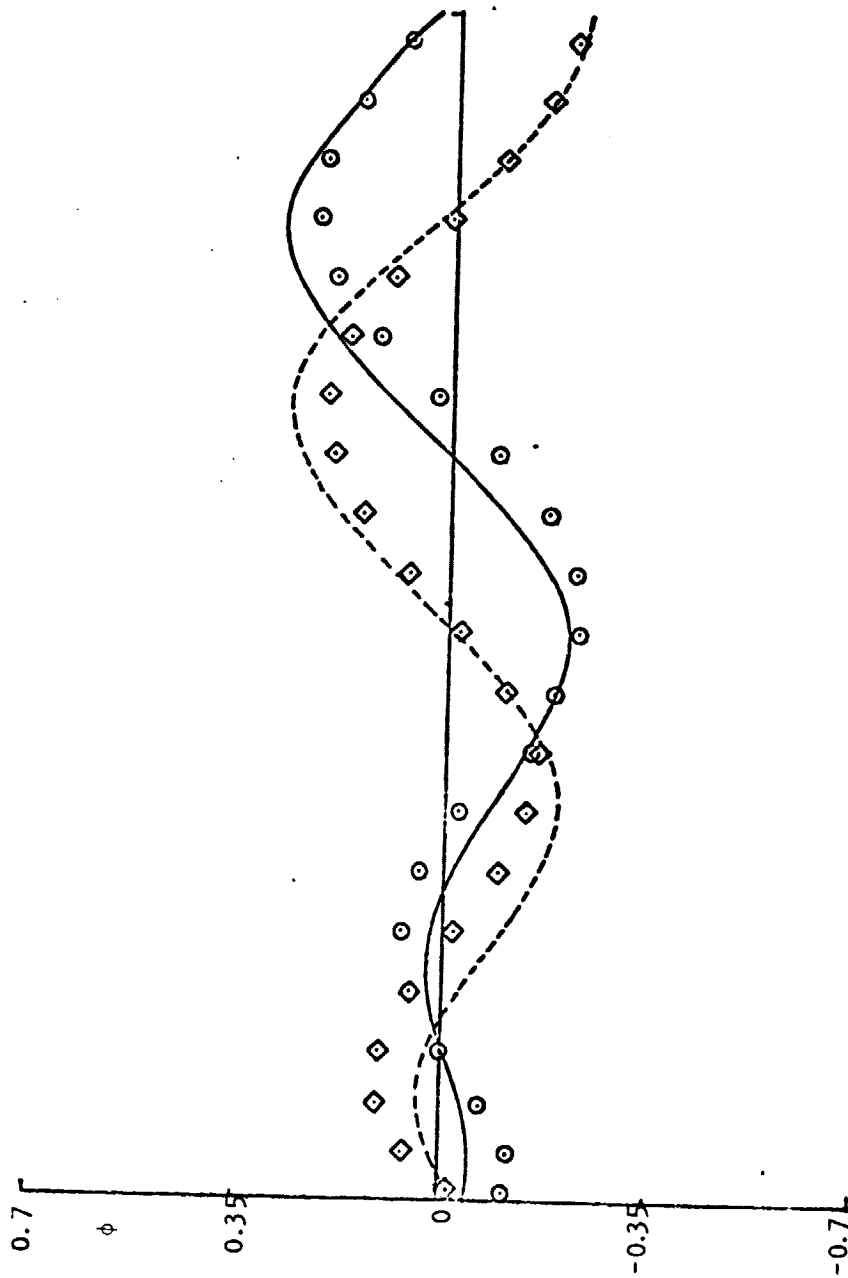


Figure 29. Acoustic Velocity Potential Distribution Along the Inlet Upper Wall ($\omega = 5.0$, No Flow, Hard Wall, Plane Wave Excitation; Symbols defined in Figure 27).

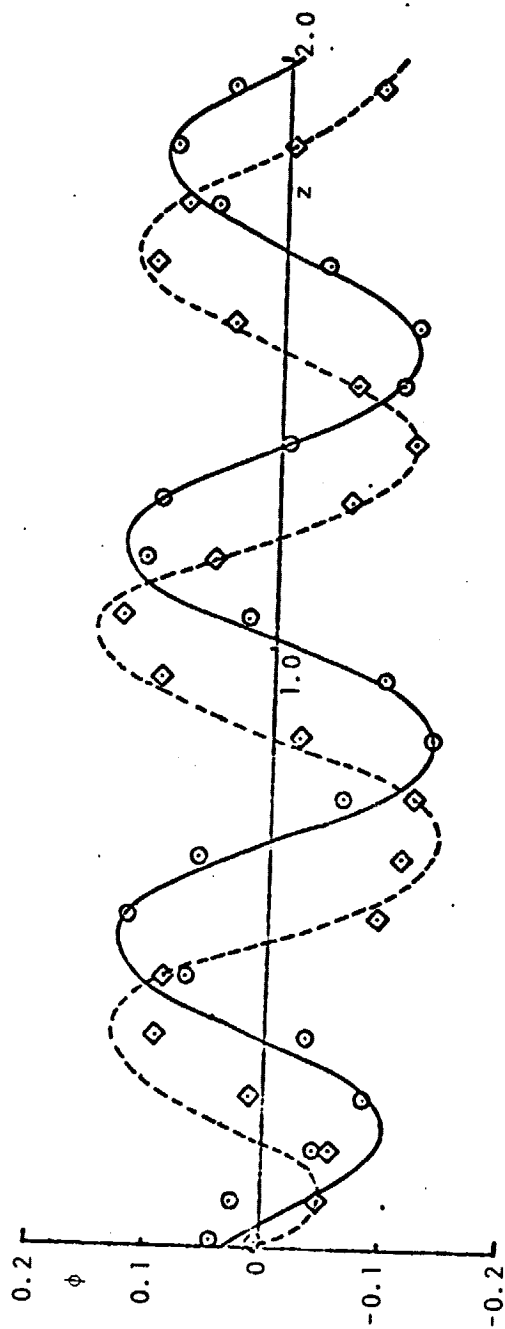


Figure 30. Acoustic Velocity Potential Distribution Along the Inlet Upper Wall
($\omega = 10.0$, No Flow, Hard Wall, Plane Wave Excitation; Symbols
defined in Figure 27).

Comparison studies have also been conducted for the case of plane wave propagation in the QCSEE inlet with lined walls. In the absence of mean flow the condition of particle displacement continuity and that of particle velocity continuity are identical. The specific acoustic impedance of the inlet upper wall is chosen to be $Z_e = 0.16 - i0.34$, a representative value chosen from Reference 2 for the case of plane wave propagation in a lined rectangular duct carrying no mean flow. The center body is still prescribed to be a hard wall. The sound excitation at the fan plane is again prescribed as a plane velocity wave of unit amplitude and a phase angle of 180° .

Table 1 shows the distribution of Z_e at the nodes located at the entrance plane of the soft walled QCSEE inlet as calculated by the integral approach for the plane wave propagation of angular frequencies $\omega = 1$ and 2. The acoustic velocity potential distribution along the lined upper wall of the inlet obtained by the FEM and the integral approach for angular frequencies $\omega = 1$ and 2 are shown in Figures 31 and 32, respectively. One observes that the agreement between the two methods for the lined wall case is also excellent. The $\text{dB}_{\text{reduction}}$ obtained for both the frequencies by the two methods agree to four significant places (for $\omega = 1$ $\text{dB}_{\text{reduction}}$ equals 24.8794 and for $\omega = 2$ $\text{dB}_{\text{reduction}}$ equals 13.3546). Figures 33 and 34 show the variation of the acoustic energy absorbed by the lined wall for $\omega = 1$ and 2 respectively. With this information the conservation of acoustic energy is checked by comparing the inflow and outflow of acoustic energy in the domain of interest. It has been found that the acoustic energy is conserved to within 3%

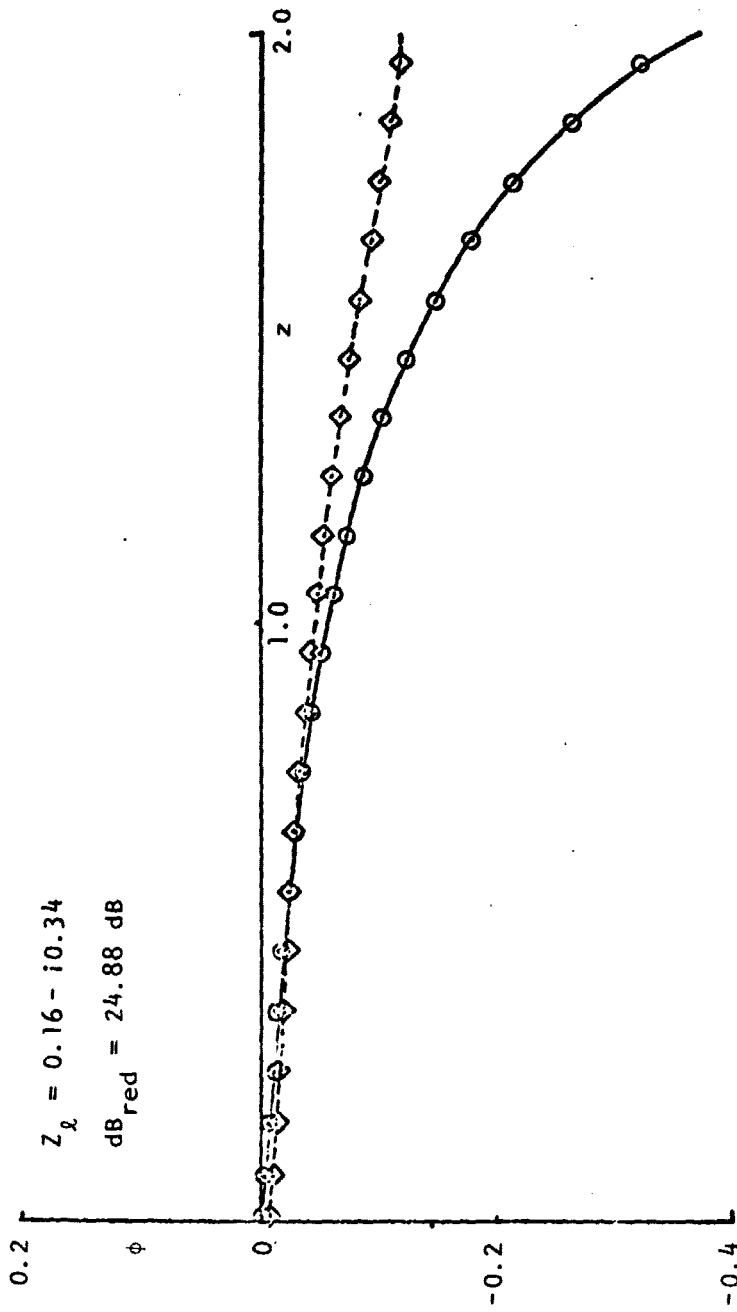


Figure 31. Acoustic Velocity Potential Distribution Along the Inlet Upper Wall ($\omega = 1.0$, No Flow, Soft Wall, Plane Wave Excitation, Symbols defined in Figure 27).

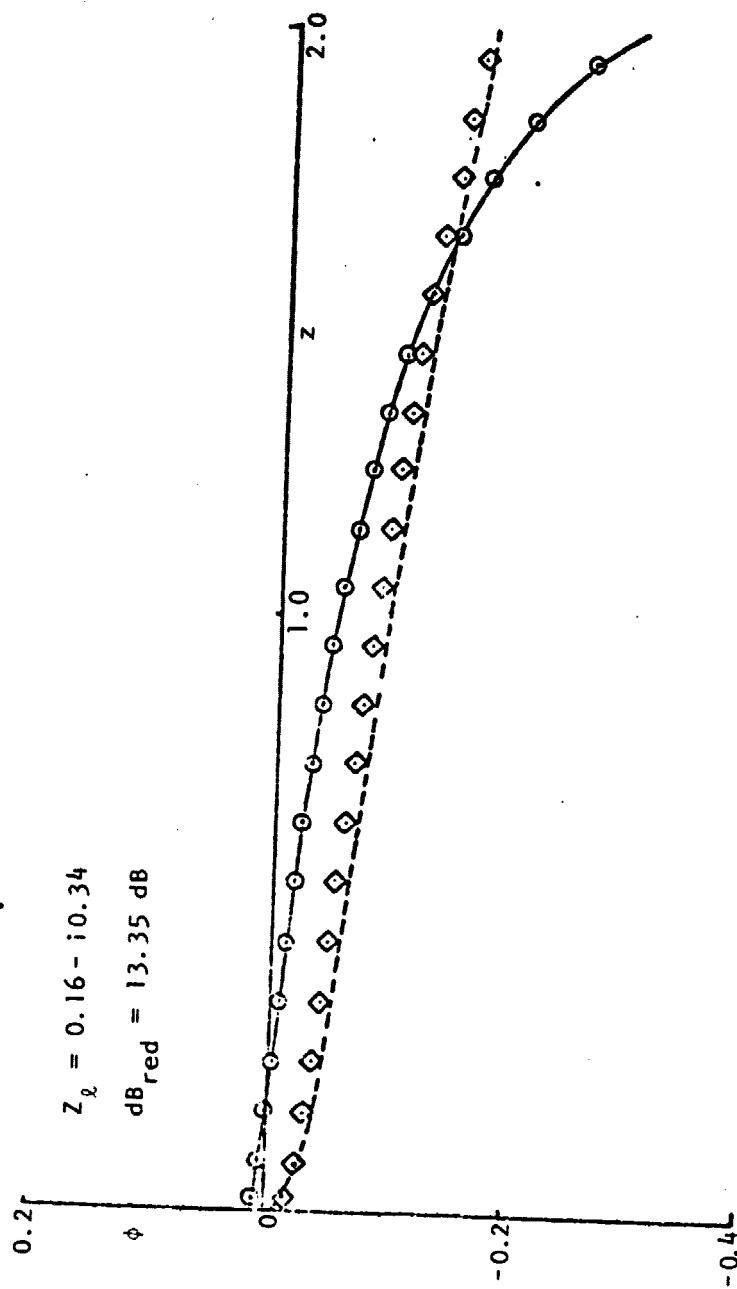


Figure 32. Acoustic Velocity Potential Distribution Along the Inlet Upper Wall ($\omega = 2.0$, No Flow, Soft Wall, Plane Wave Excitation; Symbols defined in Figure 27).

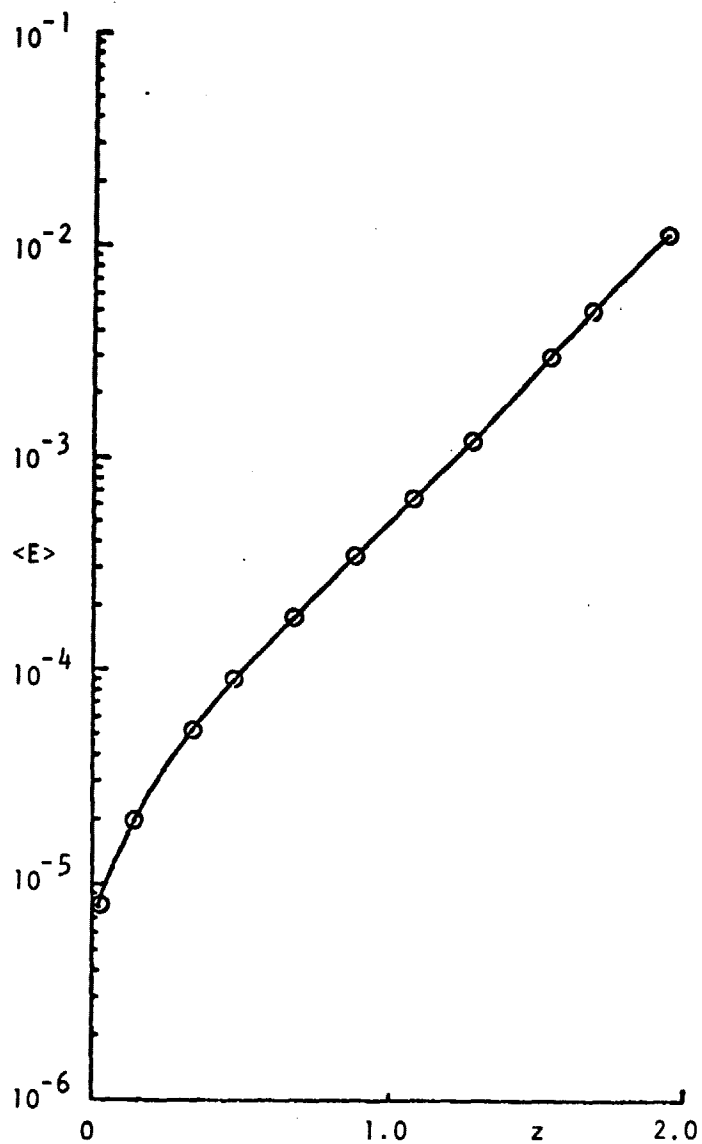


Figure 33. Acoustic Energy Absorbed by the Lined Inlet Upper Wall ($\omega = 1.0$, No Flow, Plane Wave Excitation).

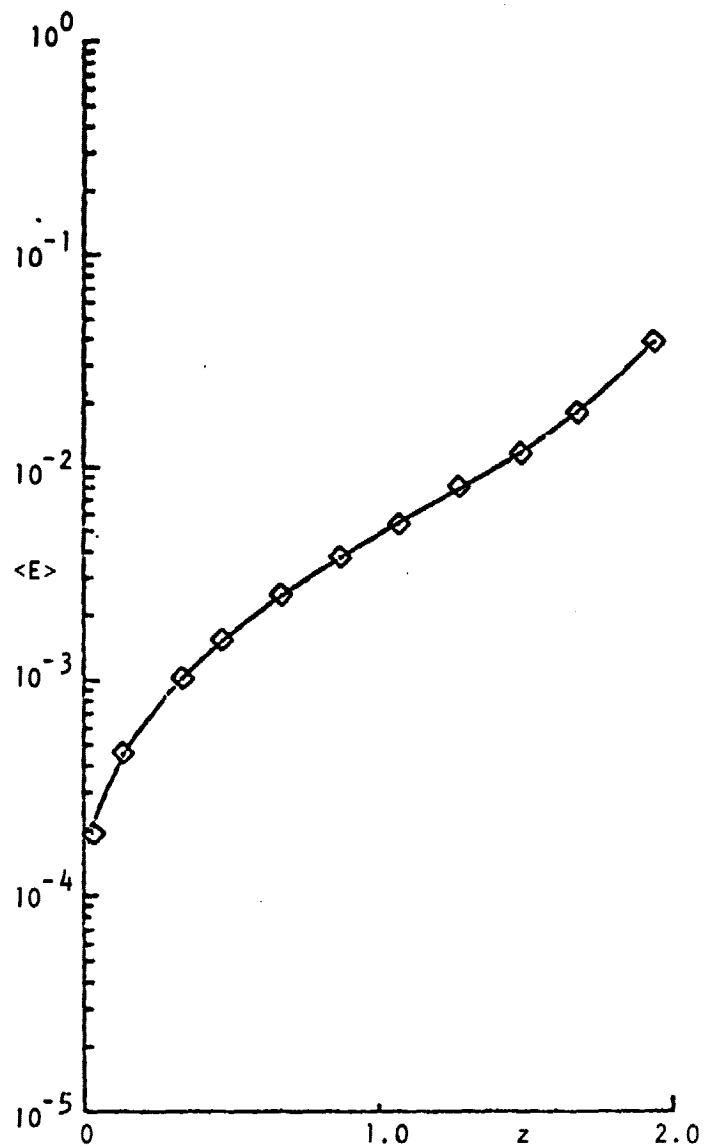


Figure 34. Acoustic Energy Absorbed by the Lined Inlet Upper Wall ($\omega = 2.0$, No Flow, Plane Wave Excitation).

Table 1. "Exact" Radiation Impedances from the Integral Technique
for the QCSEE Inlet With No Mean Flow

$Z_e = R_e + iX_e$ for the QCSEE Inlet						
Node Number	Hard Wall				Soft Wall	
	ω				ω	
	1.0	2.0	5.0	10.0	1.0	2.0
1	0.2629- i0.5333	0.4415- i0.4676	1.0942- i0.3231	0.8815- i0.1020	1.1780- i1.7072	i.7210- i2.2895
2	0.2427- i0.5084	0.7204- i0.5629	1.1589- i0.1141	0.9365- i0.0672	0.7214- i1.2168	1.5664+ i0.7554
3	0.2642- i0.6385	0.9994- i0.6583	1.2237+ i0.0949	0.9914- i0.0323	0.2648- i0.7265	1.4119- i0.7788
4	0.3100- i0.7535	1.2422- i0.6592	1.1573+ i0.0703	1.0679- i0.0600	0.2161- i0.6513	1.0600- i0.9674
5	0.3463- i0.8390	1.4175- i0.6405	1.1046- i0.0486	1.0698- i0.0788	0.1965- i0.6261	0.9196- i1.0234
6	0.3724- i0.8993	1.5344- i0.6195	1.0754- i0.1659	1.0287+ i0.0386	0.1869- i0.6173	0.8535- i1.0511
7	0.3880- i0.9348	1.6012- i0.6044	1.0625- i0.2440	1.1025+ i0.1934	0.1822- i0.6136	0.8222- i1.0655
8	0.3932- i0.9466	1.6231- i0.5991	1.0588- i0.2708	1.1572+ i0.2360	0.1808- i0.6126	0.8131- i1.0701

error for both the frequencies.

Since the prescription of the "exact" radiation impedance condition at the entrance plane of an inlet carrying a variable mean flow is not possible with the present day knowledge, the simple "no reflection" radiation impedance condition, $\bar{\rho} \bar{c}$, was used in most of the investigated cases. The $\bar{\rho} \bar{c}$ condition yields no reflection of the incident wave only if the propagation of plane waves is considered and if the reflections from the inlet walls are not significant.

In the absence of mean flow, if the inlet could be approximated as a tube of constant cross sectional area, the problem of plane wave propagation within such an inlet of finite length and in the far field can be solved by the classical Weiner Hopf integral technique²⁹ for frequencies below the cut off frequency corresponding to the lowest order spinning mode, namely the first radial mode. For the inlet modelled as a circular pipe the cut off frequency for the lowest order spinning mode is $\omega_c = 3.832$.²⁹ Hence, for frequencies greater than ω_c plane wave solutions by the Weiner Hopf technique do not exist. The integral solution obtained by the Weiner Hopf technique yields a constant (in general complex) impedance condition at the entrance plane of the inlet to be henceforth denoted as "Weiner Hopf radiation impedance condition," whose value for $\omega = 1.0$ and 2.0 equals $0.2335 - i0.5555$ and $0.8317 - i0.6528$ respectively. One could prescribe this radiation condition for the corresponding frequencies in place of $\bar{\rho} \bar{c}$ condition for the case of no mean flow.

Studies have been conducted to evaluate the influence of the "exact" radiation condition, $\bar{\rho} \bar{c}$ "no reflection" radiation condition and

the Wiener Hopf radiation impedance condition (where applicable) on the wave structure within the QCSEE inlet for the case of plane wave propagation of angular frequencies $\omega = 1, 2, 5$ and 10. Figures 35 and 36 show the influence of the above three radiation impedances on the acoustic velocity potential distribution along the hard upper wall of the inlet for $\omega = 1$ and 2 respectively. One observes in Figures 35 and 36 that the wave profile predicted by prescribing the Wiener Hopf radiation condition matches quite well with the one predicted by prescribing the "exact" radiation condition. Thus at low frequencies the Wiener Hopf radiation condition can be viewed as an "average" constant value of the exact radiation condition across the inlet entrance plane.

The wave structure obtained by imposing the "no reflection radiation condition is markedly different from the one corresponding to the "exact" radiation condition for $\omega = 1.0$ (see Figure 35). However for the case of $\omega = 2.0$, the profile corresponding to the "no reflection" radiation condition tends to approach the wave profile corresponding to the "exact" radiation condition (see Figure 36). Figure 37 shows that the wave profiles obtained by prescribing the $\bar{p} \bar{c}$ radiation condition and the "exact" radiation condition for a plane wave propagation of $\omega = 5$ match quite well along the length of the inlet. An almost exact match between the two profiles is observed for the case of $\omega = 10$ as shown in Figure 38. A physical explanation for this observation is as follows. The propagation of high frequency plane waves in a duct could be approximated as the wave propagation in a ray tube where the reflected component is negligible, in which case, the "no reflection"

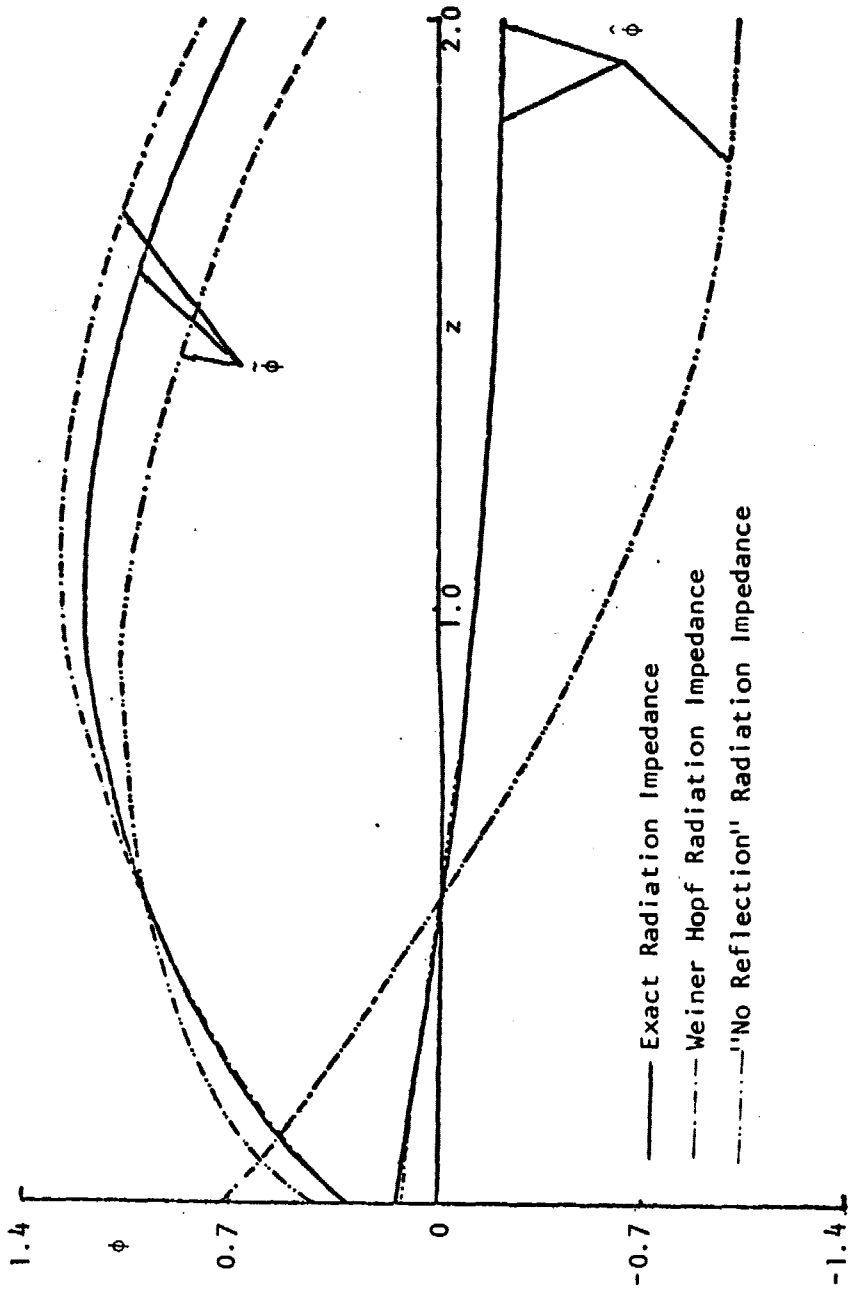


Figure 35. Influence of Different Radiation Impedances on the Acoustic Velocity Potential Distribution Along the Inlet Upper Wall ($\omega = 1.0$, No Flow, Hard Wall, Plane Wave Excitation).

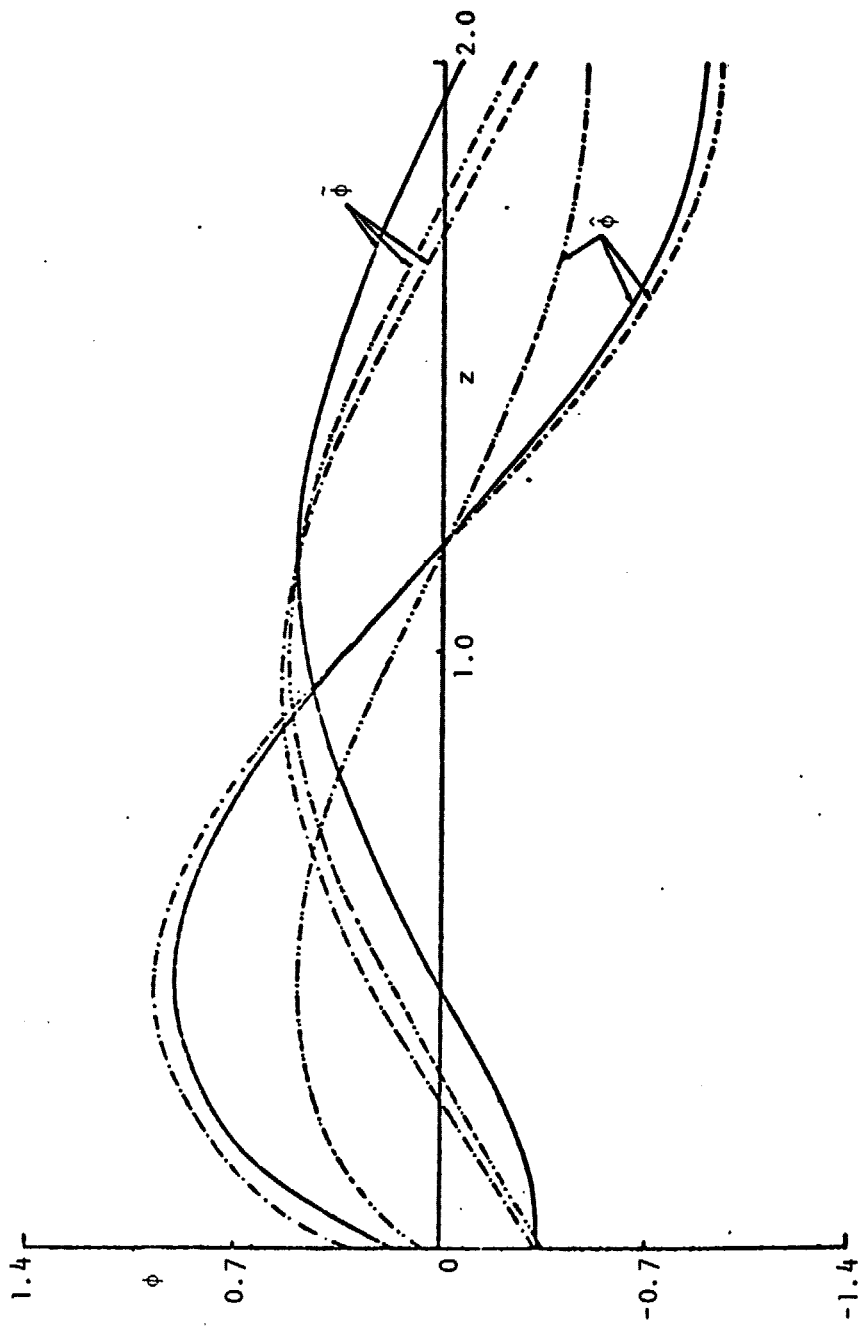


Figure 36. Influence of Different Radiation Impedances on the Acoustic Velocity Potential Distribution Along the Inlet Upper Wall ($\omega = 2.0$, No Flow, Hard Wall, Plane Wave Excitation; Symbols defined in Figure 35).

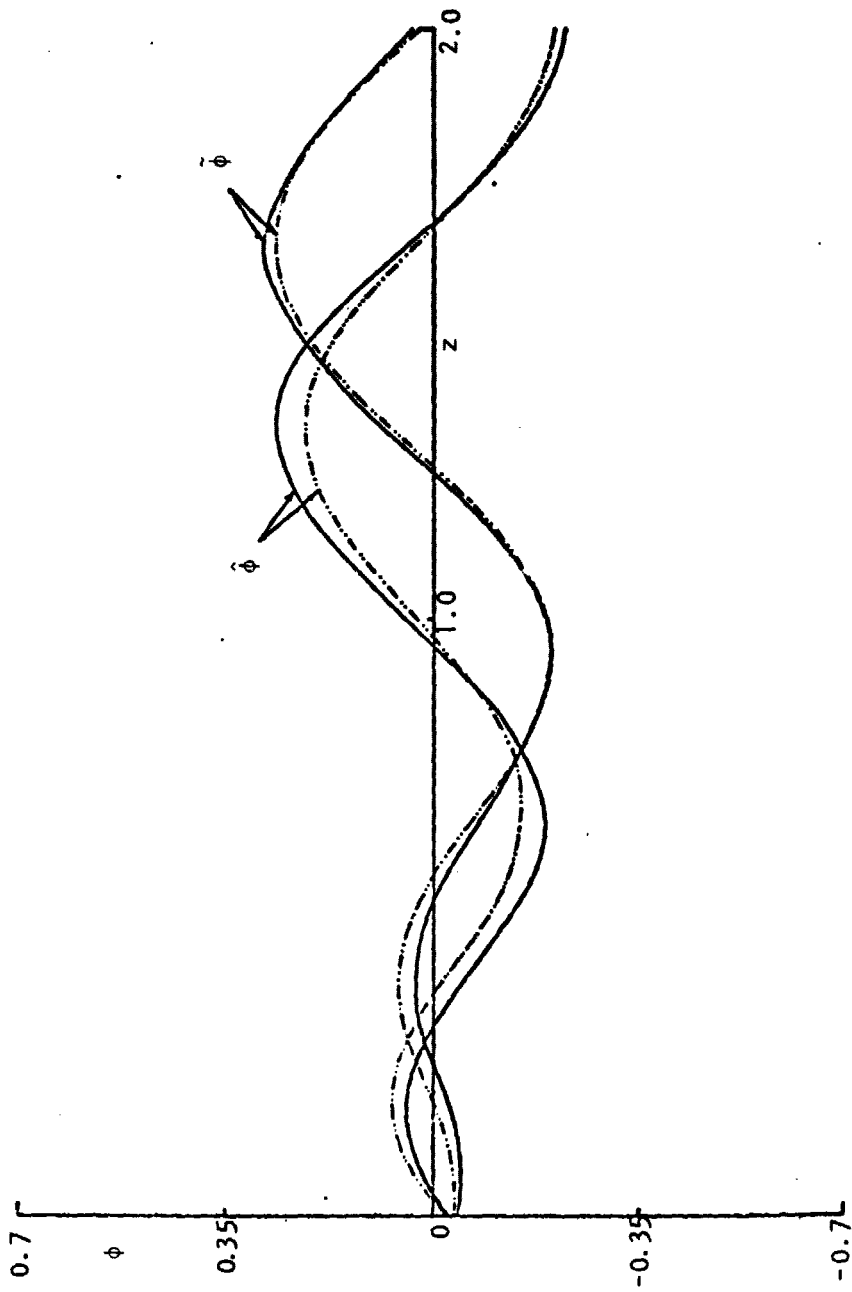


Figure 37. Influence of Different Radiation Impedances on the Acoustic Velocity Potential Distribution Along the Inlet Upper Wall ($\omega = 5.0$, No Flow, Hard Wall, Plane Wave Excitation; Symbols defined in Figure 35).

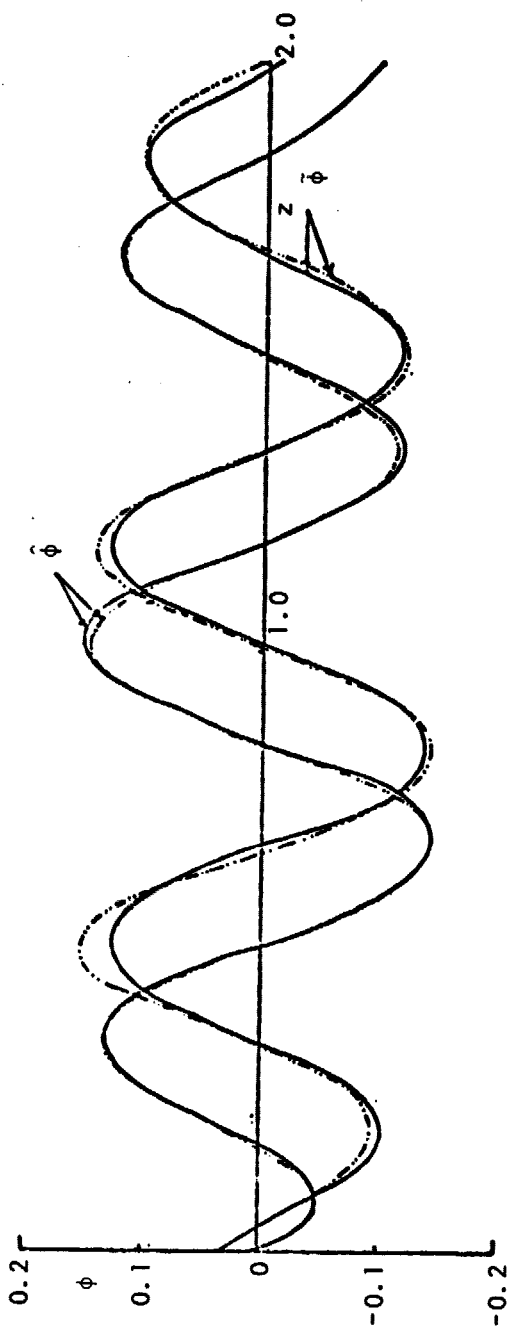


Figure 38. Influence of Different Radiator Impedances on the Acoustic Velocity Potential Distribution Along the Inlet Upper Wall ($\omega = 10.0$, No Flow, Hard Wall, Plane Wave Excitation; Symbols defined in Figure 35).

radiation condition indeed approaches the "exact" radiation condition. This fact is also evident from the values of the "exact" radiation impedances given in Table 1 for $\omega = 1, 2, 5$ and 10. As ω increases, one observes from this table that the "exact" radiation condition approaches the value of $1 + 0i$, which is the "no reflection" $\bar{\rho} \bar{c}$ radiation condition in terms of the nondimensional quantities.

4.5 "Compressible" Mean Flow Calculations for the QCSEE and Bellmouth Turbofan Inlets

To predict the acoustic properties of practical inlet configurations, the QCSEE (Quiet, Clean, Short-haul Experimental Engine) inlet⁹ and the Bellmouth inlet¹⁰ have been chosen for the present study (see Figures 1a and 1b).

Before proceeding with the inlet acoustic analysis the behavior of the inlet mean flow must be determined. As explained earlier, the steady flow in the inlets is approximated using a solution for an incompressible steady flow with a compressibility correction.

The incompressible solution was obtained by solving an integral formulation of Laplace's equation with the inlet boundary divided into a number of straight line segments. For the QCSEE inlet, the number of straight line segments equals 140 and it equals 90 only for the Bellmouth inlet, because of the simpler geometry of the Bellmouth inlet compared to the QCSEE inlet. The chosen free stream and fan plane velocities correspond to a free stream Mach number of 0.12 and an average exit Mach number of 0.52 for the QCSEE inlet⁹ and correspond to a free stream Mach number of 0.0 and an average exit Mach number of 0.52 for the

Bellmouth inlet. The resulting solutions of the Laplace's equation are superposed as described in Section 3.1.2 to yield the incompressible mean flow descriptions for both the inlets. Application of the compressibility correction to the incompressible mean flow velocities as described in Section 3.1.3 yields the "compressible" velocity description of the mean flow in the interior of the inlets.

The mean flow velocity computations needed for the acoustic equations have been performed at the nodal locations of the quadratic finite element triangulization schemes of the QCSEE and the Bellmouth inlets (see Figures 4a and 4b), Tables D.1 and D.2 in Appendix D contain the mean flow data at the corner nodal points along with the coordinates of the corner nodes. For the purpose of illustration, the compressible velocity profiles at the inlet entrance plane, the throat and the fan plane are shown in Figures 39 and 40 for the QCSEE and the Bellmouth inlets respectively. As one observes the radial profiles in Figures 39 and 40 the mean flow deviates far from the one dimensional model at the entrance plane. The axial velocity component, $\bar{\phi}_z$ becomes zero at the inlet wall as it is a stagnation point for the axial component of the velocity. The radial velocity component, $\bar{\phi}_r$ is zero at the axis of the inlet because of the axisymmetry of the problem and has a large negative value at the inlet wall, indicating the effect of the entry lip shape in sucking the flow. At the throat and the fan plane $\bar{\phi}_r$ is within 5% of $\bar{\phi}_z$ for the QCSEE inlet and within 12% for the Bellmouth inlet and $\bar{\phi}_z$ is also reasonably uniform over the inlet cross section indicating that the mean flow is almost one dimensional at the

throat and the fan planes. From Tables D.1 and D.2 one observes that the duct cross sectional area is minimum at the throat plane for the QCSEE inlet and at the fan plane for the Bellmouth inlet. Hence, on the basis of one dimensional isentropic gas dynamic relations for subsonic flows one would expect that the axial velocity is maximum at the throat plane for the QCSEE inlet and at the fan plane for the Bellmouth inlet. One indeed observes in Figures 39 and 40 and Tables D.1 and D.2 that $\bar{\phi}_z$ is on the average largest at the throat plane for the QCSEE inlet and at the fan plane for the Bellmouth inlet.

Though the mean velocity profiles at the throat and fan plane seem to indicate the presence of almost one dimensional flow at these two planes such is not the case at many other axial locations. As Tables D.1 and D.2 indicate there are very strong radial gradients in $\bar{\phi}_z$ and $\bar{\phi}_r$ in the vicinity of the inlet entrance plane and the nose of the center body which can not be accounted for by the one dimensional isentropic gas dynamic calculations.

4.6 Acoustic Calculations for the Hard Walled QCSEE Inlet

With the knowledge of the "compressible" mean flow velocities in the interior of the QCSEE inlet, one can perform the acoustic calculations for the QCSEE inlet configuration. In this section the results of the acoustic calculations for the QCSEE inlet shown in Figure 1a with hard walls will be presented for two frequencies. In order to investigate the effects of the two-dimensional nature of the mean flow on the acoustic behavior in the inlet, the mean flow was also computed using a one-dimensional, isentropic compressible flow model²³ to describe

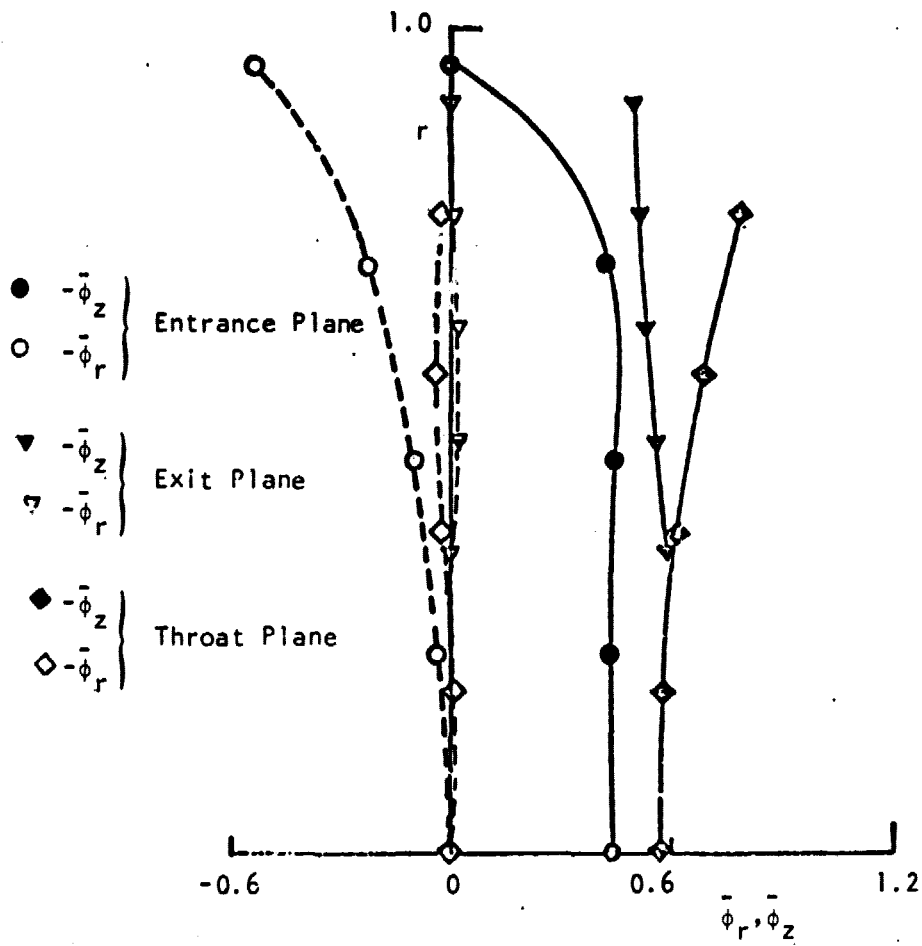


Figure 39. Radial Variation of "Compressible" Mean Flow Velocities at 3 Axial Locations for the QCSEE Inlet.

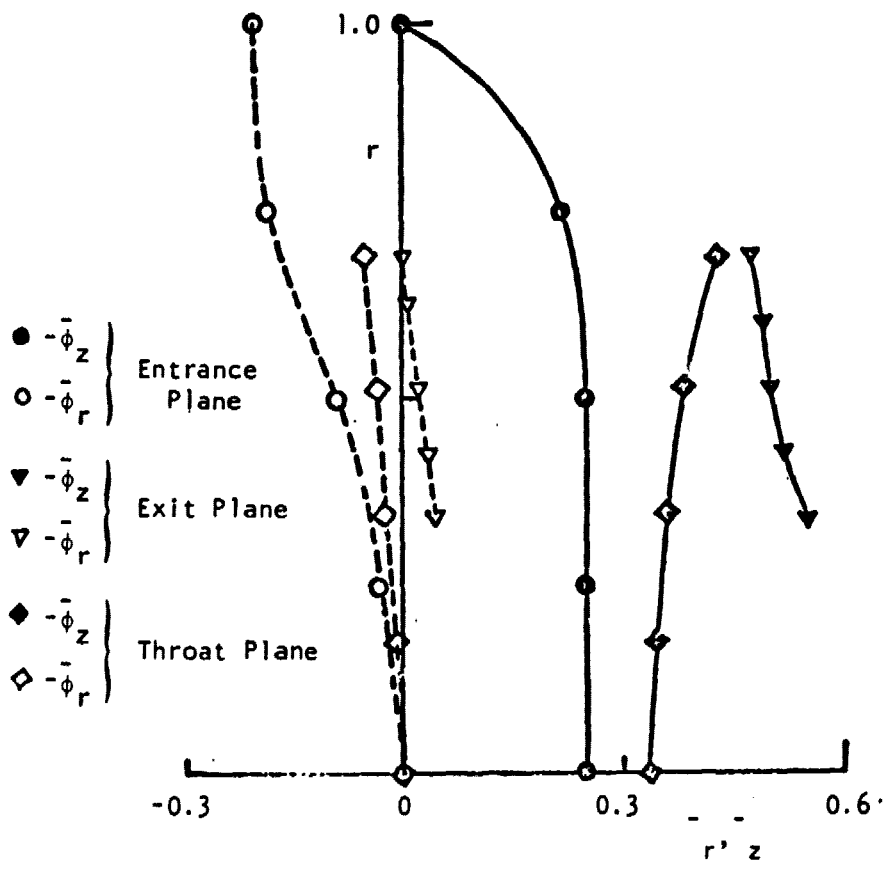


Figure 40. Radial Variation of "Compressible" Mean Flow Velocities at 3 Axial Locations for the Bellmouth Inlet.

the inlet mean flow. As in the two dimensional flow computations, a free stream Mach number of 0.12 and an exit Mach number of 0.52 have also been used in the one-dimensional flow computations. The solution domain, consisting of the inlet duct, has been subdivided into 360 3-node triangles with 212 nodes (see Figure 3). The real and imaginary parts of the acoustic potential were calculated at the nodes, and the real and imaginary parts of the acoustic axial and radial velocity components and the acoustic pressure were calculated at the centroids of the triangular elements using the linear interpolation functions for the acoustic potential (i.e., see Eq. (52)).

Calculations for plane velocity wave excitation at the inlet exit plane and the frequency ω equal 1 and 2 have been performed using the 1-D and 2-D steady flow calculations. Figure 41 shows the variation of the real and imaginary parts of the acoustic pressure along the upper inlet wall, for a frequency of 1.0. The radial variation of the acoustic pressure at the inlet entrance plane, inlet throat and inlet exit plane for $\omega = 1.0$ are shown in Figure 42, 43, and 44 respectively. Similar plots for a plane velocity wave excitation with $\omega = 2.0$ are shown in Figures 45, 46, 47, and 48.

To isolate the effect of cross sectional area variation alone on the wave propagation in the inlet, inlet acoustic calculations for the case of no mean flow have been performed for a plane velocity wave excitation at the inlet exit plane for two frequencies, $\omega = 1$ and 2. Figures 49 and 50 show the variation of the real and imaginary parts of acoustic pressure along the upper wall of the inlet for $\omega = 1$ and 2

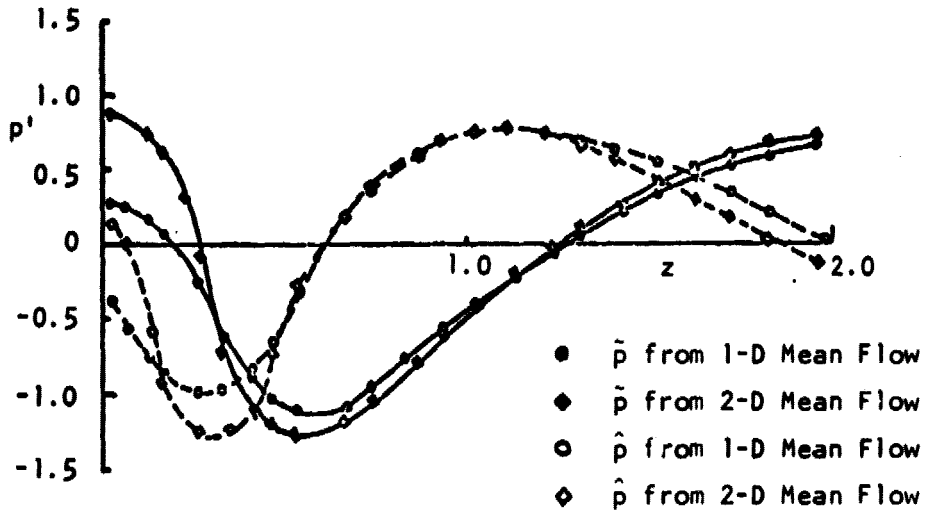


Figure 41. Acoustic Pressure Distribution Along the Inlet Upper Wall ($\omega = 1.0$; Plane Wave Excitation).

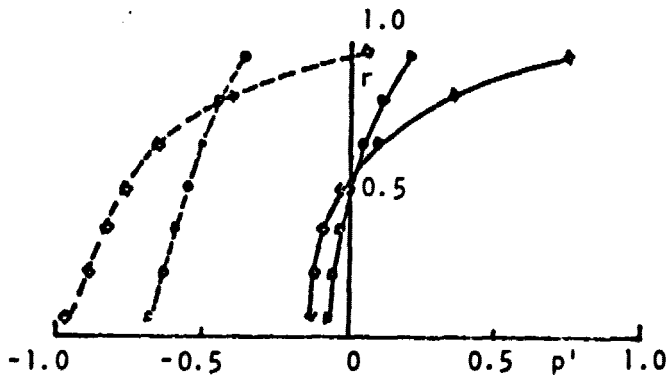


Figure 42. Radial Variation of Acoustic Pressure at the Entrance Plane for $\omega = 1.0$ (Symbols defined in Figure 41).

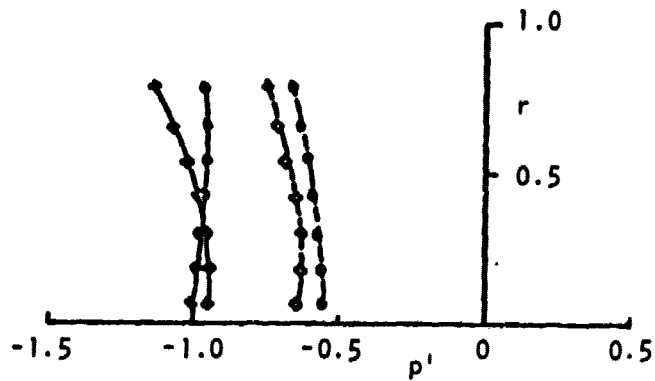


Figure 43. Radial Variation of Acoustic Pressure at the Throat Plane for $\omega = 1.0$ (Symbols defined in Figure 41).

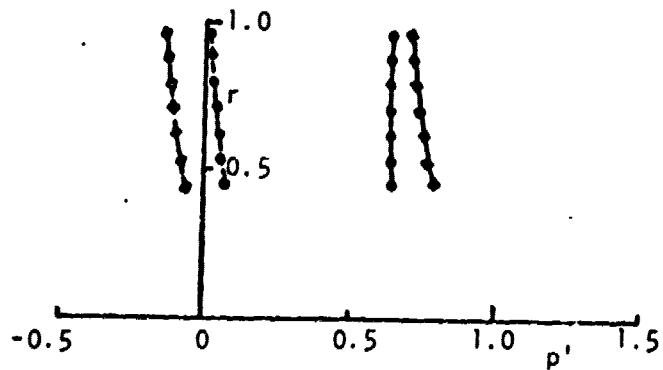


Figure 44. Radial Variation of Acoustic Pressure at the Inlet Exit Plane for $\omega = 1.0$ (Symbols defined in Figure 41).

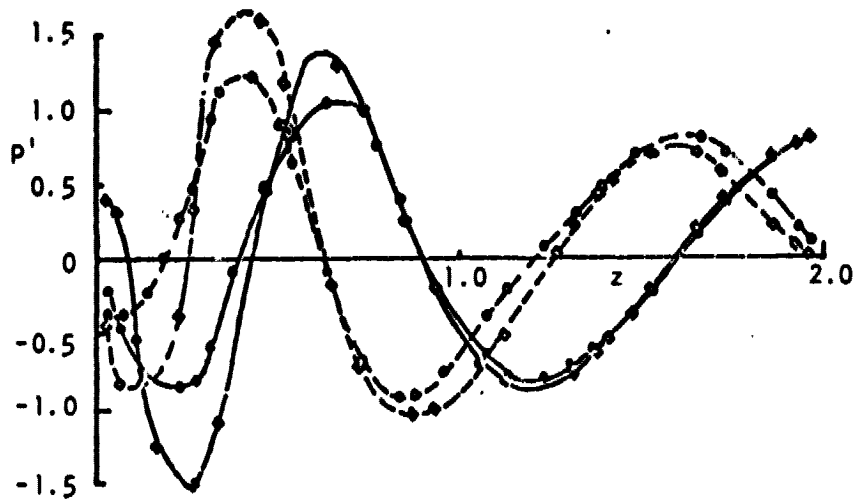


Figure 45. Acoustic Pressure Distribution Along the Inlet Upper Wall ($\omega = 2.0$, Plane Wave Excitation; Symbols defined in Figure 41).

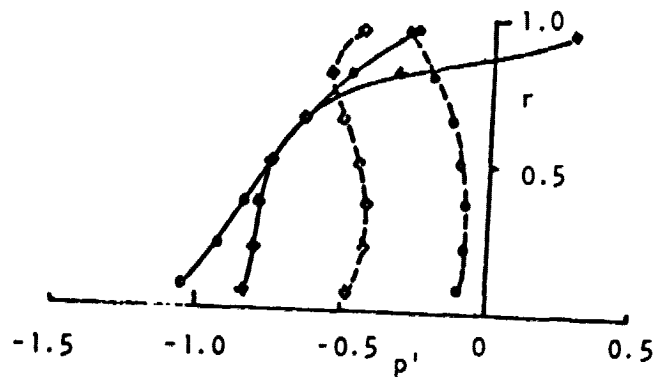


Figure 46. Radial Variation of Acoustic Pressure at the Entrance Plane for $\omega = 2.0$ (Symbols defined in Figure 41).

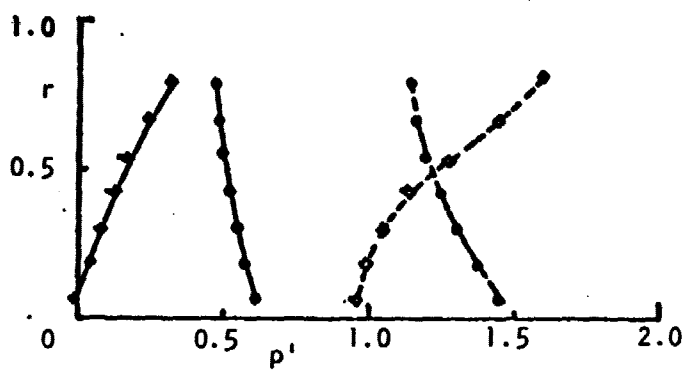


Figure 47. Radial Variation of Acoustic Pressure at the Throat Plane for $\omega = 2.0$ (Symbols defined in Figure 41).

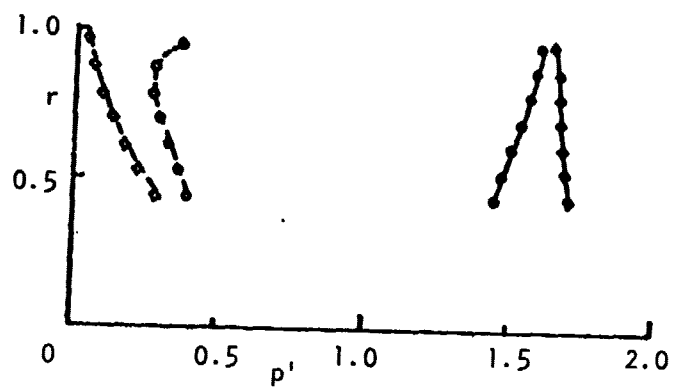


Figure 48. Radial Variation of Acoustic Pressure at the Exit Plane for $\omega = 2.0$ (Symbols defined in Figure 41).

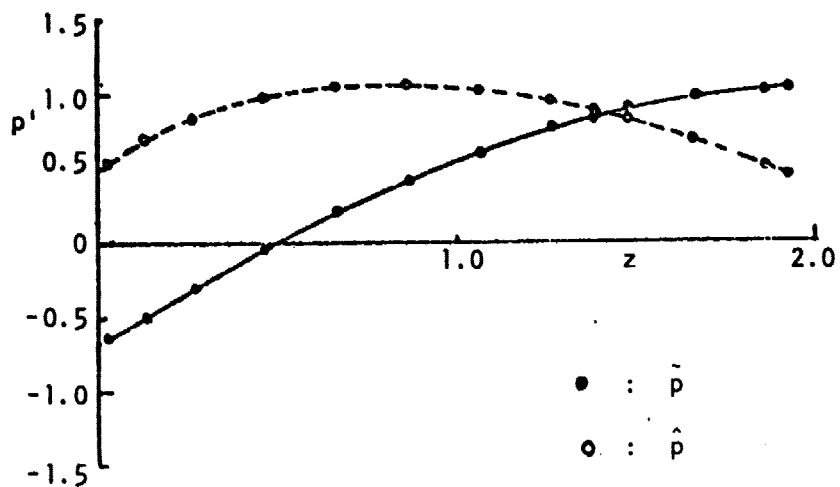


Figure 49. Acoustic Pressure Distribution Along the Upper Wall of the Inlet for the Zero Mean Flow Case ($\omega = 1.0$; Plane Wave Excitation).

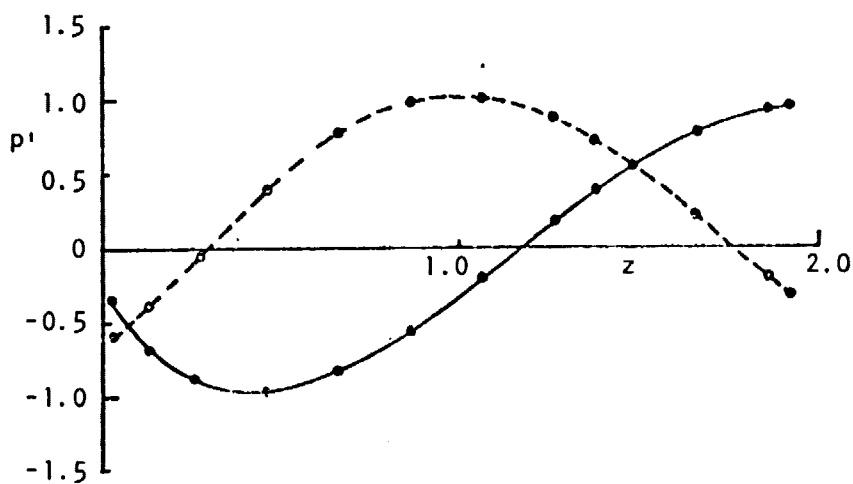


Figure 50. Acoustic Pressure Distribution Along the Upper Wall of the Inlet for the Zero Mean Flow Case (for $\omega = 2.0$; Plane Wave Excitation; Symbols defined in Figure 49).

respectively. Radial variation of the acoustic pressure for the zero mean flow case, at the inlet entrance, throat, and exit plane for $\omega = 1$ are shown in Figures 51, 52, and 53 respectively. Similar plots are shown in Figures 54, 55 and 56 for $\omega = 2$.

In the problem under consideration, the propagation of sound within the inlet will be affected by the following phenomena: (a) reflection from the inlet walls due to inlet cross sectional area variation; (b) reflection at the inlet entrance and exit planes; (c) reflection due to the presence of gradients in mean flow properties; (d) convection of sound by the mean flow which affects the local effective wavelength; and (e) refraction of sound due to the presence of transverse mean flow gradients. The presence of some of these effects will be considered below by analyzing the predicted inlet acoustic behavior.

When there is zero mean flow in the inlet, only reflection will be important. Furthermore, in this case the inlet entrance impedance $Z_e = 1$ is a good approximation for the almost no reflection condition at the entrance plane and thus only reflection from the walls should be present. Figures 51-56 show very little distortion in the plane wave shape, indicating that there is very little reflection from the inlet walls.

When the mean flow is described by a one dimensional approximation, only reflection and convection will be important. Figures 42-44 and 46-48 show very little distortion in the plane wave shape (for 1-D mean flow) except near the inlet entrance plane where there are steep area and mean axial velocity gradients, reaffirming the conclusion that

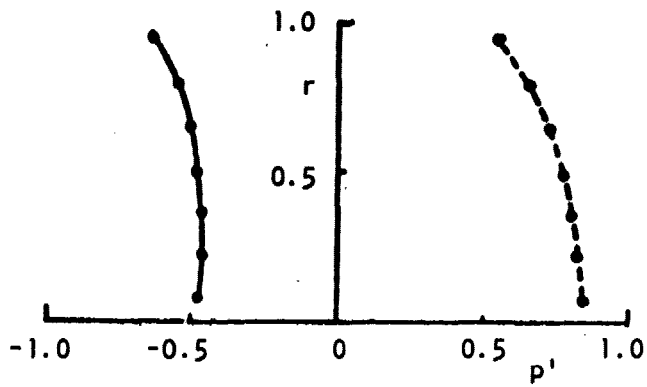


Figure 51. Radial Variation of Acoustic Pressure at the Entrance Plane for the Zero Mean Flow Case for $\omega = 1.0$ (Symbols defined in Figure 49).

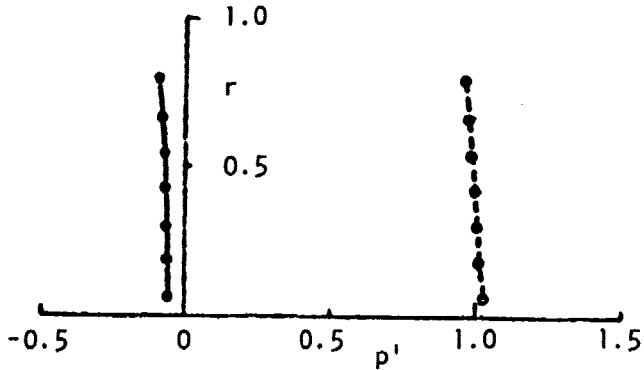


Figure 52. Radial Variation of Acoustic Pressure at the Throat Plane for the Zero Mean Flow Case for $\omega = 1.0$ (Symbols defined in Figure 49).

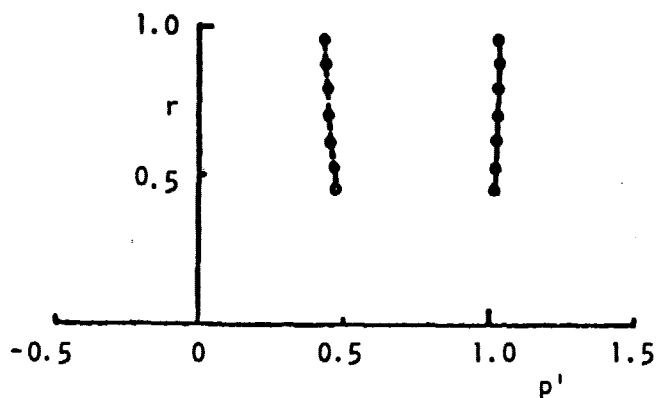


Figure 53. Radial Variation of Acoustic Pressure at the Inlet Exit Plane for the Zero Mean Flow Case for $\omega = 1.0$ (Symbols defined in Figure 49).

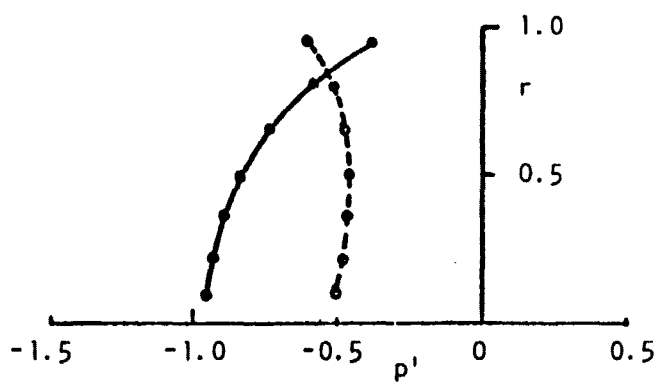


Figure 54. Radial Variation of Acoustic Pressure at the Entrance Plane for the Zero Mean Flow Case for $\omega = 2.0$ (Symbols defined in Figure 49).

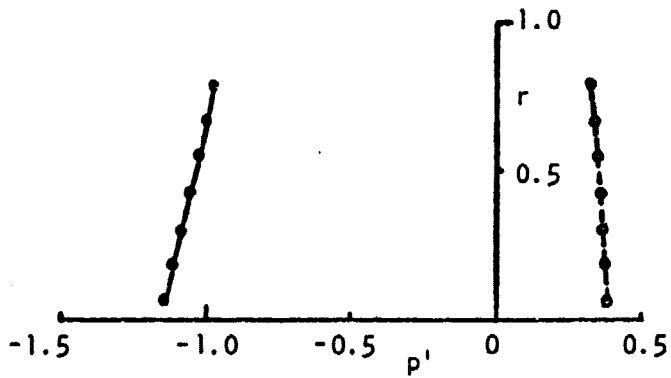


Figure 55. Radial Variation of Acoustic Pressure at the Throat Plane for the Zero Mean Flow Case for $\omega = 2.0$ (Symbols defined in Figure 49).

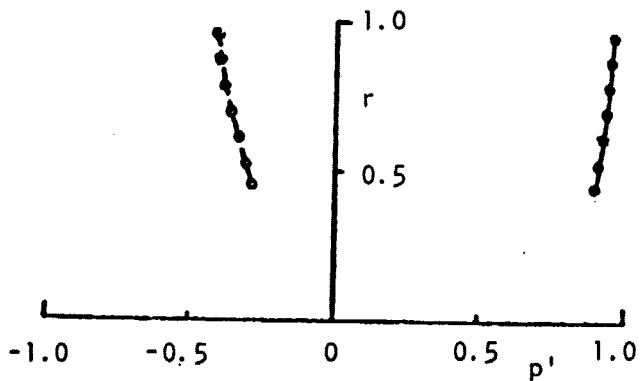


Figure 56. Radial Variation of Acoustic Pressure at the Inlet Exit Plane for the Zero Mean Flow Case for $\omega = 2.0$ (Symbols defined in Figure 49).

there is very little reflection from the inlet walls. Figures 41, 45, 49 and 50 show the convective effects of the flow as manifested by the overall decrease in effective wavelength for the case with mean flow (1-D or 2-D) as compared to the case of no mean flow. Figures 41 and 45 indicate a minimum effective wavelength near the throat where the highest mean flow Mach number exists.

When the mean flow is described by a two dimensional approximation all of the above mentioned effects are present. Furthermore, at the inlet entrance plane radial mean flow velocities are quite large and there are radial gradients in the axial component of the mean flow. Under these conditions the assumed impedance of $Z_e = 1$ will result in wave reflection at the inlet entrance plane. For the two dimensional mean flow description, Figures 42-44 and 46-48 show severe distortion in the initially plane wave shape due to reflection, convection, and refraction it is not possible to isolate the individual effects. It is known,^{1,30} however, that refraction increases with an increase in frequency. This effect is observed by comparing Figures 42-44 (for $\omega = 1$) and 46-48 (for $\omega = 2$) where the distortion of the plane front increases with an increase in frequency.

4.7 Sound Attenuation Studies for Zero Mean Flow Case for the QCSEE, Bellmouth and Cylindrical Inlets

The objective of this section is to estimate the sensitivity of duct attenuation to inlet curvature and centerbody for a practical turbofan inlet. The influence of flow gradients on the duct attenuation will be included in the next section which deals with the nonzero mean

flow case. To accomplish this task, a number of acoustic calculations on a soft walled QCSEE turbofan inlet, a bellmouth inlet and a straight open cylinder of the same overall dimensions (i.e. length and fan diameter), are performed. The specific acoustic liner impedance values chosen are the same for each inlet at a particular frequency and they correspond to the near optimum impedance values for a plane pressure wave input into an infinitely long circular duct. Rice¹⁷ presents these values for a wide range of frequencies and liner length to duct diameter ratios. In the finite element calculations for the zero mean flow case a constant acoustic axial velocity (ϕ_z) is used as the input condition and hence these impedances do not necessarily represent the optimum values in the finite element calculations. The radiation impedance condition is prescribed to be equal to $\bar{\rho} \bar{c}$.

Figure 57 shows the dependence of duct: attenuation, $\text{dB}_{\text{reduction}}$ on the frequency of wave propagation, $\eta (= -\frac{\omega}{2\pi})$ for the QCSEE, Bellmouth and cylindrical inlets for the case of the full length of the upper wall of the inlets being lined. Also shown in the figure are the near optimum specific acoustic liner impedances, Z_e for the four frequencies listed. One observes that $\text{dB}_{\text{reduction}}$ falls rapidly as frequency increases for all the three inlets which is due to focusing of the sound wave toward the inlet axis at higher frequencies. The propagation of high frequency plane waves in a duct could be approximated as the propagation in a ray tube with its axis coinciding with the inlet axis. As the frequency increases the sound power is concentrated near the duct axis and it reduces at the wall where it must be absorbed and hence the rapid drop in the duct attenuation. One also observes that there is a considerable

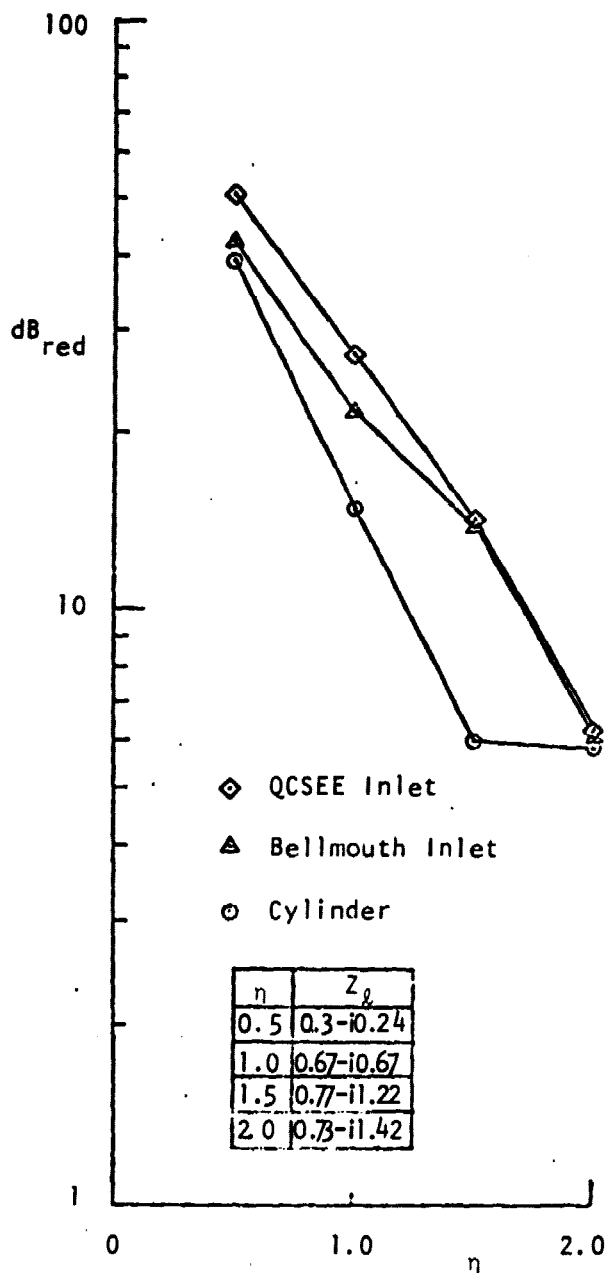


Figure 57. Dependence of dB_{red} on Frequency for the QCSEE, Bellmouth and Cylindrical Inlets for the Zero Mean Flow Case.

variation in the duct attenuation for the three inlets which can be attributed to the differences in their geometries. At lower frequencies the attenuations differ much more compared to at high frequency and fall within 0.5 dB for $n = 2$. In other words attenuation of low frequency waves is more sensitive to inlet geometry than to high frequency waves. As explained earlier the sound energy is beamed towards the duct axis as frequency increases leaving little sound energy to be absorbed at the walls. Hence the propagation of high frequency sound waves is insensitive to the area variations of the duct resulting in about the same attenuation for all the three inlets. The duct attenuation for the Bellmouth inlet falls in between the duct attenuation for the QCSEE and the cylindrical inlets since the Bellmouth inlet is geometrically "median" between the QCSEE inlet and the cylinder.

4.8 Sound Attenuation Studies for Nonzero Mean Flow Case for the QCSEE, Bellmouth and Cylindrical Inlets

The influence of mean flow gradients on duct attenuation is studied in this section using the "compressible" mean flow velocities computed in Section 4.5 (also see Appendix D). The average fan plane Mach number for both the QCSEE and the Bellmouth inlets is 0.52.

As proposed by Rice,³¹ the near optimum liner impedance values for the cylinder containing a uniform steady flow are calculated by dividing the zero mean flow near optimum values by $(1 - M)^2$ where M is the Mach number of the uniform steady flow in the cylinder. For the purpose of comparison of the acoustic performance of the inlets containing a mean flow, representative Mach numbers have to be chosen for the

cylinder to "represent" in some overall sense the two dimensional mean flow in the QCSEE and Bellmouth inlets. For this purpose, one dimensional isentropic gas dynamic calculations are performed for the QCSEE and Bellmouth inlets and the axial station chosen to "represent" the cylinder is at $Z = 0.9$ for both the QCSEE and Bellmouth inlets since they "resemble" the cylindrical duct at and in the neighborhood of this station. The one dimensional isentropic Mach number at $Z = 0.9$ for the QCSEE inlet equals 0.579 and for the Bellmouth inlet equals 0.362. The liner impedance values used in comparing the cylindrical duct and the QCSEE inlet are obtained by dividing the impedance values listed in Figure 57 by $(1 - M)^2$ where M equals 0.579. Similarly the liner impedance values used in comparing the cylindrical duct and the Bellmouth inlet are obtained by dividing the impedance values listed in Figure 57 by $(1 - M)^2$ where M equals 0.362. In the finite element calculations a constant acoustic pressure (p) is used as the input condition and the radiation condition is again prescribed to be equal to $\bar{\rho} \bar{c}$ for the nonzero mean flow case.

Figure 58 shows the acoustic performance of the QCSEE inlet and the cylindrical duct containing mean flow. As in the no mean flow case one again observes the rapid fall of attenuation as frequency increases. And also the attenuations differ considerably for the two inlets at lower frequencies but they lie within 1 dB for $\eta = 2.0$. The differences in the duct attenuations are due to a combined effect of inlet curvature, centerbody and mean flow properties. The duct attenuation for the zero mean flow case is higher compared to the corresponding non zero mean flow

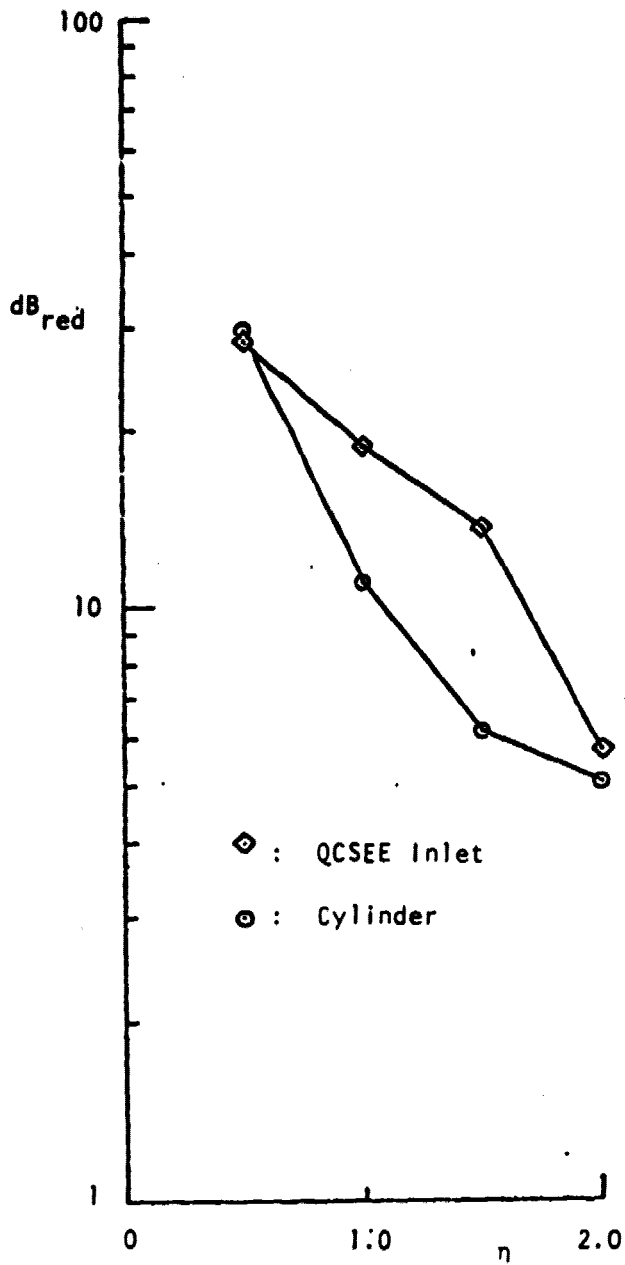


Figure 58. Dependence of dB_{red} on Frequency for the QCSEE and Cylindrical Inlets for Nonzero Mean Flow Case.

case for $\eta = 0.5$ and 1.0 for both the QCSEE inlet and cylinder. For $\eta = 0.5$ $\text{dB}_{\text{reduction}}$ for the QCSEE inlet with mean flow is about 22 dB lower than that for the no mean flow case. Also, for $\eta = 0.5$ $\text{dB}_{\text{reduction}}$ for the cylinder with mean flow is about 10 dB lower than that for the no mean flow case. However, $\text{dB}_{\text{reduction}}$ for the nonzero mean flow case for $\eta = 2.0$ falls within 1 dB of the zero mean flow case for both the QCSEE inlet and cylinder. These observations indicate that though the approximate method proposed by Rice to obtain the near optimum impedance values for the flow case is quite reasonable for high frequency waves, it leads to a rapid drift in the optimum values of the impedances for low frequency waves resulting in a considerable reduction of duct attenuation. Similar observations are noted in Figure 59 which shows the acoustic performance of the Bellmouth inlet and the cylinder containing mean flow. Since the QCSEE and Bellmouth inlets are studied for different values of the liner impedance for the mean flow case one can not compare their acoustic performance.

At the present time, the frequency range and transverse mode is limited by the maximum number of elements which the computer can handle. In the above cases, seven elements were used to resolve the transverse modes and fourteen elements were used to resolve axial variations. For a given finite element triangulization scheme, an estimate of the accuracy of the numerical solution for various frequencies may be made by comparing it with the known analytical solution for the case of a hard walled annular cylinder carrying a uniform steady flow. Even though there is no one to one correspondence between the accuracies of the

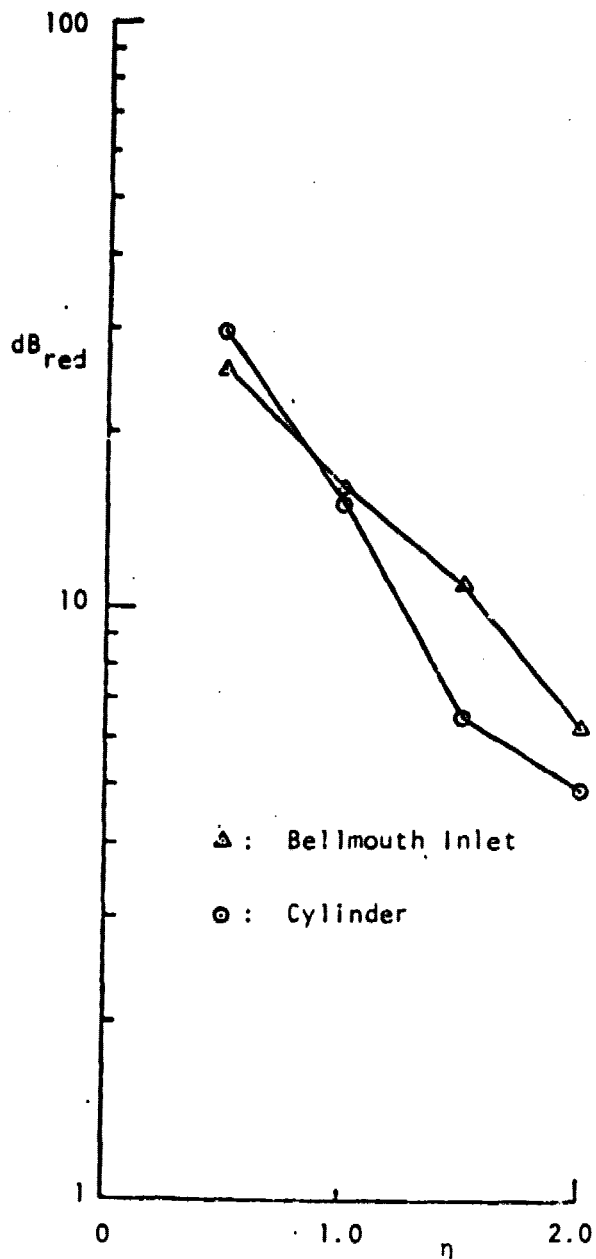


Figure 59. Dependence of dB_{red} on Frequency for the Bellmouth and Cylindrical Inlets for Nonzero Mean Flow Case.

solution obtained for a variable area inlet and an annular cylinder the above mentioned criterion, in the absense of anything better, is probably an acceptable criterion.

CHAPTER V

CONCLUSIONS AND RECOMMENDATIONS

5.1 Conclusions

An analytical technique utilizing the Finite Element Method (FEM) in combination with the Method of Weighted Residuals has been developed for predicting the acoustic performance of turbofan inlets carrying a subsonic axisymmetric steady flow. An approximate solution for the steady inviscid flow field is obtained using an integral method for calculating the incompressible potential flow field in the inlet with a correction to account for compressibility effects. Acoustic properties of the QCSEE inlet, a Bellmouth inlet and a circular cylinder for zero mean flow and non-zero mean flow situations have been determined for a limited range of frequencies ($3.14 \leq \omega \leq 12.57$) of plane wave propagation. Summarizing the results of this investigation it can be concluded that:

1. The finite element technique solutions are in excellent agreement with available analytical solutions for the problems of plane and spinning wave propagation through a hard walled annular cylinder with a constant mean flow.

2. For an equal number of finite elements, quadrant representation of the finite elements is superior to linear representation in handling high frequency ($\omega \approx 15$) plane wave propagation.

3. The duct attenuation and the acoustic pressure distributions obtained by the finite element scheme and the finite difference results of Baumeister for the case of a lined rectangular duct carrying a steady uniform flow are found to be generally in good agreement.

4. The results obtained by the finite element program using the "exact" impedance at the open end of the duct provided by the integral solution approach of Bell, Meyer and Zinn are found to be in excellent agreement with the results of the integral solution approach for plane wave propagation in hard and soft walled QCSEE inlet carrying no mean flow for a range of frequencies. The simple "no reflection" impedance condition at the open end of the inlet though inaccurate for low frequencies ($\omega \leq 2$) of plane wave propagation, approaches the "exact" impedance condition for high frequencies ($\omega = 10$).

5. Results for low frequency ($\omega \leq 2$) plane wave propagation through the hard walled QCSEE inlet containing a mean flow show that when one-dimensional steady flow is assumed to exist in the inlet, the plane wave propagates with relatively little distortion. However, propagation of a plane wave through the fully two-dimensional flow field in the inlet produces severe distortions due to the excitation of higher order modes.

6. Plane wave calculations for soft walled QCSEE inlet, a circular cylinder and a Bellmouth inlet for the near optimum liner impedance values of an infinitely long circular duct with no mean flow, indicate that the duct attenuation falls rapidly with increase in frequency for the cases of zero mean flow and fully two-dimensional

axisymmetric mean flow due to focusing of the sound wave toward the duct axis for high frequencies. Attenuation of low frequency plane waves is found to be more sensitive to inlet curvature, center body and mean flow gradients as compared to that of high frequency plane waves. The approximate method proposed by Rice to obtain the near optimum liner impedance values for the flow case from the zero mean flow case is found to be reasonable for high frequency plane waves but leads to a rapid drift in the optimum values for the low frequency plane waves resulting in a considerable reduction of duct attenuation.

5.2 Recommendations for Future Research

Several improvements over the developed theoretical analysis which could be made to broaden its range of applicability are discussed below.

1. Prediction of the Far Field Noise Levels

The present analysis predicts the ratio of the input acoustic power at the fan plane to the output acoustic power at the inlet entrance plane and thereby concludes about the effectiveness of the liner to absorb sound. However, in practice, the effectiveness of the liner is estimated by measuring the sound pressure levels in the far field.

The far field predictions could be made using the finite element technique by extending the triangulization scheme from inside the inlet to the "far field" through the inlet entrance plane. The elements external to the inlet could be made larger as one moves away from the inlet since the variation of the acoustic variables in the open space is not expected to be as large as it is inside the inlet. In this

scheme the radiation condition should be prescribed at the peripheral elements in the open space. The prescription of the simple $\bar{p} \bar{c}$ radiation condition out in the "far field" is expected to be quite good since any wave front approaches a plane wavefront locally as one moves sufficiently far away from the source. The extent of the finite element spread out in the open space to simulate the far field will be governed by the computational capabilities and mass storage space of the available computer system.

II. Effect of the Molecular Transport Properties on the Acoustic Behavior of the Inlet

In the present theoretical model the effect of viscosity and thermal conductivity of the fluid on both the mean flow field and the acoustic field have been neglected. These assumptions and the assumption of irrotational flow simplified the boundary value problem to the solution of a single complex partial differential equation with variable coefficients for the acoustic velocity potential subject to a set of complex mixed type boundary conditions. When employing the finite element technique the use of the velocity potential offers many advantages over the conventional linearized gas equations approach.³² For two dimensional mean flows the velocity potential approach reduces the computer storage and running times by an order of magnitude compared to the more general linearized gas equations approach.

The acoustic equations for sheared viscous flows were developed by Mungur et al.³³ Since the gradients in the wave motion are "small" the molecular transport of momentum and energy due to viscosity and thermal conductivity of the fluid respectively are neglected by common

practice in deriving the linearized acoustic equations, and the inviscid acoustic equations are solved using the mean flow velocity field that results from a consideration of viscosity in the mean flow field only.

Because of the significant computational advantage of the acoustic potential formulation, one is strongly motivated to extend the acoustic potential finite element program to include the case of sheared mean flows. Goldstein and Rice³⁴ suggest a very practical procedure for calculating the effect of the boundary layer in conjunction with the potential function analysis. Goldstein and Rice point out that in many cases a linear shear layer can be used to accurately model a $1/7^{\text{th}}$ power law turbulent boundary layer. For the special case of a linear shear boundary layer, they show that the following correction procedure can be applied.

The specific acoustic liner impedance, Z_{ℓ} at the inlet wall is a known parameter. For a given boundary layer thickness δ and a mean flow Mach number at the edge of the boundary layer, a specific acoustic impedance at the edge of the boundary layer, $(Z_{\ell})_{\text{effective}}$ can be calculated which is independent of the potential core flow. This effective impedance could be used as the boundary condition for the potential flow finite element calculations. The procedure is approximate because the correction procedure³⁴ assumes a uniform boundary layer in the absence of mean flow variations. Nevertheless the procedure represents a simple and effective way of accounting for shear with a potential approach for the duct acoustics problem.

III. Optimization Studies for the Liner Design

The present technique predicts the $\text{dB}_{\text{reduction}}$ for a lined duct containing a two dimensional axisymmetric mean flow for a prescribed configuration of the sound absorbing liner. The liner performance which could be measured as the $\text{dB}_{\text{reduction}}$ per unit length of the liner is a function of its specific acoustic impedance, frequency of wave propagation, mean flow characteristics and the geometry of the duct. The technology needed for a practical liner design has to predict the optimum liner configuration for a desired $\text{dB}_{\text{reduction}}$. Such a design information could be prepared by conducting optimization studies for liners over a realistic range of the independent variables. Such a study will provide the needed technology data base for the liner design.

A P P E N D I C E S

PRECEDING PAGE BLANK NOT FILLED

APPENDIX A

PROOF OF EQUATION (60)

To prove

$$I = \iint_{\Delta(e)} (L_i^e)^a (L_j^e)^b (L_k^e)^c drdz = \frac{a!b!c!}{(a+b+c+2)!} \times 2\Delta \quad (60)$$

Consider the linear transformation

$$(r, z) \rightarrow (L_i^e, L_j^e) \quad (A-1)$$

The elemental area $drdz$ is related to dL_i, dL_j through

$$drdz = J \begin{vmatrix} r & z \\ L_i^e & L_j^e \end{vmatrix} dL_i^e dL_j^e \quad (A-2)$$

where the Jacobian $J \begin{vmatrix} r & z \\ L_i^e & L_j^e \end{vmatrix}$

$$J \begin{vmatrix} r & z \\ L_i^e & L_j^e \end{vmatrix} = \begin{vmatrix} \frac{\partial r}{\partial L_i^e} & \frac{\partial r}{\partial L_j^e} \\ \frac{\partial z}{\partial L_i^e} & \frac{\partial z}{\partial L_j^e} \end{vmatrix} \quad (A-3)$$

Substituting Eqs. (51) in (A-3) one obtains

$$\begin{aligned} J \begin{vmatrix} r & z \\ L_i^e & L_j^e \end{vmatrix} &= (z_i - z_k)(r_j - r_k) - (r_i - r_k)(z_j - z_k) \\ &= 2x (\text{Area of triangle } ijk) = 2\Delta \end{aligned} \quad (A-4)$$

Hence, Eq. (60) becomes

$$I = \int_{L_i^{(e)}=0}^1 \int_{L_j^{(e)}=0}^{1-L_i^{(e)}} (L_i^{(e)})^a (L_j^{(e)})^b (1-L_i^{(e)}-L_j^{(e)})^c 2\Delta x dL_i^{(e)} dL_j^{(e)} \quad (A-5)$$

That is,

$$I = 2\Delta x \int_{L_i^{(e)}=0}^1 (L_i^{(e)})^a dL_i^{(e)} \int_{L_j^{(e)}=0}^{1-L_i^{(e)}} (L_j^{(e)})^b (1-L_i^{(e)}-L_j^{(e)})^c dL_j^{(e)}$$

Using the definition of Beta function and Gamma function, the inner integral is equal to³⁵

$$(1-L_i^{(e)})^{b+c+1} \times \frac{b!c!}{(b+c+1)!}$$

Hence,

$$I = 2\Delta x \int_{L_i^{(e)}=0}^1 (L_i^{(e)})^a \times (1-L_i^{(e)})^{b+c+1} \times \frac{b!c!}{(b+c+1)!} dL_i^{(e)}$$

Again using the same formula above,

$$I = 2\Delta x \frac{a!b!c!}{(a+b+c+2)!} \quad (60)$$

APPENDIX B

DEVELOPMENT OF ELEMENTAL RELATIONS

B.1 Application of Galerkin's Technique to a Finite Element

Equation (59) when applied to a single finite element yields

$$\iiint_{\Delta(e)} N_{\mu}^{(e)} L(\phi') dV^{(e)} = 0, \mu = 1, 2, \dots, \sigma \quad (B-1)$$

where σ is the total number of nodes in the element e (σ is 3 for a linear and 6 for a quadratic element). For illustration purposes the Galerkin's technique is applied to Eq. (6) in this development. Exactly same procedure applies to Eq. (7) also. Hereafter, the superscript e is dropped since this derivation is for one element only.

The first three terms in Eq. (6) contain second order partial derivatives of $\tilde{\phi}$ which are reduced to first order by using Green's theorem in a plane. Green's theorem in a plane region R bounded by a curve C for two functions $U(r, Z)$ and $V(r, Z)$ is²⁴ (see Figure B.1 and note that C is traversed in a direction that R lies to the left of C)

$$\iint_R \left[\frac{\partial V}{\partial z} - \frac{\partial U}{\partial r} \right] dr dz = \oint_C U dz + \oint_C V dr \quad (B-2)$$

Identifying

$$U = -N_{\mu} r^2 (\bar{c}^2 - \phi_r^2) \phi_r$$

and

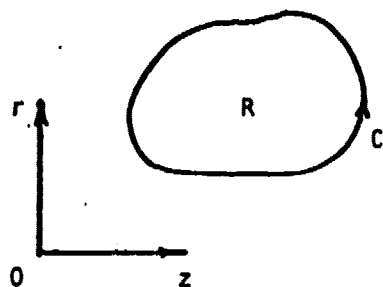


Figure B-1. Green's Theorem in a Plane Region, R Bounded by a Curve, C .

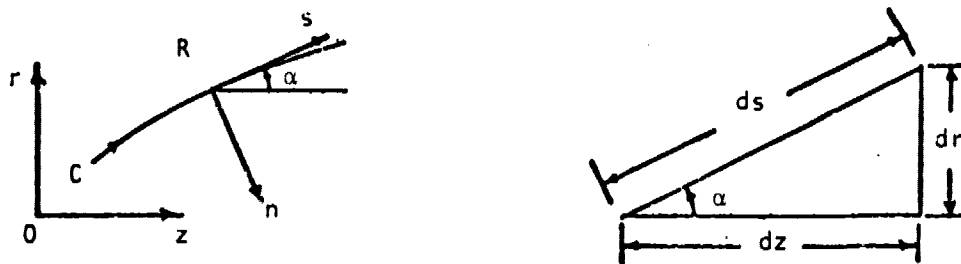


Figure B-2. Transformation of (r, z) Coordinate System to the Natural Coordinate System.

$$V = N_{\mu} r^2 [(\bar{c}^2 - \bar{\phi}_z^2) \bar{\phi}_z - 2\bar{\phi}_r \bar{\phi}_z \bar{\phi}_r]$$

and applying Eq. (B-2) yields after some manipulations

$$\begin{aligned} & \iint_R \left\{ \bar{\phi}_r \left[\frac{\partial}{\partial r} (N_{\mu} r^2 (\bar{c}^2 - \bar{\phi}_r^2)) \right] - \frac{\partial}{\partial z} (2N_{\mu} r^2 \bar{\phi}_r \bar{\phi}_z) \right. \\ & \quad + \left. \left\{ (\gamma+1) \bar{\phi}_{rr} \bar{\phi}_r + 2\bar{\phi}_{rz} \bar{\phi}_z - \frac{\bar{c}^2}{r} + (\gamma-1) \frac{\bar{\phi}_r^2}{r} + (\gamma-1) \bar{\phi}_r \bar{\phi}_{zz} \right\} N_{\mu} r^2 \right\} \\ & \quad + \bar{\phi}_z \left[\frac{\partial}{\partial z} (N_{\mu} r^2 (\bar{c}^2 - \bar{\phi}_z^2)) \right] \\ & \quad + \left. \left\{ (\gamma+1) \bar{\phi}_{zz} \bar{\phi}_z + 2\bar{\phi}_{rz} \bar{\phi}_r + (\gamma-1) \bar{\phi}_{rr} \bar{\phi}_z - (\gamma-1) \frac{\bar{\phi}_z \bar{\phi}_r}{r} \right\} N_{\mu} r^2 \right] \\ & \quad - \left[\omega^2 - \frac{m^2 \bar{c}^2}{r^2} \right] N_{\mu} r^2 \bar{\phi} + 2\omega \bar{\phi}_r N_{\mu} r^2 \hat{\phi}_r + 2\omega \bar{\phi}_z N_{\mu} r^2 \hat{\phi}_z \\ & \quad + \omega (\gamma-1) \left[\bar{\phi}_{rr} + \frac{\bar{\phi}_r}{r} + \bar{\phi}_{zz} \right] N_{\mu} r^2 \hat{\phi} \} dr dz \\ & = \oint_C N_{\mu} r^2 [(\bar{c}^2 - \bar{\phi}_z^2) \bar{\phi}_z - 2\bar{\phi}_r \bar{\phi}_z \bar{\phi}_r] dr - \oint_C N_{\mu} r^2 (\bar{c}^2 - \bar{\phi}_r^2) \bar{\phi}_r dz, \\ & \qquad \qquad \qquad \mu = 1, 2, \dots, \sigma \quad (B-3) \end{aligned}$$

It is simpler to evaluate the boundary integrals in Eq. (B-3) in terms of the natural coordinates (s, n) where s is the coordinate along the curve C and n is the coordinate normal to C and pointing away from the region R (see Figure B-2). Differential lengths dr and dz along the curve C are related to ds by

$$\begin{aligned} dr &= ds \sin \alpha \\ dz &= ds \cos \alpha \end{aligned} \quad (B-4)$$

and the velocity components are related by

$$\begin{aligned}\phi_r &= \phi_s \sin\alpha - \phi_n \cos\alpha \\ \phi_z &= \phi_s \sin\alpha + \phi_n \sin\alpha\end{aligned}\tag{B-5}$$

Substituting Eqs. (B-4) and (B-5) in the boundary integral of Eq. (B-3) one obtains

$$\begin{aligned}\bar{B}_\mu &= \oint_C N_\mu r^2 [\bar{\phi}_s \{(\bar{\phi}_r^2 - \bar{\phi}_z^2) \cos\alpha \sin\alpha - 2\bar{\phi}_r \bar{\phi}_z \sin^2\alpha\} \\ &\quad + \bar{\phi}_n \{c^2 - (\bar{\phi}_z \sin\alpha - \bar{\phi}_r \cos\alpha)^2\}] ds, \quad \mu = 1, 2, \dots, \sigma\end{aligned}\tag{B-6}$$

It is to be noted that the contributions to the boundary integral in Eq. (B-6) come only from the elements located on the boundary surfaces of the inlet as the individual element contributions located in the interior of the inlet are cancelled as the element boundaries are traversed in exactly opposite directions for the two neighboring elements. Hence, though the individual element boundary integrals will be nonzero, when the elements are assembled into a global matrix form, the internal element contributions to the boundary integrals vanish. So Eq. (B-6) is evaluated only for elements located along the boundary of the inlet.

B.2 Element Relations for an Internal Element

For an internal element the right hand side of Eq. (B-3) is not evaluated as discussed above. The left hand side of Eq. (B-3) is evaluated by using linear interpolation functions for 3-node triangles and quadratic interpolation functions for 6-node triangles (see Eqs. 51-58).

B.2.1 Evaluation for a 3-Node Triangle (See Figure 5)

For a 3-node triangle the variation of the acoustic potential over the element is given by

$$\bar{\phi}(r, z) = L_i(r, z)\bar{\phi}_i + L_j(r, z)\bar{\phi}_j + L_k(r, z)\bar{\phi}_k \quad (53)$$

and

$$\hat{\phi}(r, z) = L_i(r, z)\hat{\phi}_i + L_j(r, z)\hat{\phi}_j + L_k(r, z)\hat{\phi}_k \quad (54)$$

For the sake of simplicity in evaluating terms in Eq. (B-3) the mean flow quantities \bar{c} , $\bar{\phi}_r$ and $\bar{\phi}_z$ within each element are assumed to be constant and equal to the arithmetic average of their respective values at the nodes i , j and k . However, the derivatives of the mean flow quantities like $\bar{\phi}_{rr}$, $\bar{\phi}_{rz}$, $\bar{\phi}_{zz}$, \bar{c}_r , \bar{c}_z etc. are evaluated assuming that the mean flow quantities are varying linearly over the element just like the acoustic potential. Also the coordinate r is assumed to have a constant value \bar{r} equal to the r -coordinate of the centroid of the element except where the derivatives with respect to r are to be evaluated.

The following polynomial integrations of the area coordinates need to be performed:

$$a. \iint_{\Delta} L_{\mu} drdz, \quad \mu = i, j \text{ and } k$$

and

$$b. \iint_{\Delta} L_{\mu} [L_i\phi_i + L_j\phi_j + L_k\phi_k] drdz, \quad \mu = i, j \text{ and } k$$

Application of Eq. (60) to integrals a and b yields

$$\iint_{\Delta} L_{\mu} drdz = \frac{2\Delta}{6},$$

and

$$\left. \begin{aligned} \mu &= i, j \text{ and } k \\ \eta &= i, j \text{ and } k \end{aligned} \right\} \text{(B-7)}$$

$$\iint_{\Delta} L_{\mu} [L_i \phi_i + L_j \phi_j + L_k \phi_k] drdz = \frac{2\Delta}{24} [\phi_i + \phi_j + \phi_k + \delta_{\mu\eta} \phi_{\eta}],$$

where $\delta_{\mu\eta}$ is the Kroneker's delta having the property

$$\delta_{\mu\eta} = \begin{cases} 1 & \text{if } \mu = \eta \\ 0 & \text{if } \mu \neq \eta \end{cases} \quad \text{(B-8)}$$

Substituting Eqs. (B-7) in Eq. (B-3) one obtains the desired element relation for an internal element:

$$\begin{aligned} & \frac{(c_i \tilde{\phi}_i + c_j \tilde{\phi}_j + c_k \tilde{\phi}_k)}{2\Delta} \times \left[\frac{c_{\mu}}{2} \bar{r}^2 (\bar{c}^2 - \bar{\phi}_r^2) + \frac{4\Delta}{6} \{ \bar{r} (\bar{c}^2 - \bar{\phi}_r^2) \right. \\ & + \bar{r}^2 (\bar{c} \bar{c}_r - \bar{\phi}_r \bar{\phi}_{rr}) \} + \{ (\gamma+1) \bar{\phi}_{rr} \bar{\phi}_r + 2 \bar{\phi}_{rz} \bar{\phi}_z - \frac{\bar{c}^2}{r} \\ & + (\gamma-1) \frac{\bar{\phi}_r^2}{r} + (\gamma-1) \bar{\phi}_r \bar{\phi}_{zz} \} \frac{\bar{r}^2 \times 2\Delta}{6} - 2 \bar{r}^2 \{ \frac{b_{\mu}}{2} \bar{\phi}_r \bar{\phi}_z \\ & + (\bar{\phi}_{rz} \bar{\phi}_z + \bar{\phi}_r \bar{\phi}_{zz}) \frac{2\Delta}{6} \} + \frac{(b_i \tilde{\phi}_i + b_j \tilde{\phi}_j + b_k \tilde{\phi}_k) \bar{r}^2}{2\Delta} \times \\ & \left[\frac{b_{\mu}}{2} (\bar{c}^2 - \bar{\phi}_z^2) + \frac{4\Delta}{6} (\bar{c} \bar{c}_z - \bar{\phi}_z \bar{\phi}_{zz}) + \{ (\gamma+1) \bar{\phi}_{zz} \bar{\phi}_z + 2 \bar{\phi}_{rz} \bar{\phi}_r \right. \\ & + (\gamma-1) \bar{\phi}_{rr} \bar{\phi}_z - (\gamma-1) \frac{\bar{\phi}_z \bar{\phi}_r}{r} \} \times \frac{2\Delta}{6} \left. \right] \\ & - (\omega^2 - m^2 \frac{\bar{c}^2}{r^2}) \bar{r}^2 \times (\tilde{\phi}_i + \tilde{\phi}_j + \tilde{\phi}_k + \delta_{\mu\eta} \tilde{\phi}_{\eta}) \times \frac{2\Delta}{24} \\ & + 2\omega_{\bar{r}} \bar{r}^2 \frac{(c_i \hat{\phi}_i + c_j \hat{\phi}_j + c_k \hat{\phi}_k)}{6} + 2\omega_{\bar{z}} \bar{r}^2 \frac{(b_i \hat{\phi}_i + b_j \hat{\phi}_j + b_k \hat{\phi}_k)}{6} \\ & + \omega(\gamma-1) \times [\bar{\phi}_{rr} + \frac{\bar{\phi}_r}{r} + \bar{\phi}_{zz}] \bar{r}^2 (\hat{\phi}_i + \hat{\phi}_j + \hat{\phi}_k + \delta_{\mu\eta} \hat{\phi}_{\eta}) \times \frac{2\Delta}{24} = 0, \\ & \mu = i, j \text{ and } k \quad \eta = i, j \text{ and } k \quad \text{(B-9)} \end{aligned}$$

B.2.2 Evaluation for a 6-Node Triangle (See Figure 5)

For a 6-node triangle the variation of acoustic potential over the element is given by

$$\begin{aligned}\tilde{\phi}(r,z) = & N_i(r,z)\tilde{\phi}_i + N_j(r,z)\tilde{\phi}_j + N_k(r,z)\tilde{\phi}_k + N_\ell(r,z)\tilde{\phi}_\ell \\ & + N_m(r,z)\tilde{\phi}_m + N_n(r,z)\tilde{\phi}_n\end{aligned}\quad (55)$$

and

$$\begin{aligned}\hat{\phi}(r,z) = & N_i(r,z)\hat{\phi}_i + N_j(r,z)\hat{\phi}_j + N_k(r,z)\hat{\phi}_k + N_\ell(r,z)\hat{\phi}_\ell \\ & + N_m(r,z)\hat{\phi}_m + N_n(r,z)\hat{\phi}_n\end{aligned}\quad (56)$$

where for corner nodes

$$\begin{aligned}N_i &= 2L_i^2 - L_i \\ N_j &= 2L_j^2 - L_j \\ N_k &= 2L_k^2 - L_k\end{aligned}\quad (57)$$

and for mid-size nodes

$$\begin{aligned}N_\ell &= 4L_iL_j \\ N_m &= 4L_jL_k \\ N_n &= 4L_kL_i\end{aligned}\quad (58)$$

The same assumptions regarding the mean flow quantities and the coordinate r made in Section B.2.1 are applied to the quadratic elements also.

The following polynomial integrations of the area coordinates need to be performed:

$$I_{a\mu} = \iint_{\Delta} N_{\mu} \phi_r \, drdz$$

$$I_{b\mu} = \iint_{\Delta} N_{\mu} \phi_z \, drdz$$

$$I_{c\mu} = \iint_{\Delta} \frac{\partial N_{\mu}}{\partial r} \phi_r \, drdz$$

$$\mu = i, j, k, \ell, m \text{ and } n \quad (B-10)$$

$$I_{d\mu} = \iint_{\Delta} \frac{\partial N_{\mu}}{\partial z} \phi_r \, drdz$$

$$I_{e\mu} = \iint_{\Delta} \frac{\partial N_{\mu}}{\partial z} \phi_z \, drdz$$

$$I_{f\mu} = \iint_{\Delta} N_{\mu} \phi \, drdz$$

The integrations will be performed for $\mu = i$ and $\mu = \ell$. The integrations for $\mu = j$ and k and $\mu = m$ and n can be obtained by a proper cyclic rotation of indices i, j and k and ℓ, m and n (see Eqs. (52)).

Case 1 $\mu = i$

Consider

$$I_{a_i} = \iint_{\Delta} N_i \phi_r \, drdz$$

Substituting Eqs. (55/56), (57) and (58) into I_{a_i} yields

$$I_{a_i} = \iint_{\Delta} (2L_i^2 - L_i) \times \frac{1}{2\Delta} \times \left[(4L_i - 1)c_i \phi_i + (4L_j - 1)c_j \phi_j + (4L_k - 1)c_k \phi_k \right. \\ \left. + 4(c_i L_j + c_j L_i) \phi_{\ell} + 4(c_j L_k + c_k L_j) \phi_m \right. \\ \left. + 4(c_k L_i + c_i L_k) \phi_n \right] \, drdz$$

Simplifying and evaluating the integrals using Eq. (60) yields

$$I_{ai} = \frac{1}{30} [2c_i \phi_i - c_j \phi_j - c_k \phi_k + \phi_\ell (2c_j - c_i) - \phi_m (c_j + c_k) + \phi_n (2c_k - c_i)] \quad (B-11)$$

Consider

$$I_{bi} = \iint_{\Delta} N_i \phi_z \, drdz$$

Substituting Eqs. (55/56), (57) and (58) into I_{bi} yields

$$I_{bi} = \iint_{\Delta} (2L_i^2 - L_i) \frac{1}{2\Delta} \times [4L_i - 1] b_i \phi_i + (4L_j - 1) b_j \phi_j + (4L_k - 1) b_k \phi_k + 4(b_i L_j + b_j L_i) \phi_\ell + 4(b_j L_k + b_k L_j) \phi_m + 4(b_k L_i + b_i L_k) \phi_n] \, drdz$$

Simplifying and evaluating the integrals using Eq. (60) yields

$$I_{bi} = \frac{1}{30} [2b_i \phi_i - b_j \phi_j - b_k \phi_k + (2b_j - b_i) \phi_\ell - (b_j + b_k) \phi_m + (2b_k - b_i) \phi_n] \quad (B-12)$$

Consider

$$I_{ci} = \iint_{\Delta} \frac{\partial N_i}{\partial r} \phi_r \, drdz$$

Substituting as above from Eqs. (55/56), (57) and (58) into I_{ci} yields

$$I_{ci} = \iint_{\Delta} \frac{1}{(2\Delta)^2} (4L_i - 1)c_i \times [(4L_i - 1)c_i\phi_i + (4L_j - 1)c_j\phi_j + (4L_k - 1)c_k\phi_k + 4(c_iL_j + c_jL_i)\phi_\ell + 4(c_jL_k + c_kL_j)\phi_m + 4(c_kL_i + c_iL_k)\phi_n] drdz$$

Simplifying and evaluating the integrals using Eq. (60) yields

$$I_{ci} = \frac{c_i}{2\Delta} \times [c_i\phi_i \left(\frac{1}{2}\right) + c_j\phi_j \left(-\frac{1}{6}\right) + c_k\phi_k \left(-\frac{1}{6}\right) + c_j\phi_\ell \left(\frac{2}{3}\right) + \phi_m(0) + c_k\phi_n \left(\frac{2}{3}\right)] \quad (B-13)$$

Consider

$$I_{di} = \iint_{\Delta} \frac{\partial N_i}{\partial z} \phi_r drdz$$

Substituting as above from Eqs. (55/56), (57) and (58) into I_{di} yields

$$I_{di} = \iint_{\Delta} \frac{1}{(2\Delta)^2} (4L_i - 1)b_i [(4L_i - 1)c_i\phi_i + (4L_j - 1)c_j\phi_j + (4L_k - 1)c_k\phi_k + 4(c_iL_j + c_jL_i)\phi_\ell + 4(c_jL_k + c_kL_j)\phi_m + 4(c_kL_i + c_iL_k)\phi_n] drdz$$

Simplifying and evaluating the integrals using Eq. (60) yields

$$I_{di} = \frac{b_i}{2\Delta} \times [c_i\phi_i \left(\frac{1}{2}\right) + c_j\phi_j \left(-\frac{1}{6}\right) + c_k\phi_k \left(-\frac{1}{6}\right) + c_j\phi_\ell \left(\frac{2}{3}\right) + \phi_m(0) + c_k\phi_n \left(\frac{2}{3}\right)] \quad (B-14)$$

Consider

$$I_{ei} = \iint_{\Delta} \frac{\partial N_i}{\partial z} \phi_z \, drdz$$

Substituting Eqs. (55/56), (57) and (58) into I_{ei} yields

$$\begin{aligned} I_{ei} = \iint_{\Delta} \frac{1}{(2\Delta)^2} (4L_i - 1)bi \times & [(4L_i - 1)b_i\phi_i + (4L_j - 1)b_j\phi_j \\ & + (4L_k - 1)b_k\phi_k + 4(b_iL_j + b_jL_i)\phi_\ell + 4(b_jL_k + b_kL_j)\phi_m \\ & + 4(b_kL_i + b_iL_k)\phi_n] \, drdz \end{aligned}$$

Simplifying and evaluating the integrals using Eq. (60) yields

$$\begin{aligned} I_{ei} = \frac{bi}{2\Delta} \times & [b_i\phi_i\left(\frac{1}{2}\right) + b_j\phi_j\left(-\frac{1}{6}\right) + b_k\phi_k\left(-\frac{1}{6}\right) \\ & + b_j\phi_\ell\left(\frac{2}{3}\right) + \phi_m(0) + b_k\phi_n\left(\frac{2}{3}\right)] \end{aligned} \quad (B-15)$$

Consider

$$I_{fi} = \iint_{\Delta} N_i \phi \, drdz$$

Substituting Eqs. (55/56), (57) and (58) into I_{fi} yields

$$\begin{aligned} I_{fi} = \iint_{\Delta} (2L_i^2 - L_i) \times & [(2L_i^2 - L_i)\phi_i + (2L_j^2 - L_j)\phi_j \\ & + (2L_k^2 - L_k)\phi_k + 4L_iL_j\phi_\ell + 4L_jL_k\phi_m + 4L_kL_i\phi_n] \, drdz \end{aligned}$$

Simplifying and evaluating the integrals using Eq. (60) yields

$$\begin{aligned} I_{fi} = 24 \times & [\phi_i\left(-\frac{1}{60}\right) + \phi_j\left(-\frac{1}{360}\right) + \phi_k\left(-\frac{1}{360}\right) + \phi_\ell(0) \\ & + \phi_m\left(-\frac{1}{90}\right) + \phi_n(0)] \end{aligned} \quad (B-16)$$

Substituting Eqs. (B-11) - (B-16) into Eq. (B-3) yields the following quadratic element equation for an internal element for the corner node i.

$$\begin{aligned}
& \tilde{I}_{ai} \times [2\bar{r}(\bar{c}^2 - \bar{\phi}_r^2) + 2\bar{r}^2(\bar{c} \bar{c}_r - \bar{\phi}_r \bar{\phi}_{rr}) - 2\bar{r}^2 \bar{\phi}_{rz} \bar{\phi}_z - 2\bar{r}^2 \bar{\phi}_r \bar{\phi}_{zz}] \\
& \quad + \{(\gamma+1)\bar{\phi}_{rr} \bar{\phi}_r + 2\bar{\phi}_{rz} \bar{\phi}_z - \frac{\bar{c}^2}{\bar{r}} + (\gamma-1)\frac{\bar{\phi}_r^2}{\bar{r}} + (\gamma-1)\bar{\phi}_r \bar{\phi}_{zz}\} \bar{r}^2] \\
& + \tilde{I}_{bi} \times [2\bar{r}^2(\bar{c} \bar{c}_z - \bar{\phi}_z \bar{\phi}_{zz}) + \{(\gamma+1)\bar{\phi}_{zz} \bar{\phi}_z + 2\bar{\phi}_{rz} \bar{\phi}_r + \\
& \quad + (\gamma-1)\bar{\phi}_{rr} \bar{\phi}_z - (\gamma-1)\frac{\bar{\phi}_z \bar{\phi}_r}{\bar{r}}\} \bar{r}^2] \\
& + \tilde{I}_{ci} [\bar{r}^2(\bar{c}^2 - \bar{\phi}_r^2)] - \tilde{I}_{di} [2\bar{r}^2 \bar{\phi}_r \bar{\phi}_z] + \tilde{I}_{ei} [\bar{r}^2(\bar{c}^2 - \bar{\phi}_z^2)] \\
& \quad - \tilde{I}_{fi} \bar{r}^2 [\omega^2 - m^2 \frac{\bar{c}^2}{\bar{r}^2}] + \hat{I}_{ai} 2\omega \bar{r}^2 \bar{\phi}_r + \hat{I}_{bi} 2\omega \bar{r}^2 \bar{\phi}_z \\
& \quad + \hat{I}_{fi} \omega(\gamma-1) \bar{r}^2 [\bar{\phi}_{rr} + \frac{\bar{\phi}_r}{\bar{r}} + \bar{\phi}_{zz}] = 0 \tag{B-17}
\end{aligned}$$

where the superscripts \sim and $\hat{\sim}$ refer to the real and imaginary parts of the complex integrals in Eqs. (B-11) - (B-16) respectively. Element equations similar to Eq. (B-17) for nodes j and k may be obtained by the cyclic rotation of indices i, j and k and ℓ , m and n in the Eqs. (B-11) - (B-16).

Case 2 $\mu = \ell$

Following exactly the procedure indicated in Case 1 one obtains the following expressions for the integrals in Eq. (B-10) for $\mu = \ell$:

$$\begin{aligned}
I_{a\ell} &= \iint_{\Delta} N_{\ell} \phi_r \, drdz \\
&= [c_i \phi_i \left(\frac{1}{10}\right) + c_j \phi_j \left(\frac{1}{10}\right) + c_k \phi_k \left(-\frac{1}{30}\right) + \frac{4}{15} (c_i + c_j) \phi_{\ell} \\
&\quad + \frac{2}{15} (c_j + 2c_k) \phi_m + \frac{2}{15} (c_i + 2c_k) \phi_n] \quad (B-18)
\end{aligned}$$

$$\begin{aligned}
I_{b\ell} &= \iint_{\Delta} N_{\ell} \phi_z \, drdz \\
&= [b_i \phi_i \left(\frac{1}{10}\right) + b_j \phi_j \left(\frac{1}{10}\right) + b_k \phi_k \left(-\frac{1}{30}\right) + \frac{4}{15} (b_i + b_j) \phi_{\ell} \\
&\quad + \frac{2}{15} (b_j + 2b_k) \phi_m + \frac{2}{15} (b_i + 2b_k) \phi_n] \quad (B-19)
\end{aligned}$$

$$\begin{aligned}
I_{c\ell} &= \iint_{\Delta} \frac{\partial N_{\ell}}{\partial r} \phi_r \, drdz \\
&= \frac{4}{2\Delta} \left[\phi_i \left(\frac{c_i c_j}{6}\right) + \phi_j \left(\frac{c_j c_i}{6}\right) + \phi_k (0) + \frac{\phi_{\ell}}{3} (c_i^2 + c_i c_j + c_j^2) \right. \\
&\quad + \frac{\phi_m}{6} (c_i c_j + 2c_i c_k + c_j^2 + c_j c_k) + \frac{\phi_n}{6} (c_i c_k + c_i^2 \\
&\quad \left. + 2c_j c_k + c_j c_i) \right] \quad (B-20)
\end{aligned}$$

$$\begin{aligned}
I_{d\ell} &= \iint_{\Delta} \frac{\partial N_{\ell}}{\partial z} \phi_r \, drdz \\
&= \frac{4}{2\Delta} \times \left[\phi_i \left(\frac{c_i b_j}{6}\right) + \phi_j \left(\frac{c_j b_i}{6}\right) + \phi_k (0) + \frac{\phi_{\ell}}{6} (2b_i c_i + b_i c_j + b_j c_i \right. \\
&\quad \left. + 2b_j c_j) + \frac{\phi_m}{6} (b_i c_j + 2b_i c_k + b_j c_j + b_j c_k) \right. \\
&\quad \left. + \frac{\phi_n}{6} (b_i c_k + b_i c_i + 2b_j c_k + b_j c_i) \right] \quad (B-21)
\end{aligned}$$

$$\begin{aligned}
I_{e\ell} &= \iint_{\Delta} \frac{\partial N_{\ell}}{\partial z} \phi_z \, drdz \\
&= \frac{4}{2\Delta} \left[\phi_i \left(\frac{b_i b_j}{6} \right) + \phi_j \left(\frac{b_j b_i}{6} \right) + \phi_k(0) + \frac{\phi_{\ell}}{3} (b_i^2 + b_i b_j + b_j^2) \right. \\
&\quad + \frac{\phi_m}{6} (b_i b_j + 2b_i b_k + b_j^2 + b_j b_k) + \frac{\phi_n}{6} (b_i b_k + b_i^2 \\
&\quad \left. + 2b_j b_k + b_j b_i) \right] \tag{B-22}
\end{aligned}$$

$$\begin{aligned}
I_{f\ell} &= \iint_{\Delta} N_{\ell} \phi \, drdz \\
&= 2\Delta \left[\phi_i(0) + \phi_j(0) + \phi_k \left(-\frac{1}{90} \right) + \phi_{\ell} \left(\frac{4}{45} \right) + \phi_m \left(\frac{2}{45} \right) \right. \\
&\quad \left. + \phi_n \left(\frac{2}{45} \right) \right] \tag{B-23}
\end{aligned}$$

Substituting Eqs. (B-18) - (B-23) into Eq. (B-3) yields the following quadratic element relation for an internal element for the mid-side node

$$\begin{aligned}
&\tilde{I}_{a\ell} \times [2\bar{r}(\bar{c}^2 - \bar{\phi}_r^2) + 2\bar{r}^2(\bar{c} \bar{c}_r - \bar{\phi}_r \bar{\phi}_{rr}) - 2\bar{r}^2 \bar{\phi}_{rz} \bar{\phi}_z - 2\bar{r}_r^2 \bar{\phi}_r \bar{\phi}_{zz} \\
&\quad + \{(\gamma+1)\bar{\phi}_{rr} \bar{\phi}_r + 2\bar{\phi}_{rz} \bar{\phi}_z - \frac{\bar{c}^2}{\bar{r}} + (\gamma-1) \frac{\bar{\phi}_r}{\bar{r}} + (\gamma-1)\bar{\phi}_r \bar{\phi}_{zz}\} \bar{r}^2] \\
&+ \tilde{I}_{b\ell} \times [2\bar{r}^2(\bar{c} \bar{c}_z - \bar{\phi}_z \bar{\phi}_{zz}) + \{(\gamma+1)\bar{\phi}_{zz} \bar{\phi}_z + 2\bar{\phi}_{rz} \bar{\phi}_r \\
&\quad + (\gamma-1)\bar{\phi}_{rr} \bar{\phi}_z - (\gamma-1) \frac{\bar{\phi}_r \bar{\phi}_z}{\bar{r}}\} \bar{r}^2] \\
&+ \tilde{I}_{c\ell} \times [\bar{r}^2(\bar{c}^2 - \bar{\phi}_r^2)] - \tilde{I}_{d\ell} [2\bar{r}^2 \bar{\phi}_r \bar{\phi}_z] + \tilde{I}_{e\ell} [\bar{r}^2 (\bar{c}^2 - \bar{\phi}_z^2)]
\end{aligned}$$

$$\begin{aligned}
& -\bar{i}_{f\ell} \bar{r}^2 \left[\omega^2 - m^2 \frac{c^2}{r^2} \right] + \hat{i}_{a\ell} 2\omega \bar{r}^2 \bar{\phi}_r + \hat{i}_{b\ell} 2\omega \bar{r}^2 \bar{\phi}_z \\
& + \hat{i}_{f\ell} \omega(r-1) \bar{r}^2 \left[\bar{\phi}_{rr} + \frac{\bar{\phi}_r}{r} + \bar{\phi}_{zz} \right] = 0
\end{aligned} \tag{B-24}$$

where the superscripts \sim and $\hat{\cdot}$ refer to the real and imaginary parts of the complex integrals in Eqs. (B-18) - (B-23) respectively. Element relations similar to Eq. (B-24) for mid-side nodes m and n may be obtained by the cyclic rotation of indices i, j and k and ℓ, m and n in the Eqs. (B-18) - (B-23).

B.3 Boundary Integral Evaluation for a Hard Wall

The boundary condition at a hard wall of the duct in terms of real and imaginary parts is

$$\bar{\phi}_n = 0$$

and

$$\hat{\phi}_n = 0$$

(15)

B.3.1 Evaluation of Hard Wall Boundary Condition for a 3-Node Triangle (See Figure B.3)

Substituting Eq. (15) in the boundary integral expression given by Eq. (B-6) one obtains

$$\bar{\beta}_\mu = \oint_C N_\mu r^2 \left[(\bar{\phi}_r^2 - \bar{\phi}_z^2) \cos\alpha \sin\alpha - 2\bar{\phi}_r \bar{\phi}_z \sin^2\alpha \right] \bar{\phi}_s ds \tag{B-25}$$

For the 3-node element configuration shown in Figure B-3 the interpolation functions along c reduce to

$$\left. \begin{aligned} N_i &= 1 - \xi \\ N_j &= \xi \\ N_k &\equiv 0 \end{aligned} \right\} 0 \leq \xi \leq 1 \quad (\text{B-26})$$

Hence the variation of $\tilde{\phi}$ along c becomes

$$\tilde{\phi} = (1 - \xi)\tilde{\phi}_i + \xi\tilde{\phi}_j \quad (\text{B-27})$$

Application of the chain rule for differentiation yields

$$\tilde{\phi}_s ds = (\tilde{\phi}_j - \tilde{\phi}_i) d\xi \quad (\text{B-28})$$

Substituting Eq. (B-28) into Eq. (B-25) one obtains

$$\tilde{\beta}_j = r^2 [(\bar{\phi}_r^2 - \bar{\phi}_z^2) \cos\alpha \sin\alpha - 2\bar{\phi}_r \bar{\phi}_z \sin^2\alpha] \int_{\xi=0}^1 \frac{(1-\xi)[\tilde{\phi}_j - \tilde{\phi}_i]}{(\xi)} d\xi$$

That is

$$\tilde{\beta}_\mu = r^2 [(\bar{\phi}_r^2 - \bar{\phi}_z^2) \cos\alpha \sin\alpha - 2\bar{\phi}_r \bar{\phi}_z \sin^2\alpha] \frac{(\tilde{\phi}_j - \tilde{\phi}_i)}{2}, \quad \mu = i \text{ and } j \quad (\text{B-29})$$

Since $\tilde{\phi}_j$ and $\tilde{\phi}_i$ are unknown as of now, $\tilde{\beta}_\mu$ is transported to the left hand side of Eqs. (B-3).

B.3.2 Evaluation of Hard Wall Boundary Condition for a 6-Node Triangle (See Figure B-3)

The boundary integral to be evaluated is given by Eq. (B-25).

For the 6-node element configuration shown in Figure B-3 the interpolation functions along c reduce to

$$\begin{array}{l}
 N_i = 2\xi^2 - 3\xi + 1 \\
 N_j = 2\xi^2 - \xi \\
 N_\ell = 4(\xi - \xi^2) \\
 N_k = N_m = N_n = 0
 \end{array}
 \left. \vphantom{\begin{array}{l} N_i \\ N_j \\ N_\ell \\ N_k \end{array}} \right\} 0 \leq \xi \leq 1 \quad (\text{B-30})$$

Hence the variation of $\bar{\phi}$ along c becomes

$$\bar{\phi} = (2\xi^2 - 3\xi + 1)\phi_i + (2\xi^2 - \xi)\phi_j + 4(\xi - \xi^2)\bar{\phi}_\ell \quad (\text{B-31})$$

Application of the chain rule for differentiation yields

$$\bar{\phi}_s \phi_s = [(4\xi - 3)\bar{\phi}_i + (4\xi - 1)\bar{\phi}_j + 4(1 - 2\xi)\bar{\phi}_\ell] d\xi \quad (\text{B-32})$$

Substituting Eq. (B-32) into Eq. (B-25) and evaluating the polynomial integrals leads to

$$\begin{aligned}
 \bar{\beta}_i = \bar{r}^2 [(\bar{\phi}_r^2 - \bar{\phi}_z^2) \cos\alpha \sin\alpha - 2\bar{\phi}_r \bar{\phi}_z \sin^2\alpha] \times \\
 [\bar{\phi}_i(-\frac{1}{2}) + \bar{\phi}_j(-\frac{1}{6}) + \bar{\phi}_\ell(\frac{2}{3})] \quad (\text{B-33})
 \end{aligned}$$

$$\begin{aligned}
 \bar{\beta}_j = \bar{r}^2 [(\bar{\phi}_r^2 - \bar{\phi}_z^2) \cos\alpha \sin\alpha - 2\bar{\phi}_r \bar{\phi}_z \sin^2\alpha] \times \\
 [\bar{\phi}_i(\frac{1}{6}) + \bar{\phi}_j(\frac{1}{2}) + \bar{\phi}_\ell(-\frac{2}{3})] \quad (\text{B-34})
 \end{aligned}$$

and

$$\begin{aligned}
 \bar{\beta}_\ell = \bar{r}^2 [(\bar{\phi}_r^2 - \bar{\phi}_z^2) \cos\alpha \sin\alpha - 2\bar{\phi}_r \bar{\phi}_z \sin^2\alpha] \times \\
 [\bar{\phi}_i(-\frac{2}{3}) + \bar{\phi}_j(\frac{2}{3}) + \bar{\phi}_\ell(0)] \quad (\text{B-35})
 \end{aligned}$$

As $\tilde{\phi}_i$, $\tilde{\phi}_j$ and $\tilde{\phi}_l$ are unknown, $\tilde{\beta}_i$, $\tilde{\beta}_j$ and $\tilde{\beta}_l$ are transported to the left hand sides of the corresponding equations in (B-3) for nodes i , j and l respectively.

B.4 Boundary Integral Evaluation for a Soft Wall (See Figure B-3)

The boundary conditions at a soft wall using the concept of continuity of particle displacement are given by

$$\begin{aligned} \theta \tilde{\phi}_n - x \hat{\phi}_n = & -\bar{\rho} [\omega \tilde{\phi} + \bar{\phi}_s \tilde{\phi}_s] + \frac{\bar{\rho} \bar{\phi}_s}{\omega} [-\omega \tilde{\phi}_s + \bar{\phi}_{ss} \hat{\phi}_s + \bar{\phi}_s \hat{\phi}_{ss}] \\ & + \left(\frac{2}{\gamma-1} \right) \frac{\bar{\rho}}{c} \frac{\partial \bar{c}}{\partial s} \frac{\bar{\phi}_s}{\omega} [-\omega \tilde{\phi} + \bar{\phi}_s \hat{\phi}_s] \end{aligned} \quad (29)$$

and

$$\begin{aligned} x \tilde{\phi}_n + \theta \hat{\phi}_n = & -\bar{\rho} [-\omega \tilde{\phi} + \bar{\phi}_s \hat{\phi}_s] - \frac{\bar{\rho} \bar{\phi}_s}{\omega} [\omega \hat{\phi}_s + \bar{\phi}_{ss} \tilde{\phi}_s + \bar{\phi}_s \tilde{\phi}_{ss}] \\ & - \left(\frac{2}{\gamma-1} \right) \frac{\bar{\rho}}{c} \frac{\partial \bar{c}}{\partial s} \frac{\bar{\phi}_s}{\omega} [\omega \hat{\phi} + \bar{\phi}_s \tilde{\phi}_s] \end{aligned} \quad (30)$$

In the absence of mean flow the above equations reduce to

$$\theta \tilde{\phi}_n - x \hat{\phi}_n = -\omega \hat{\phi} \quad (B-36)$$

$$x \tilde{\phi}_n + \theta \hat{\phi}_n = \omega \tilde{\phi} \quad (B-37)$$

Since Eqs. (B-36) and (B-37) do not contain the second derivatives of the acoustic potential, one could use 3-node triangles to evaluate the soft wall boundary conditions.

B.4.1 Evaluation of Soft Wall Boundary Condition for a 3-Node Triangle (No mean flow case only)

The boundary integral given by Eq. (B-6) reduce to the following for the case of no mean flow:

$$\tilde{\beta}_{\mu} = \oint_C N_{\mu} r^2 \tilde{\phi}_n ds \quad (\text{B-38})$$

The soft wall boundary condition for the case of no mean flow given by Eqs. (B-36) and (B-37) are solved for $\tilde{\phi}_n$ and $\hat{\phi}_n$ and on substitution into Eq. (B-38) leads to

$$\tilde{\beta}_{\mu} = \oint_C N_{\mu} r^2 \left[\frac{-\omega\theta\hat{\phi} + \omega x\tilde{\phi}}{\theta^2 + x^2} \right] ds \quad (\text{B-39})$$

Using the interpolation functions given by Eq. (B-26) for the element configuration shown in Figure B-3 one may write

$$\tilde{\phi} = (1 - \xi)\tilde{\phi}_i + \xi\tilde{\phi}_j \quad (\text{B-40})$$

and

$$\hat{\phi} = (1 - \xi)\hat{\phi}_i + \xi\hat{\phi}_j$$

The differential length ds along C is given by

$$ds = [(Z_j - Z_i)^2 + (r_j - r_i)^2]^{1/2} d\xi = L_{ij} d\xi \quad (\text{B-41})$$

Substituting Eqs. (B-40) and (B-41) into Eq. (B-39) yields

$$\hat{\beta}_{\mu} = \int_{\xi=0}^1 r^2 N_{\mu} \left[\frac{-\omega\theta\{(1-\xi)\hat{\phi}_i + \xi\hat{\phi}_j\} + \omega x\{(1-\xi)\tilde{\phi}_i + \xi\tilde{\phi}_j\}}{\theta^2 + x^2} \right] L_{ij} d\xi$$

$$\mu = i \text{ and } j$$

Substituting for N_{ij} from Eq. (B-26) and evaluating the polynomial integrals yields

$$\tilde{\beta}_{\mu} = \frac{\bar{r}^2 \omega L_{ij}}{6(\theta^2 + x^2)} \times \begin{bmatrix} -\theta(\hat{\phi}_i + \hat{\phi}_j + \delta_{\mu\eta} \hat{\phi}_{\eta}) \\ +x(\tilde{\phi}_i + \tilde{\phi}_j + \delta_{\mu\eta} \tilde{\phi}_{\eta}) \end{bmatrix}, \quad (\text{B-42})$$

$\mu = i \text{ and } j \quad \eta = i \text{ and } j$

Since the nodal values of the acoustic potentials are unknown, $\tilde{\beta}_{\mu}$ is transported to the left hand side of Eq. (B-3).

B.4.2 Evaluation of Soft Wall Boundary Condition for a 6-Node Triangle

Since the soft wall boundary conditions given by Eqs. (29) and (30) contain second derivatives of acoustic potential in the presence of a slip flow at the liner, quadratic elements or higher order elements are to be employed to treat such boundary conditions, Eq. (29) and (30) can be solved simultaneously for $\tilde{\phi}_n$ and $\hat{\phi}_n$ to yield

$$\begin{aligned} \tilde{\phi}_n = & \frac{1}{c^2 + x^2} \left[\theta \times \left\{ -\bar{\rho}(\omega\hat{\phi} + \bar{\phi}_s \tilde{\phi}_s) + \frac{\bar{\rho} \bar{\phi}_s}{\omega} (-\omega\tilde{\phi}_s + \bar{\phi}_{ss} \hat{\phi}_s + \bar{\phi}_s \hat{\phi}_{ss}) \right. \right. \\ & + \left. \left. \left(\frac{2}{\gamma-1} \right) \frac{\bar{\rho}}{c} \frac{\partial \bar{c}}{\partial s} \frac{\bar{\phi}_s}{\omega} (-\omega\tilde{\phi} + \bar{\phi}_s \hat{\phi}_s) \right\} \right. \\ & + x \times \left\{ -\bar{\rho}(-\omega\tilde{\phi} + \bar{\phi}_s \hat{\phi}_s) - \frac{\bar{\rho} \bar{\phi}_s}{\omega} (\omega\hat{\phi}_s + \bar{\phi}_{ss} \tilde{\phi}_s + \bar{\phi}_s \tilde{\phi}_{ss}) \right. \\ & \left. \left. - \left(\frac{2}{\gamma-1} \right) \frac{\bar{\rho}}{c} \frac{\partial \bar{c}}{\partial s} \frac{\bar{\phi}_s}{\omega} (\omega\hat{\phi} + \bar{\phi}_s \tilde{\phi}_s) \right\} \right] \quad (\text{B-43}) \end{aligned}$$

and

$$\begin{aligned}
\hat{\phi}_n = & \frac{1}{\theta^2 + x^2} \left[\theta \times \{ -\bar{\rho}(-\omega\hat{\phi} + \bar{\phi}_s\hat{\phi}_s) - \frac{\bar{\rho}\bar{\phi}_s}{\omega} (\omega\hat{\phi}_s + \bar{\phi}_{ss}\tilde{\phi}_s + \bar{\phi}_s\tilde{\phi}_{ss}) \right. \\
& - \left. \left(\frac{2}{\gamma-1} \right) \frac{\bar{\rho}}{c} \frac{\partial \bar{c}}{\partial s} \frac{\bar{\phi}_s}{\omega} (\omega\hat{\phi} + \bar{\phi}_s\tilde{\phi}_s) \right] \\
& - x \times \{ -\bar{\rho}(\omega\hat{\phi} + \bar{\phi}_s\tilde{\phi}_s) + \frac{\bar{\rho}\bar{\phi}_s}{\omega} (-\omega\tilde{\phi}_s + \bar{\phi}_{ss}\hat{\phi}_s + \bar{\phi}_s\hat{\phi}_{ss}) \\
& + \left. \left(\frac{2}{\gamma-1} \right) \frac{\bar{\rho}}{c} \frac{\partial \bar{c}}{\partial s} \frac{\bar{\phi}_s}{\omega} (-\omega\tilde{\phi} + \bar{\phi}_s\hat{\phi}_s) \right\} \quad (B-44)
\end{aligned}$$

Substituting Eqs. (B-32), (B-41) and (B-43) into the boundary integral in Eq. (B-6) and regrouping the terms one obtains

$$\begin{aligned}
\tilde{\beta}_\mu = & r^2 [(\bar{\phi}_r^{-2} - \bar{\phi}_z^{-2}) \cos\alpha \sin\alpha - 2\bar{\phi}_r\bar{\phi}_z \sin^2\alpha] \int_{\xi=0}^1 N_\mu \tilde{\phi}_\xi d\xi \\
& + \frac{r^2}{\theta^2 + x^2} [\bar{c}^2 - (\bar{\phi}_z \sin\alpha - \bar{\phi}_r \cos\alpha)^2] L_{ij} \times \\
& \int_{\xi=0}^1 N_\mu [\tilde{\phi}_{ss} (-\frac{\bar{\rho}}{\omega} x \bar{\phi}_s^{-2}) + \hat{\phi}_{ss} (\frac{\bar{\rho}}{\omega} \theta \bar{\phi}_s^{-2}) \\
& + \tilde{\phi}_s \{ -2\bar{\rho}\bar{\phi}_s\theta - \frac{\bar{\rho}\bar{\phi}_s\bar{\phi}_{ss}}{\omega} x - \left(\frac{2}{\gamma-1} \right) \frac{\bar{\rho}}{c} \frac{\partial \bar{c}}{\partial s} \frac{x}{\omega} \bar{\phi}_s^{-2} \} \\
& + \hat{\phi}_s \{ -2\bar{\rho}\bar{\phi}_s x + \frac{\bar{\rho}\bar{\phi}_s\bar{\phi}_{ss}}{\omega} \theta + \left(\frac{2}{\gamma-1} \right) \frac{\bar{\rho}}{c} \frac{\partial \bar{c}}{\partial s} \frac{\theta}{\omega} \bar{\phi}_s^{-2} \} \\
& + \tilde{\phi} \{ -\left(\frac{2}{\gamma-1} \right) \frac{\bar{\rho}}{c} \frac{\partial \bar{c}}{\partial s} \bar{\phi}_s\theta + \bar{\rho}\omega x \} \\
& + \hat{\phi} \{ -\left(\frac{2}{\gamma-1} \right) \frac{\bar{\rho}}{c} \frac{\partial \bar{c}}{\partial s} \bar{\phi}_s x - \bar{\rho}\omega\theta \}] d\xi, \quad \mu = 1, j \text{ and } \ell \quad (B-45)
\end{aligned}$$

The required polynomial integrals in Eq. (B-45) are evaluated below by using Eqs. (B-30).

$$S_{ai} = \int_{\xi=0}^1 N_i d\xi = \int_{\xi=0}^1 (2\xi^2 - 3\xi + 1) d\xi = \frac{1}{6} \quad (\text{B-46})$$

$$S_{aj} = \int_{\xi=0}^1 N_j d\xi = \int_{\xi=0}^1 (2\xi^2 - \xi) d\xi = \frac{1}{6} \quad (\text{B-47})$$

$$S_{al} = \int_{\xi=0}^1 N_l d\xi = \int_{\xi=0}^1 4\xi(1-\xi) d\xi = \frac{2}{3} \quad (\text{B-48})$$

$$\begin{aligned} S_{bi} &= \int_{\xi=0}^1 N_i \phi_{\xi} d\xi = \int_{\xi=0}^1 (2\xi^2 - 3\xi + 1) [(4\xi - 3)\phi_i + (4\xi - 1)\phi_j \\ &\quad + 4(1 - 2\xi)\phi_l] d\xi \\ &= \phi_i \left(-\frac{1}{2}\right) + \phi_j \left(-\frac{1}{6}\right) + \phi_l \left(\frac{2}{3}\right) \end{aligned} \quad (\text{B-49})$$

$$\begin{aligned} S_{bj} &= \int_{\xi=0}^1 N_j \phi_{\xi} d\xi = \int_{\xi=0}^1 (2\xi^2 - \xi) [(4\xi - 3)\phi_i + (4\xi - 1)\phi_j \\ &\quad + 4(1 - 2\xi)\phi_l] d\xi \\ &= \phi_i \left(\frac{1}{6}\right) + \phi_j \left(\frac{1}{2}\right) + \phi_l \left(-\frac{2}{3}\right) \end{aligned} \quad (\text{B-50})$$

$$\begin{aligned} S_{bl} &= \int_{\xi=0}^1 N_l \phi_{\xi} d\xi = \int_{\xi=0}^1 4(\xi - \xi^2) [(4\xi - 3)\phi_i + (4\xi - 1)\phi_j \\ &\quad + 4(1 - 2\xi)\phi_l] d\xi \\ &= \phi_i \left(-\frac{2}{3}\right) + \phi_j \left(\frac{2}{3}\right) + \phi_l (0) \end{aligned} \quad (\text{B-51})$$

$$\begin{aligned} S_{ci} &= \int_{\xi=0}^1 N_i \phi d\xi = \int_{\xi=0}^1 (2\xi^2 - 3\xi + 1) [(2\xi^2 - 3\xi + 1)\phi_i + (2\xi^2 - \xi)\phi_j \\ &\quad + 4(\xi - \xi^2)\phi_l] d\xi \\ &= \phi_i \left(\frac{2}{15}\right) + \phi_j \left(-\frac{1}{30}\right) + \phi_l \left(\frac{1}{15}\right) \end{aligned} \quad (\text{B-52})$$

$$\begin{aligned}
S_{cj} &= \int_{\xi=0}^1 N_j \phi d\xi = \int_{\xi=0}^1 (2\xi^2 - \xi) [(2\xi^2 - 3\xi + 1)\phi_i + (2\xi^2 - \xi)\phi_j \\
&\quad + 4(\xi - \xi^2)\phi_\ell] d\xi \\
&= \phi_i \left(-\frac{1}{30}\right) + \phi_j \left(\frac{2}{15}\right) + \phi_\ell \left(\frac{1}{15}\right) \quad (B-53)
\end{aligned}$$

$$\begin{aligned}
S_{c\ell} &= \int_{\xi=0}^1 N_\ell \phi d\xi = \int_{\xi=0}^1 4(\xi - \xi^2) [(2\xi^2 - 3\xi + 1)\phi_i + (2\xi^2 - \xi)\phi_j \\
&\quad + 4(\xi - \xi^2)\phi_\ell] d\xi \\
&= \phi_i \left(\frac{1}{15}\right) + \phi_j \left(\frac{1}{15}\right) + \phi_\ell \left(\frac{8}{15}\right) \quad (B-54)
\end{aligned}$$

Also from Eq. (B-30) one may obtain

$$\phi_{ss} = \frac{4}{L_{ij}^2} [\phi_i + \phi_j - 2\phi_\ell] \quad (B-55)$$

Substitution of Eqs. (B-46), (B-49) and (B-52) into Eq. (B-45), for $\mu = i$ yields the desired evaluated boundary integral

$$\begin{aligned}
\tilde{\beta}_i &= \bar{r}^2 [(\bar{\phi}_r^2 - \bar{\phi}_z^2) \cos\alpha \sin\alpha - 2\bar{\phi}_r \bar{\phi}_z \sin^2\alpha] \tilde{S}_{bi} \\
&+ \frac{\bar{r}^2 L_{ij}}{\theta^2 + x^2} [\bar{c}^2 - (\bar{\phi}_z \sin\alpha - \bar{\phi}_r \cos\alpha)^2] \times \\
&\left[\tilde{\phi}_{ss} \left(-\frac{\bar{\rho}}{\omega} \times \bar{\phi}_s^2\right) S_{ai} + \hat{\phi}_{ss} \left(\frac{\bar{\rho}}{\omega} \theta \bar{\phi}_s^2\right) S_{ai} \right. \\
&\quad \left. + \left\{ -2\bar{\rho} \bar{\phi}_s \theta - \frac{\bar{\rho} \bar{\phi}_s \bar{\phi}_{ss}}{\omega} \times - \left(\frac{2}{\gamma-1}\right) \frac{\bar{\rho}}{c} \frac{\partial \bar{c}}{\partial s} \frac{x}{\omega} \bar{\phi}_s^2 \right\} \frac{\tilde{S}_{bi}}{L_{ij}} \right. \\
&\quad \left. + \left\{ -2\bar{\rho} \bar{\phi}_s x + \frac{\bar{\rho} \bar{\phi}_s \bar{\phi}_{ss}}{\omega} \theta + \left(\frac{2}{\gamma-1}\right) \frac{\bar{\rho}}{c} \frac{\partial \bar{c}}{\partial s} \frac{\theta}{\omega} \bar{\phi}_s^2 \right\} \frac{\hat{S}_{bi}}{L_{ij}} \right]
\end{aligned}$$

$$\begin{aligned}
& + \left\{ -\left(\frac{2}{\gamma-1}\right) \frac{\bar{\rho}}{c} \frac{\partial \bar{c}}{\partial s} \bar{\phi}_s \theta + \bar{\rho} \omega x \right\} \tilde{S}_{ci} \\
& + \left\{ -\left(\frac{2}{\gamma-1}\right) \frac{\bar{\rho}}{c} \frac{\partial \bar{c}}{\partial s} \bar{\phi}_s x - \bar{\rho} \omega \theta \right\} \hat{S}_{ci} \left. \right] \quad (B-56)
\end{aligned}$$

where the superscripts \sim and $\hat{\cdot}$ refer to the real and imaginary parts of Eqs. (B-49) and (B-52) respectively.

Similarly, substitution of Eqs. (B-47) (B-50) and (B-53) into Eq. (B-45) for $\mu=j$ yields

$$\begin{aligned}
\tilde{\beta}_j &= \bar{r}^2 [(\bar{\phi}_r^2 - \bar{\phi}_z^2) \cos \alpha \sin \alpha - 2\bar{\phi}_r \bar{\phi}_z \sin^2 \alpha] \tilde{S}_{bj} \\
&+ \frac{\bar{r}^2 L_{ij}}{\theta^2 + x^2} [\bar{c}^2 - (\bar{\phi}_z \sin \alpha - \bar{\phi}_r \cos \alpha)^2] \times \\
&[\bar{\phi}_{ss} (-\frac{\bar{\rho}}{\omega} x \bar{\phi}_s^2) S_{aj} + \hat{\phi}_{ss} (\frac{\bar{\rho}}{\omega} \theta \bar{\phi}_s^2) S_{aj} \\
&+ \{-2\bar{\rho} \bar{\phi}_s \theta - \frac{\bar{\rho} \bar{\phi}_s \bar{\phi}_{ss}}{\omega} x - (\frac{2}{\gamma-1}) \frac{\bar{\rho}}{c} \frac{\partial \bar{c}}{\partial s} \frac{x}{\omega} \bar{\phi}_s^{-2}\} \frac{\tilde{S}_{bj}}{L_{ij}} \\
&+ \{-2\bar{\rho} \bar{\phi}_s x + \frac{\bar{\rho} \bar{\phi}_s \bar{\phi}_{ss}}{\omega} \theta + (\frac{2}{\gamma-1}) \frac{\bar{\rho}}{c} \frac{\partial \bar{c}}{\partial s} \frac{\theta}{\omega} \bar{\phi}_s^{-2}\} \frac{\hat{S}_{bj}}{L_{ij}} \\
&+ \left\{ -\left(\frac{2}{\gamma-1}\right) \frac{\bar{\rho}}{c} \frac{\partial \bar{c}}{\partial s} \bar{\phi}_s \theta + \bar{\rho} \omega x \right\} \tilde{S}_{cj} \\
&+ \left\{ -\left(\frac{2}{\gamma-1}\right) \frac{\bar{\rho}}{c} \frac{\partial \bar{c}}{\partial s} \bar{\phi}_s x - \bar{\rho} \omega \theta \right\} \hat{S}_{cj} \quad (B-57)
\end{aligned}$$

On similar lines, substitution of Eqs. (B-48), (B-51) and (B-54) into Eq. (B-45) for $\mu = l$ yields

$$\begin{aligned}
\tilde{\beta}_\ell = & \bar{r}^2 [(\bar{\phi}_r^2 - \bar{\phi}_z^2) \cos\alpha \sin\alpha - 2\bar{\phi}_r\bar{\phi}_z \sin^2\alpha] \tilde{S}_{b\ell} \\
& + \frac{\bar{r}^2 L_{ij}}{\theta^2 + x^2} [\bar{c}^2 - (\bar{\phi}_z \sin\alpha - \bar{\phi}_r \cos\alpha)^2] , \\
& [\bar{\phi}_{ss} (-\frac{\bar{\rho}}{\omega} x \bar{\phi}_s^2) S_{a\ell} + \hat{\phi}_{ss} (\frac{\bar{\rho}}{\omega} \theta \bar{\phi}_s^2) S_{a\ell} \\
& + \{-2\bar{\rho} \bar{\phi}_s \theta - \frac{\bar{\rho} \bar{\phi}_s \bar{\phi}_{ss}}{\omega} x - (\frac{2}{\gamma-1}) \frac{\bar{\rho}}{c} \frac{\partial \bar{c}}{\partial s} \frac{x}{\omega} \bar{\phi}_s^2\} \frac{\tilde{S}_{b\ell}}{L_{ij}} \\
& + \{-2\bar{\rho} \bar{\phi}_s x + \frac{\bar{\rho} \bar{\phi}_s \bar{\phi}_{ss}}{\omega} \theta + (\frac{2}{\gamma-1}) \frac{\bar{\rho}}{c} \frac{\partial \bar{c}}{\partial s} \frac{\theta}{\omega} \bar{\phi}_s^2\} \frac{\hat{S}_{b\ell}}{L_{ij}} \\
& + \{- (\frac{2}{\gamma-1}) \frac{\bar{\rho}}{c} \frac{\partial \bar{c}}{\partial s} \bar{\phi}_s \theta + \bar{\rho} \omega x\} \tilde{S}_{c\ell} \\
& + \{- (\frac{2}{\gamma-1}) \frac{\bar{\rho}}{c} \frac{\partial \bar{c}}{\partial s} \bar{\phi}_s x - \bar{\rho} \omega \theta\} \hat{S}_{c\ell}] \tag{B-58}
\end{aligned}$$

As ϕ_i , ϕ_j and ϕ_ℓ are unknowns, $\tilde{\beta}_i$, $\tilde{\beta}_j$ and $\tilde{\beta}_\ell$ are transported to the left hand sides of the corresponding equations in (B-3) for nodes i , j and ℓ respectively.

B.5 Boundary Integral Evaluation for Fan Plane Source Condition

The sound excitation condition at the inlet fan plane could be prescribed as velocity source (Eqs. 10 and 11) or a pressure source (Eqs. 13 and 14). The boundary integral will be evaluated for both types of source conditions.

B.5.1 Evaluation of a Velocity Source Fan Plane Condition for a 3-Node Triangle (See Figure B.4)

Along the curve C α is equal to 90° and assuming that the radial component of the mean velocity is zero (which has been found to be reasonable from the mean flow computations) the boundary integral in Eq. (B-6) reduces to

$$\tilde{\beta}_\mu = \oint_C N_\mu r^2 (\bar{c}^2 - \bar{\phi}_z^2) \tilde{\phi}_n ds \quad (\text{B-59})$$

The boundary condition in terms of a radially varying velocity source is

$$\tilde{\phi}_n = \tilde{f}(r) \quad (10)$$

and

$$\hat{\phi}_n = \hat{f}(r) \quad (11)$$

since the direction of the outward normal is in the positive z direction. Using the interpolation functions given by Eq. (B-26) one may write

$$\begin{aligned} \tilde{\phi}_n &= (1-\xi)\tilde{f}_i + \xi\tilde{f}_j \\ r &= (1-\xi)r_i + \xi r_j \quad 0 \leq \xi \leq 1 \end{aligned} \quad (\text{B-60})$$

and

$$ds = (r_j - r_i)d\xi$$

Substituting Eqs. (B-60) into Eq. (B-59) one obtains

$$\tilde{\beta}_{ij} = \int_{\xi=0}^1 \frac{(1-\xi)}{(\xi)} \frac{[(1-\xi)r_j + \xi r_i]^2 (\bar{c}^2 - \bar{\phi}_2^2)}{[(1-\xi)\tilde{f}_i + \xi\tilde{f}_j]} (r_j - r_i) d\xi$$

Evaluation of the various polynomials in the above integrals yield the following forcing boundary conditions for the linear element in terms of a velocity source which form the right hand side of Eq. (B-3)

$$\begin{aligned} \tilde{\beta}_i = (r_j - r_i) (\bar{c}^2 - \bar{\phi}_2^2) \times & [\tilde{f}_i \{ r_i^2 (\frac{1}{5} + r_i r_j (\frac{1}{10}) + r_j^2 (\frac{1}{30}) \} \\ & + \tilde{f}_j \{ r_i^2 (\frac{1}{20}) + r_i r_j (\frac{1}{15}) + r_j^2 (\frac{1}{20}) \}] \end{aligned} \quad (B-61)$$

and

$$\begin{aligned} \tilde{\beta}_j = (r_j - r_i) (\bar{c}^2 - \bar{\phi}_2^2) \times & [\tilde{f}_i \{ r_i^2 (\frac{1}{20}) + r_i r_j (\frac{1}{15}) + r_j^2 (\frac{1}{20}) \} \\ & + \tilde{f}_j \{ r_i^2 (\frac{1}{30}) + r_i r_j (\frac{1}{10}) + r_j^2 (\frac{1}{5}) \}] \end{aligned} \quad (B-62)$$

B.5.2 Evaluation of a Velocity Source Fan Plane Condition for a 6-Node Triangle (See Figure B-4)

The boundary integral to be evaluated is Eq. (B-59). Making use of the interpolation functions for quadratic elements given by Eq.

(B-30) one may write

$$\begin{aligned} \tilde{\phi}_n &= (2\xi^2 - 3\xi + 1)\tilde{f}_i + (2\xi^2 - \xi)\tilde{f}_j + 4(\xi - \xi^2)\tilde{f}_l \\ r &= (1 - \xi)r_i + \xi r_j \quad 0 \leq \xi \leq 1 \\ ds &= (r_j - r_i) d\xi \end{aligned} \quad (B-63)$$

Substituting Eqs. (B-63) into Eq. (B-59) one obtains

$$\begin{aligned} \tilde{\beta}_{i,j} = \int_{\xi=0}^1 & \frac{(2\xi^2 - 3\xi + 1)}{(2\xi^2 - \xi)} \times [((1-\xi)r_i + \xi r_j)^2 (\bar{c}^2 - \bar{\phi}_z^2) \times \\ & (2\xi^2 - 3\xi + 1)\tilde{f}_i + (2\xi^2 - \xi)\tilde{f}_j + 4(\xi - \xi^2)\tilde{f}_\ell] \\ & \times (r_j - r_i) d\xi \end{aligned}$$

Evaluation of the polynomials in the above integrals leads to the following forcing boundary conditions for the quadratic element in terms of a velocity source which form the right hand side of Eq. (B-3)

$$\begin{aligned} \tilde{\beta}_i = (r_j - r_i) (\bar{c}^2 - \bar{\phi}_z^2) \times & [\tilde{f}_i \{r_i^2 (\frac{11}{105}) + r_i r_j (\frac{1}{42}) + r_j^2 (\frac{1}{210})\} \\ & + \tilde{f}_j \{r_i^2 (-\frac{1}{84}) + r_i r_j (-\frac{1}{105}) + r_j^2 (-\frac{1}{84})\} \\ & + 4\tilde{f}_\ell \{r_i^2 (\frac{1}{70}) + r_i r_j (\frac{1}{210}) + r_j^2 (-\frac{1}{420})\}] \quad (B-64) \end{aligned}$$

$$\begin{aligned} \tilde{\beta}_j = (r_j - r_i) (\bar{c}^2 - \bar{\phi}_z^2) \times & [\tilde{f}_i \{r_i^2 (-\frac{1}{84}) + r_i r_j (-\frac{1}{105}) + r_j^2 (-\frac{1}{84})\} \\ & + \tilde{f}_j \{r_i^2 (-\frac{1}{210}) + r_i r_j (\frac{1}{42}) + r_j^2 (\frac{11}{105})\} \\ & + 4\tilde{f}_\ell \{r_i^2 (-\frac{1}{420}) + r_i r_j (\frac{1}{210}) + r_j^2 (\frac{1}{70})\}] \quad (B-65) \end{aligned}$$

and

$$\begin{aligned} \tilde{\beta}_\ell = 4(r_j - r_i) (\bar{c}^2 - \bar{\phi}_z^2) \times & [\tilde{f}_i \{r_i^2 (\frac{1}{70}) + r_i r_j (\frac{1}{210}) + r_j^2 (-\frac{1}{420})\} \\ & + \tilde{f}_j \{r_i^2 (-\frac{1}{420}) + r_i r_j (\frac{1}{210}) + r_j^2 (\frac{1}{70})\} \\ & + 4\tilde{f}_\ell \{r_i^2 (\frac{1}{105}) + r_i r_j (\frac{1}{70}) + r_j^2 (\frac{1}{105})\}] \quad (B-66) \end{aligned}$$

B.5.3 Evaluation of a Pressure Source Fan Plane Condition for a 3-Node Triangle (See Figure B-4)

The boundary integral to be evaluated is given by Eq. (B-59). The

boundary condition in terms of a radially varying pressure source is

$$\tilde{p} = \tilde{g}(r) \quad (13)$$

and

$$\hat{p} = \hat{g}(r) \quad (14)$$

One could solve for $\tilde{\phi}_n/\hat{\phi}_n$ ($\tilde{\phi}_z/\hat{\phi}_z$ in this case) in terms of \tilde{p} from Eq. (8) only if $\tilde{\phi}_z \neq 0$ to obtain

$$\tilde{\phi}_z = - \frac{[\omega\hat{\phi} + \tilde{p}/\bar{\rho}]}{\tilde{\phi}_z} \quad (B-67)$$

and

$$\hat{\phi}_z = \frac{[\omega\tilde{\phi} - \hat{p}/\bar{\rho}]}{\tilde{\phi}_z} \quad (B-68)$$

Substituting Eqs. (13) and (B-67) into Eq. (B-59) one obtains,

$$\hat{\beta}_\mu = - \oint N_\mu r^2 (\bar{c}^2 - \tilde{\phi}_z^{-2}) \frac{[\omega\hat{\phi} + \tilde{g}(r)/\bar{\rho}]}{\tilde{\phi}_z} ds \quad (B-69)$$

Following the procedure indicated in Section B.5.1 and using the interpolation functions given by Eq. (B-26) one may write

$$\begin{aligned} \tilde{g} &= (1-\xi)\tilde{g}_i + \xi\tilde{g}_j \\ r &= (1-\xi)r_i + \xi r_j \end{aligned} \quad (B-70)$$

$$\hat{\phi} = (1-\xi)\hat{\phi}_i + \xi\hat{\phi}_j$$

and

$$ds = (r_j - r_i)d\xi$$

Substituting Eqs. (B-70) into Eq. (B-69) yields

$$\begin{aligned} \bar{\beta}_j = - \int_{\xi=0}^1 \frac{(1-\xi)}{(\xi)} \times [\{ (1-\xi)r_i + \xi r_j \}^2 \frac{(\bar{c}^2 - \bar{\phi}_z^2)}{\bar{\phi}_z} \times \\ \{ \omega [(1-\xi)\hat{\phi}_i + \hat{\phi}_j] \\ + \frac{1}{\rho} [(1-\xi)\tilde{g}_i + \xi\tilde{g}_j] \}] (r_j - r_i) d\xi \end{aligned}$$

Evaluating the various polynomials in the above integrals yield the following forcing boundary conditions for the linear element in terms of a pressure source which form the right hand side of Eq. (B-3) (note that the terms involving $\hat{\phi}_i$ and $\hat{\phi}_j$ are transported to the left hand side of Eq. (B-3) as they are unknown yet)

$$\begin{aligned} \bar{\beta}_i = - \frac{(\bar{c}^2 - \bar{\phi}_z^2)}{\bar{\phi}_z} (r_j - r_i) \times \\ \left[\left(\frac{\tilde{g}_i}{\rho} + \omega\hat{\phi}_i \right) \left\{ r_i^2 \left(\frac{1}{5} \right) + r_i r_j \left(\frac{1}{10} \right) + r_j^2 \left(\frac{1}{30} \right) \right\} \right. \\ \left. + \left(\frac{\tilde{g}_j}{\rho} + \omega\hat{\phi}_j \right) \left\{ r_i^2 \left(\frac{1}{20} \right) + r_i r_j \left(\frac{1}{15} \right) + r_j^2 \left(\frac{1}{20} \right) \right\} \right] \quad (B-71) \end{aligned}$$

and

$$\begin{aligned} \tilde{\beta}_j = - \frac{(\bar{c}^2 - \bar{\phi}_z^2)}{\bar{\phi}_z} (r_j - r_i) \times \\ \left[\left(\frac{\tilde{g}_i}{\rho} + \omega\hat{\phi}_i \right) \left\{ r_i^2 \left(\frac{1}{20} \right) + r_i r_j \left(\frac{1}{15} \right) + r_j^2 \left(\frac{1}{20} \right) \right\} \right. \\ \left. + \left(\frac{\tilde{g}_j}{\rho} + \omega\hat{\phi}_j \right) \left\{ r_i^2 \left(\frac{1}{30} \right) + r_i r_j \left(\frac{1}{10} \right) + r_j^2 \left(\frac{1}{5} \right) \right\} \right] \quad (B-72) \end{aligned}$$

B.5.4 Evaluation of a Pressure Source Fan Plane Condition for a 6-Node Triangle (See Figure B-4)

The boundary integral to be evaluated for the case of a pressure source is given by Eq. (B-69). Incorporating the interpolation functions for quadratic elements given by Eq. (B-30) one may write

$$\begin{aligned}
 \bar{g} &= (2\xi^2 - 3\xi + 1)\bar{g}_i + (2\xi^2 - \xi)\bar{g}_j + 4(\xi - \xi^2)\bar{g}_\ell \\
 \hat{\phi} &= (2\xi^2 - 3\xi + 1)\hat{\phi}_i + (2\xi^2 - \xi)\hat{\phi}_j + 4(\xi - \xi^2)\hat{\phi}_\ell \\
 r &= (1 - \xi)r_i + \xi r_j \\
 ds &= (r_j - r_i)d\xi
 \end{aligned}
 \tag{B-73}$$

Substituting Eqs. (B-73) into Eq. (B-69) yields

$$\begin{aligned}
 \bar{B}_{ij\ell} &= - \int_{\xi=0}^1 \frac{(2\xi^2 - 3\xi + 1)}{(2\xi^2 - \xi)} \times \left[\left\{ \left[(1 - \xi)r_i + \xi r_j \right]^2 \frac{(\bar{c}^2 - \bar{\phi}_z^2)}{\bar{\phi}_z} \times \right. \right. \\
 &\quad \left. \left\{ \omega [(2\xi^2 - 3\xi + 1)\hat{\phi}_i + (2\xi^2 - \xi)\hat{\phi}_j + 4(\xi - \xi^2)\hat{\phi}_\ell] \right. \right. \\
 &\quad \left. \left. + \frac{1}{\bar{\rho}} [(2\xi^2 - 3\xi + 1)\bar{g}_i + (2\xi^2 - \xi)\bar{g}_j + 4(\xi - \xi^2)\bar{g}_\ell] \right\} \right] \\
 &\quad \times (r_j - r_i)d\xi
 \end{aligned}$$

Evaluating the various polynomials in the above integrals yield the following forcing boundary conditions for the quadratic element in terms of a pressure source which form the right hand side of Eq. (B-3) (note that the terms involving $\hat{\phi}_i$, $\hat{\phi}_j$ and $\hat{\phi}_\ell$ are transported to the left hand side of Eq. (B-3) as they are unknown yet)

$$\tilde{\beta}_i = \frac{(\bar{c}^2 - \bar{\phi}_z^2)(r_j - r_i)}{\bar{\phi}} \times$$

$$\left[\begin{aligned} & \left(\frac{\tilde{g}_i}{\bar{\rho}} + \omega \hat{\phi}_i \right) \left\{ r_i^2 \left(\frac{11}{105} \right) + r_i r_j \left(\frac{1}{42} \right) + r_j^2 \left(\frac{1}{210} \right) \right\} \\ & + \left(\frac{\tilde{g}_j}{\bar{\rho}} + \omega \hat{\phi}_j \right) \left\{ r_i^2 \left(-\frac{1}{84} \right) + r_i r_j \left(-\frac{1}{105} \right) + r_j^2 \left(-\frac{1}{84} \right) \right\} \\ & + 4 \left(\frac{\tilde{g}_\ell}{\bar{\rho}} + \omega \hat{\phi}_\ell \right) \left\{ r_j^2 \left(\frac{1}{70} \right) + r_i r_j \left(\frac{1}{210} \right) + r_i^2 \left(-\frac{1}{420} \right) \right\} \end{aligned} \right] \quad (B-74)$$

$$\tilde{\beta}_j = -\frac{(\bar{c}^2 - \bar{\phi}_z^2)(r_j - r_i)}{\bar{\phi}_z} \times$$

$$\left[\begin{aligned} & \left(\frac{\tilde{g}_i}{\bar{\rho}} + \omega \hat{\phi}_i \right) \left\{ r_i^2 \left(-\frac{1}{84} \right) + r_i r_j \left(-\frac{1}{105} \right) + r_j^2 \left(-\frac{1}{84} \right) \right\} \\ & + \left(\frac{\tilde{g}_j}{\bar{\rho}} + \omega \hat{\phi}_j \right) \left\{ r_i^2 \left(\frac{1}{210} \right) + r_i r_j \left(\frac{1}{42} \right) + r_j^2 \left(\frac{11}{105} \right) \right\} \\ & + 4 \left(\frac{\tilde{g}_\ell}{\bar{\rho}} + \omega \hat{\phi}_\ell \right) \left\{ r_i^2 \left(-\frac{1}{420} \right) + r_i r_j \left(\frac{1}{210} \right) + r_j^2 \left(\frac{1}{70} \right) \right\} \end{aligned} \right] \quad (B-75)$$

$$\tilde{\beta}_\ell = -4 \frac{(\bar{c}^2 - \bar{\phi}_z^2)(r_j - r_i)}{\bar{\phi}_z} \times$$

$$\left[\begin{aligned} & \left(\frac{\tilde{g}_i}{\bar{\rho}} + \omega \hat{\phi}_i \right) \left\{ r_i^2 \left(\frac{1}{70} \right) + r_i r_j \left(\frac{1}{210} \right) + r_j^2 \left(-\frac{1}{420} \right) \right\} \\ & + \left(\frac{\tilde{g}_j}{\bar{\rho}} + \omega \hat{\phi}_j \right) \left\{ r_i^2 \left(-\frac{1}{420} \right) + r_i r_j \left(\frac{1}{210} \right) + r_j^2 \left(\frac{1}{70} \right) \right\} \\ & + 4 \left(\frac{\tilde{g}_\ell}{\bar{\rho}} + \omega \hat{\phi}_\ell \right) \left\{ r_j^2 \left(\frac{1}{105} \right) + r_i r_j \left(\frac{1}{70} \right) + r_i^2 \left(\frac{1}{105} \right) \right\} \end{aligned} \right] \quad (B-76)$$

B.6 Boundary Integral Evaluation for Inlet Entrance Plane

The boundary condition at the inlet entrance plane in terms of a general radially varying radiation impedance is expressed in Eqs. (34) and (35):

$$\tilde{\phi}_z (\bar{c} \theta_e - \bar{\phi}_z) - \bar{c} x_e \hat{\phi}_z = \omega \hat{\phi} + \bar{\phi}_r \tilde{\phi}_r \quad (34)$$

$$\tilde{\phi}_z \bar{c} x_e + \hat{\phi}_z (\bar{c} \theta_e - \bar{\phi}_z) = -\omega \tilde{\phi} + \bar{\phi}_r \hat{\phi}_r \quad (35)$$

B.6.1 Evaluation of Entrance Plane Radiation Condition for a 3-Node Triangle (See Figure B-5)

Noting that along the curve C α is equal to 270° the boundary integral in Eq. (B-6) reduces to

$$\tilde{\beta}_\mu = \oint_C N_\mu r^2 [\tilde{\phi}_s (-2 \bar{\phi}_r \bar{\phi}_z) + \tilde{\phi}_n (\bar{c}^2 - \bar{\phi}_z^2)] ds \quad (B-77)$$

Noting that for the configuration in Figure B-5 s and n are in the opposite directions to r and z respectively

$$\tilde{\beta}_\mu = \oint N_\mu r^2 [-2 \bar{\phi}_r \bar{\phi}_z \tilde{\phi}_r + (\bar{c}^2 - \bar{\phi}_z^2) \tilde{\phi}_z] dr \quad (B-78)$$

The boundary conditions given by Eqs. (34) and (35) can be solved for $\tilde{\phi}_z$ and $\hat{\phi}_z$ and on substitution into Eq. (B-78) yields

$$\tilde{\beta}_\mu = \oint r^2 N_\mu \left[-2 \bar{\phi}_r \bar{\phi}_z \tilde{\phi}_r + \frac{(\bar{c}^2 - \bar{\phi}_z^2)}{\Delta e} \left\{ (\bar{c} \theta_e - \bar{\phi}_z) (\omega \hat{\phi} + \bar{\phi}_r \tilde{\phi}_r) + \bar{c} x_e (-\omega \tilde{\phi} + \bar{\phi}_r \hat{\phi}_r) \right\} \right] dr \quad (B-79)$$

where $\Delta e = (\bar{c} \theta_e - \bar{\phi}_z)^2 + (\bar{c} x_e)^2$

Incorporating the interpolation functions given by Eq. (B-26) one may write

$$\begin{aligned}\phi &= (1 - \xi)\phi_i + \xi\phi_j \\ r &= (1 - \xi)r_i + \xi r_j\end{aligned}\tag{B-80}$$

Substituting Eqs. (B-80) into Eq. (B-79) one obtains

$$\begin{aligned}\beta_{ij} &= \int_{\xi=0}^1 \binom{1-\xi}{\xi} \times [(1 - \xi)r_i + \xi r_j]^2 \times \\ &\quad \left[\begin{aligned} &2\bar{\phi}_r \bar{\phi}_z (\tilde{\phi}_i - \tilde{\phi}_j) / (r_i - r_j) \\ &+ \frac{(\bar{c}^2 - \bar{\phi}_z^2)}{\Delta e} \times \left\{ (\bar{c} \theta_e - \bar{\phi}_z) (\omega \{ (1 - \xi)\hat{\phi}_i + \xi\hat{\phi}_j \} \right. \right. \\ &\quad \left. \left. + \frac{\bar{\phi}_r}{(r_i - r_j)} (\tilde{\phi}_i - \tilde{\phi}_j)) \right. \right. \\ &\quad \left. \left. + (\bar{c} \times_e (-\omega \{ (1 - \xi)\tilde{\phi}_i + \xi\tilde{\phi}_j \} \right. \right. \\ &\quad \left. \left. + \frac{\bar{\phi}_r}{(r_i - r_j)} (\hat{\phi}_i - \hat{\phi}_j)) \right\} \right] \\ &\quad \times (r_j - r_i) d\xi\end{aligned}\tag{B-81}$$

Evaluating the various polynomial integrals assuming that the mean flow variables and the radiation impedance to be constant over the element leads to

$$\begin{aligned}
\tilde{\beta}_i &= 2\bar{\phi}_r \bar{\phi}_z (\tilde{\phi}_i - \tilde{\phi}_j) \left[r_i^2 \left(\frac{1}{4} \right) + r_i r_j \left(\frac{1}{6} \right) + r_j^2 \left(\frac{1}{12} \right) \right] \\
&\quad - \frac{(\bar{c}^2 - \bar{\phi}_z^2)}{\Delta e} \times \left[(\bar{c} \theta_e - \bar{\phi}_z) \omega (r_i - r_j) \left\{ \hat{\phi}_i \left[r_i^2 \left(\frac{1}{5} \right) + r_i r_j \left(\frac{1}{10} \right) + r_j^2 \left(\frac{1}{30} \right) \right] \right. \right. \\
&\quad \quad \quad \left. \left. + \hat{\phi}_j \left[r_i^2 \left(\frac{1}{20} \right) + r_i r_j \left(\frac{1}{15} \right) + r_j^2 \left(\frac{1}{20} \right) \right] \right\} \right. \\
&\quad \quad \quad \left. + (\bar{c} \theta_e - \bar{\phi}_z) \bar{\phi}_r (\tilde{\phi}_i - \tilde{\phi}_j) \left\{ r_i^2 \left(\frac{1}{4} \right) + r_i r_j \left(\frac{1}{6} \right) + r_j^2 \left(\frac{1}{12} \right) \right\} \right. \\
&\quad \quad \quad \left. - \bar{c} x_e \omega (r_i - r_j) \left\{ \tilde{\phi}_i \left[r_i^2 \left(\frac{1}{5} \right) + r_i r_j \left(\frac{1}{10} \right) + r_j^2 \left(\frac{1}{30} \right) \right] \right. \right. \\
&\quad \quad \quad \left. \left. + \tilde{\phi}_j \left[r_i^2 \left(\frac{1}{20} \right) + r_i r_j \left(\frac{1}{15} \right) + r_j^2 \left(\frac{1}{20} \right) \right] \right\} \right. \\
&\quad \quad \quad \left. + \bar{c} x_e \bar{\phi}_r (\hat{\phi}_i - \hat{\phi}_j) \left\{ r_i^2 \left(\frac{1}{4} \right) + r_i r_j \left(\frac{1}{6} \right) + r_j^2 \left(\frac{1}{12} \right) \right\} \right] \quad (B-82)
\end{aligned}$$

and

$$\begin{aligned}
\tilde{\beta}_j &= 2\bar{\phi}_r \bar{\phi}_z (\tilde{\phi}_i - \tilde{\phi}_j) \left[r_i^2 \left(\frac{1}{12} \right) + r_i r_j \left(\frac{1}{6} \right) + r_j^2 \left(\frac{1}{4} \right) \right] \\
&\quad - \frac{(\bar{c}^2 - \bar{\phi}_z^2)}{\Delta e} \times \left[(\bar{c} \theta_e - \bar{\phi}_z) \omega (r_i - r_j) \left\{ \hat{\phi}_i \left[r_i^2 \left(\frac{1}{20} \right) + r_i r_j \left(\frac{1}{15} \right) + r_j^2 \left(\frac{1}{20} \right) \right] \right. \right. \\
&\quad \quad \quad \left. \left. + \hat{\phi}_j \left[r_i^2 \left(\frac{1}{30} \right) + r_i r_j \left(\frac{1}{10} \right) + r_j^2 \left(\frac{1}{5} \right) \right] \right\} \right. \\
&\quad \quad \quad \left. + (\bar{c} \theta_e - \bar{\phi}_z) \bar{\phi}_r (\tilde{\phi}_i - \tilde{\phi}_j) \left\{ r_i^2 \left(\frac{1}{12} \right) + r_i r_j \left(\frac{1}{6} \right) + r_j^2 \left(\frac{1}{4} \right) \right\} \right. \\
&\quad \quad \quad \left. - (\bar{c} x_e \omega (r_i - r_j) \left\{ \tilde{\phi}_i \left[r_i^2 \left(\frac{1}{20} \right) + r_i r_j \left(\frac{1}{15} \right) + r_j^2 \left(\frac{1}{20} \right) \right] \right. \right. \\
&\quad \quad \quad \left. \left. + \tilde{\phi}_j \left[r_i^2 \left(\frac{1}{30} \right) + r_i r_j \left(\frac{1}{10} \right) + r_j^2 \left(\frac{1}{5} \right) \right] \right\} \right. \\
&\quad \quad \quad \left. + \bar{c} x_e \bar{\phi}_r (\hat{\phi}_i - \hat{\phi}_j) \left\{ r_i^2 \left(\frac{1}{12} \right) + r_i r_j \left(\frac{1}{6} \right) + r_j^2 \left(\frac{1}{4} \right) \right\} \right] \quad (B-83)
\end{aligned}$$

Since the acoustic potentials are unknown yet, $\tilde{\beta}_i$ and $\tilde{\beta}_j$ are transported to the left hand sides of the corresponding equations in (B-3) for nodes i and j respectively.

B.6.2 Evaluation of Entrance Plane Radiation Condition for a 6-Node Triangle (See Figure B-5)

The boundary integral to be evaluated is given by Eq. (B-79).

Incorporating the interpolation functions given by Eqs. (B-30) one may write

$$\begin{aligned}\phi &= (2\xi^2 - 3\xi + 1)\phi_i + (2\xi^2 - \xi)\phi_j + 4(\xi - \xi^2)\phi_\ell \\ r &= (1 - \xi)r_i + \xi r_j\end{aligned}\tag{B-84}$$

Substituting Eqs. (B-84) into Eq. (B-79) one obtains

$$\tilde{\beta}_i = \int_{\xi=0}^1 \frac{(2\xi^2 - 3\xi + 1)}{4(\xi - \xi^2)} \times \left[\frac{(\bar{c}^2 - \bar{\phi}_z^2)}{\Delta e} \{ (\bar{c} \theta_e - \bar{\phi}_z)(\omega\hat{\phi} + \bar{\phi}_r\tilde{\phi}_r) + \bar{c} \times_e (-\omega\tilde{\phi} + \bar{\phi}_r\hat{\phi}_r) \} \right. \\ \left. - 2\bar{\phi}_r\bar{\phi}_z\tilde{\phi}_r \right] r^2 dr$$

Evaluating the various polynomials in the above integrals yields

$$\begin{aligned}\tilde{\beta}_i &= -\frac{\bar{r}^2(r_i - r_j)(\bar{c}^2 - \bar{\phi}_z^2)}{\Delta e} \times \\ &\left[(\bar{c} \theta_e - \bar{\phi}_z) \left\{ \omega \left[\hat{\phi}_i \left(\frac{2}{15} \right) + \phi_j \left(-\frac{1}{30} \right) + \phi_\ell \left(\frac{1}{15} \right) \right] \right. \right. \\ &\quad \left. \left. - \frac{\bar{\phi}_r}{(r_i - r_j)} \left[\tilde{\phi}_i \left(-\frac{1}{2} \right) + \tilde{\phi}_j \left(-\frac{1}{6} \right) + \tilde{\phi}_\ell \left(\frac{2}{3} \right) \right] \right\} \right. \\ &\quad \left. - \bar{c} \times_e \left\{ \omega \left[\tilde{\phi}_i \left(\frac{2}{15} \right) + \tilde{\phi}_j \left(-\frac{1}{30} \right) + \tilde{\phi}_\ell \left(\frac{1}{15} \right) \right] \right. \right. \\ &\quad \left. \left. + \frac{\bar{\phi}_r}{(r_i - r_j)} \left[\hat{\phi}_i \left(-\frac{1}{2} \right) + \hat{\phi}_j \left(-\frac{1}{6} \right) + \hat{\phi}_\ell \left(\frac{2}{3} \right) \right] \right\} \right]\end{aligned}$$

$$-2\bar{r}^2 \bar{\phi}_r \bar{\phi}_z [\tilde{\phi}_i(-\frac{1}{2}) + \tilde{\phi}_j(-\frac{1}{6}) + \tilde{\phi}_\ell(\frac{2}{3})] \quad (\text{B-}$$

where $\bar{r} = (r_i + r_j)/2$

$$\begin{aligned} \tilde{\beta}_j = & - \frac{\bar{r}^2 (r_i - r_j) (\bar{c}^2 - \bar{\phi}_z^2)}{\Delta e} \times \\ & \left[(\bar{c} \theta_e - \bar{\phi}_z) \left\{ \omega [\hat{\phi}_i(-\frac{1}{30}) + \hat{\phi}_j(\frac{2}{15}) + \hat{\phi}_\ell(\frac{1}{15})] \right. \right. \\ & \quad \left. \left. - \frac{\bar{\phi}_r}{(r_i - r_j)} [\tilde{\phi}_i(\frac{1}{6}) + \tilde{\phi}_j(\frac{1}{2}) + \phi_\ell(-\frac{2}{3})] \right\} \right. \\ & \left. - \bar{c} \times_e \left\{ \omega [\tilde{\phi}_i(-\frac{1}{30}) + \tilde{\phi}_j(-\frac{2}{15}) + \tilde{\phi}_\ell(\frac{1}{15})] \right. \right. \\ & \quad \left. \left. + \frac{\bar{\phi}_r}{(r_i - r_j)} [\hat{\phi}_i(\frac{1}{6}) + \hat{\phi}_j(\frac{1}{2}) + \hat{\phi}_\ell(-\frac{2}{3})] \right\} \right] \\ & - 2\bar{r}^2 \bar{\phi}_r \bar{\phi}_z [\tilde{\phi}_i(\frac{1}{6}) + \tilde{\phi}_j(\frac{1}{2}) + \tilde{\phi}_\ell(-\frac{2}{3})] \end{aligned} \quad (\text{B-86})$$

and

$$\begin{aligned} \tilde{\beta}_\ell = & - \frac{\bar{r}^2 (r_i - r_j) (\bar{c}^2 - \bar{\phi}_z^2)}{\Delta e} \times \\ & \left[(\bar{c} \theta_e - \bar{\phi}_z) \left\{ \omega [\hat{\phi}_i(\frac{1}{15}) + \hat{\phi}_j(\frac{1}{15}) + \hat{\phi}_\ell(\frac{8}{15})] \right. \right. \\ & \quad \left. \left. - \frac{\bar{\phi}_r}{(r_i - r_j)} [\tilde{\phi}_i(-\frac{2}{3}) + \tilde{\phi}_j(\frac{2}{3}) + \tilde{\phi}_\ell(0)] \right\} \right. \\ & \left. - \bar{c} \times_e \left\{ \omega [\tilde{\phi}_i(\frac{1}{15}) + \tilde{\phi}_j(\frac{1}{15}) + \tilde{\phi}_\ell(\frac{8}{15})] \right. \right. \\ & \quad \left. \left. + \frac{\bar{\phi}_r}{(r_i - r_j)} [\hat{\phi}_i(-\frac{2}{3}) + \hat{\phi}_j(\frac{2}{3}) + \hat{\phi}_\ell(0)] \right\} \right] \\ & - 2\bar{r}^2 \bar{\phi}_r \bar{\phi}_z [\tilde{\phi}_i(-\frac{2}{3}) + \tilde{\phi}_j(\frac{2}{3}) + \tilde{\phi}_\ell(0)] \end{aligned} \quad (\text{B-87})$$

Since the acoustic potentials are unknown yet, $\tilde{\beta}_i$, $\tilde{\beta}_j$ and $\tilde{\beta}_\ell$ are transported to the left hand sides of the corresponding equations in (B-3) for nodes i , j and ℓ respectively.

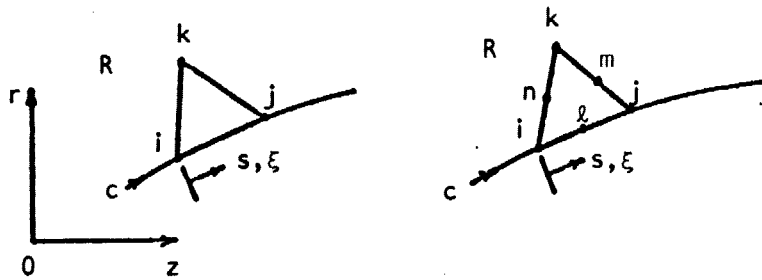


Figure B-3. Linear and Quadratic Elements on Inlet Wall.

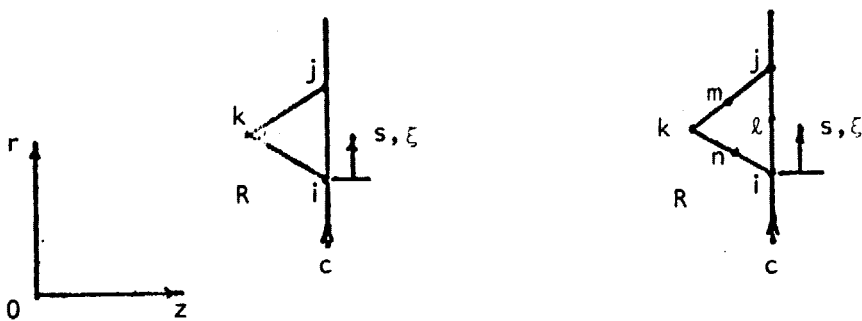


Figure B-4. Linear and Quadratic Elements on Fan Plane.

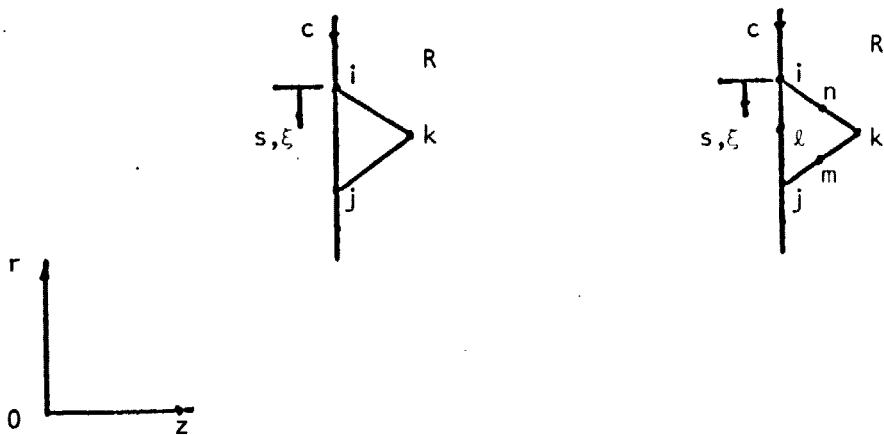


Figure B-5. Linear and Quadratic Elements on Inlet Entrance Plane.

APPENDIX C

ACOUSTIC INTENSITY AND POWER CALCULATIONS

C.1 Derivation of Equation (64) for Acoustic Intensity

Recall that the assumptions of the theoretical model are: fluid is inviscid, non-heat conducting and satisfies the ideal gas law. The fluid flow is isentropic. Hence the steady state stagnation enthalpy is constant. The present objective is to evaluate an expression for acoustic intensity for a wave propagating in a flow with gradients.

For any closed surface S fixed in flow the total outward energy flow, E is

$$E = \int_S \underline{N} \cdot \hat{n} \, ds \quad (C-1)$$

where \underline{N} is the energy flux vector
and \hat{n} is the unit outward normal vector.

And

$$\underline{N} = J \underline{m} \quad (C-2)$$

where J is the specific stagnation enthalpy
and \underline{m} is the mass flux vector.

Substituting Eq. (C-2) into Eq. (C-1) and taking the time average of the equation one obtains

$$\langle E \rangle = \left\langle \int_S J \underline{m} \cdot \hat{n} \, ds \right\rangle \quad (C-3)$$

where the operator $\langle () \rangle = \lim_{T \rightarrow \infty} \frac{1}{2T} \int_{-T}^T () dt$

Since S is fixed the time averaging operator and the integral operator can be exchanged and noting that \hat{n} is not a function of time Eq. (C-3) reduces to

$$\langle E \rangle = \int_S \langle J_{\underline{m}} \rangle \cdot \hat{n} dS \quad (C-4)$$

The energy flux vector, \underline{N} , is a second order quantity in terms of acoustic perturbations. Hence in the development of an expression for \underline{N} one needs to retain terms up to second order in J and \underline{m} individually rather than considering \underline{N} as made up of product of only first order perturbations. This subtle point has been noted by Zinn³⁶ in the context of evaluating acoustic losses in short rocket motor nozzles. By performing time averaging operation on the continuity equation containing terms up to second order perturbations and also assuming periodic first order perturbations, Zinn has shown that the time averaged value of the second order perturbation of \underline{m} is a constant that can be chosen to be equal to zero without any loss of generality. An identical operation on Euler's equation for the case of compressible irrotational flows shows that the time averaged value of the second order perturbation of J is also zero.³⁶ Hence, the contribution of second order perturbations of J and \underline{m} towards the time averaged acoustic intensity is zero. Subject to this qualification, one can express J and \underline{m} as composed of only a steady state component and a periodic acoustic component, i.e.,

$$J(\underline{x}, t) = \bar{J}(\underline{x}) + J'(\underline{x}, t)$$

and

(C-5)

$$\underline{m}(\underline{x}, t) = \bar{\underline{m}}(\underline{x}) + \underline{m}'(\underline{x}, t)$$

Under the isentropic assumption made the steady state stagnation enthalpy \bar{J} is a constant and not a function of the position vector, \underline{x} . Substituting Eq. (C-5) into Eq. (C-4) and noting that \bar{J} and $\bar{\underline{m}}$ are independent of time and that the time averaged values of the periodic acoustic quantities are equal to zero, one obtains

$$\langle E \rangle = \bar{J} \int_S \bar{\underline{m}} \cdot \hat{n} \, dS + \int_S \langle \bar{J}' \underline{m}' \rangle \cdot \hat{n} \, dS \quad (C-6)$$

The continuity equation corresponding to the steady state quantities in the integral form reads

$$\int_S \bar{\underline{m}} \cdot \hat{n} \, dS = 0 \quad (C-7)$$

Hence the first term in Eq. (C-6) contributes nothing towards the outward energy flow, that is

$$\langle E \rangle = \int_S \langle \bar{J}' \underline{m}' \rangle \cdot \hat{n} \, dS \quad (C-8)$$

Since $\bar{J} \bar{\underline{m}}$ corresponds to intensity in the absence of acoustic perturbations one may define the time averaged acoustic intensity as the difference in intensities $\langle \underline{J} \underline{m} \rangle$ and $\bar{J} \bar{\underline{m}}$, that is

$$\langle I_{\text{acoustic}} \rangle = \langle \underline{J} \underline{m} \rangle - \bar{J} \bar{\underline{m}} = \langle \bar{J}' \underline{m}' \rangle \quad (C-9)$$

The specific stagnation enthalpy J is given by

$$J = h + \frac{1}{2} |\underline{v}|^2 \quad (C-10)$$

where h is the specific enthalpy

and $\frac{1}{2} |\underline{v}|^2$ is the specific kinetic energy.

An acoustic perturbation of Eq. (C-10) yields

$$J' = h' + \bar{\underline{v}} \cdot \underline{v}' \quad (C-11)$$

A similar acoustic perturbation of mass flux vector \underline{m} yields

$$\underline{m}' = \bar{\rho} \underline{v}' + \rho' \bar{\underline{v}} \quad (C-12)$$

The classical Maxwell's relations³⁷ for the isentropic situation yield

$$h' = \left(\frac{\partial h}{\partial p} \right)_s p' = \frac{p'}{\rho}$$

and

$$p' = \left(\frac{\partial p}{\partial s} \right)_s s' = \frac{p'}{c^2}$$

(C-13)

where s is the specific entropy of the system.

Substituting Eqs. (C-11) - (C-13) into Eq. (C-9) yields the desired expression for the time averaged acoustic intensity

$$\langle \underline{I}_{\text{acoustic}} \rangle = \langle p' \underline{v}' + \frac{\rho'^2 \bar{\underline{v}}}{\rho c^2} + \bar{\rho} (\bar{\underline{v}} \cdot \underline{v}') \underline{v}' + (\bar{\underline{v}} \cdot \underline{v}') \frac{\rho'}{c^2} \bar{\underline{v}} \rangle \quad (C-14)$$

For the case of an irrotational and uniform entropy flow, the mean and acoustic velocities $\bar{\underline{v}}$ and \underline{v}' in Eq. (C-14) can be expressed as gradients

of mean and acoustic potentials $\bar{\phi}$ and ϕ' respectively. Hence the acoustic intensity in the direction of a unit vector \underline{a} is

$$\begin{aligned} \langle I_{\text{acoustic}} \rangle \cdot \underline{a} = & \langle \rho' \nabla \phi' \rangle \cdot \underline{a} + \frac{\nabla \bar{\phi} \cdot \underline{a}}{\bar{\rho} \bar{c}^2} \langle p'^2 \rangle \\ & + \bar{\rho} [\nabla \bar{\phi} \cdot \langle \nabla \phi' \nabla \phi' \rangle] \cdot \underline{a} + \frac{(\nabla \bar{\phi} \cdot \underline{a})}{\bar{c}^2} \nabla \bar{\phi} \cdot \langle p' \nabla \phi' \rangle \quad (64) \end{aligned}$$

which is the desired relationship.

The time averaged energy flow across a surface S is then

$$\langle E \rangle = \int_S \langle I_{\text{acoustic}} \rangle \cdot \hat{n} \, dS \quad (65)$$

C.2 Evaluation of Acoustic Power at the Inlet Boundaries and dB Calculations

Equation (65) has to be evaluated at the fan plane, inlet entrance plane and the inlet walls to determine the acoustic power input into the inlet, the acoustic power output of the inlet and the acoustic power absorbed by the lined inlet walls respectively.

In this context, it can be shown easily that for two sinusoidal functions given by

$$q = \text{Re}[Q e^{-i\omega t}]$$

and

$$r = \text{Re}[R e^{-i\omega t}]$$

where $\text{Re}[] = \text{Real part of } []$,

Q and R are complex quantities given by

$$Q = \tilde{Q} + i\hat{Q} \quad \text{and} \quad R = \tilde{R} + i\hat{R}$$

the time averaged value of qr is

$$\langle qr \rangle = \frac{1}{2} \text{Re}[Q^* R] \quad (\text{C-15})$$

where R^* is the complex conjugate of R.

This result is used repeatedly in evaluating the various time averages occurring in Eq. (64).

C.2.1 Acoustic Power Input into the Inlet at the Fan Plane

At the fan plane the unit outward normal points in the positive Z-direction. Hence the acoustic power input is

$$\langle E \rangle_{\text{input}} = \int_{\text{Fan plane}} \langle I_{\text{acoustic}} \rangle_2 \, dS \quad (\text{C-16})$$

Since the integrand is independent of the azimuthal angle θ , Eq. (C-16) can be integrated with respect to θ to yield

$$\langle E \rangle_{\text{input}} = 2\pi \int_{r_{if}}^{r_{of}} \langle I_{\text{acoustic}} \rangle_2 \, r \, dr \quad (\text{C-17})$$

where r_{if} and r_{of} are the inner and outer radii at the fan plane respectively. Application of Eq. (C-15) and (64) along the positive Z-direction yields

$$\begin{aligned} \langle I_{\text{acoustic}} \rangle_2 = \frac{1}{2} \left[\left(1 + \frac{\bar{\phi}_z}{c^2} \right) (\bar{p} \hat{\phi}_z + \hat{p} \bar{\phi}_z) + \frac{\bar{\phi}_z}{\rho c^2} (\bar{p}^2 + \hat{p}^2) + \bar{\rho} \bar{\phi}_z (\hat{\phi}_z^2 + \bar{\phi}_z^2) \right. \\ \left. + \bar{\rho} \bar{\phi}_r (\hat{\phi}_r \hat{\phi}_z + \hat{\phi}_r \bar{\phi}_z) + \frac{\bar{\phi}_r \bar{\phi}_z}{c^2} (\bar{p} \hat{\phi}_r + \hat{p} \bar{\phi}_r) \right] \quad (\text{C-18}) \end{aligned}$$

Equation (C-17) is evaluated for the finite elements located on the fan plane by calculating the time averaged acoustic intensity in terms of the element centroidal values of the acoustic variables for the sake of simplicity. Hence the acoustic intensity as calculated by Eq. (C-18) over each such element is constant and can be taken out of the integral in Eq. (C-17). Hence the contribution of one element located on the fan plane to Eq. (C-17) is (see Figure B-4)

$$\begin{aligned} \langle E^e \rangle_{\text{input}} &= 2\pi \langle I_{\text{acoustic}}^e \rangle_z \int_{r=r_i}^{r_j} r \, dr \\ &= \pi \langle I_{\text{acoustic}}^e \rangle_z (r_j^2 - r_i^2) \end{aligned} \quad (\text{C-19})$$

Summation of Eq. (C-19) for all the elements located on the fan plane yields the total time averaged acoustic power input, i.e.,

$$\langle E \rangle_{\text{input}} = \sum_{e=1}^{N_F} \langle E^e \rangle_{\text{input}} \quad (\text{C-20})$$

where N_F is the number of elements located on the fan plane.

C.2.2 Acoustic Power Output at the Inlet Entrance Plane

At the inlet entrance plane the unit outward normal points in the negative Z-direction. Hence the acoustic power output is

$$\langle E \rangle_{\text{output}} = - \int_{\text{Entrance plane}} \langle I_{\text{acoustic}} \rangle_z \, dS \quad (\text{C-21})$$

Again Eq. (C-21) can be integrated with respect to θ to yield

$$\langle E \rangle_{\text{output}} = -2\pi \int_{r_{ie}}^{r_{oe}} \langle I_{\text{acoustic}} \rangle_z r dr \quad (\text{C-22})$$

where r_{ie} and r_{oe} are the inner and outer radii at the inlet entrance plane respectively.

Equation (C-22) is evaluated for the finite elements located on the entrance plane by calculating the time averaged acoustic intensity as in Section C.2.1. Hence the contribution of one element located on the entrance plane to Eq. (C-22) is (see Figure B-5)

$$\begin{aligned} \langle E^e \rangle_{\text{output}} &= -2\pi \langle I_{\text{acoustic}}^e \rangle_z \int_{r_j}^{r_i} r dr \\ &= -\pi \langle I_{\text{acoustic}}^e \rangle_z (r_i^2 - r_j^2) \end{aligned} \quad (\text{C-23})$$

Summing of Eq. (C-23) for all elements located on the entrance plane yields the total time averaged acoustic power output, i.e.,

$$\langle E \rangle_{\text{output}} = \sum_{e=1}^{N_e} \langle E^e \rangle_{\text{output}} \quad (\text{C-24})$$

where N_e is the number of elements located on the inlet entrance plane.

C.2.3 Acoustic Power Absorbed at the Inlet Walls

The acoustic power absorbed by the inlet walls is

$$\langle E \rangle_{\text{absorbed}} = \int_{\text{Inlet wall}} \langle I_{\text{acoustic}} \rangle_n dS \quad (\text{C-25})$$

Since the integrand is independent of θ , Eq. (C-25) can be integrated with respect to θ to yield (see Figure B-3)

$$\langle E \rangle_{\text{absorbed}} = 2\pi \int_s \langle I_{\text{acoustic}} \rangle_n r ds \quad (\text{C-26})$$

where s is the natural coordinate along the inlet wall. Substituting Eq. (B-4) into Eq. (C-26) leads to the expression for $\langle E \rangle_{\text{absorbed}}$ for a single element located on the inlet wall

$$\langle E^e \rangle_{\text{absorbed}} = 2\pi \int_{\xi=0}^1 \langle I_{\text{acoustic}}^e \rangle_n [(1-\xi)r_i + \xi r_j] L_{ij} d\xi \quad (\text{C-27})$$

Noting that at the inlet walls the normal component of the mean flow velocity is zero, Eq. (64) reduces to the following expression for the acoustic intensity normal to the inlet wall

$$\langle I_{\text{acoustic}} \rangle_n = \langle p' \frac{\partial \phi'}{\partial n} + \bar{\rho} (\nabla \bar{\phi} \cdot \nabla \phi') \frac{\partial \phi'}{\partial n} \rangle \quad (\text{C-28})$$

Evaluating the vector dot product in terms of the natural coordinates ($s \cdot n$) and using Eq. (C-15), Eq. (C-28) reduces to

$$\langle I_{\text{acoustic}} \rangle_n = \frac{1}{2} [(\bar{p} \bar{\phi}_n + \hat{p} \hat{\phi}_n) + \bar{\rho} \bar{\phi}_s (\bar{\phi}_s \bar{\phi}_n + \hat{\phi}_s \hat{\phi}_n)] \quad (\text{C-29})$$

Equation (C-27) is evaluated for the finite elements located on the inlet wall by calculating the normal component of the time averaged acoustic intensity in terms of the centroidal values of the acoustic variables using Eq. (C-29). Hence the contribution of one element located on the inlet wall to Eq. (C-27) is

$$\begin{aligned} \langle E^e \rangle_{\text{absorbed}} &= 2\pi \langle I_{\text{acoustic}}^e \rangle_n \int_{\xi=0}^1 [(1-\xi)r_i + \xi r_j] L_{ij} d\xi \\ &= \pi \langle I_{\text{acoustic}}^e \rangle_n L_{ij} (r_i + r_j) \end{aligned} \quad (\text{C-30})$$

Summing of Eq. (C-30) for all elements located on the inlet wall yields the total time averaged acoustic power absorbed by the inlet wall, i.e.,

$$\langle E \rangle_{\text{absorbed}} = \sum_{e=1}^{N_{\omega}} \langle E^e \rangle_{\text{absorbed}} \quad (\text{C-31})$$

where N_{ω} is the number of elements located on the upper and lower walls of the inlet. An obvious conclusion from Eq. (C-29) is, the normal component of the acoustic intensity at a hard wall is zero since $\tilde{\phi}_n$ and $\hat{\phi}_n$ are prescribed to be zero there. Hence for a hard wall the acoustic power absorbed is zero.

C.2.4 DB Calculations and the Principle of Conservation of Acoustic Energy

Once the energy fluxes at the inlet boundaries are determined by Eqs. (C-20), (C-24) and (C-31) the dB calculations are performed to estimate the effectiveness of a liner. The $\text{dB}_{\text{reduction}}$ for a liner is defined by

$$\text{dB}_{\text{reduction}} = 10 \log_{10} \left| \frac{\langle E \rangle_{\text{input}}}{\langle E \rangle_{\text{output}}} \right| \quad (66)$$

The principle of conservation of acoustic energy states that the acoustic power input should equal the sum of acoustic power output and the acoustic power absorbed, i.e.,

$$\langle E \rangle_{\text{input}} = \langle E \rangle_{\text{output}} + \langle E \rangle_{\text{absorbed}} \quad (\text{C-32})$$

For a hard walled inlet Eq. (C-32) reduces to

$$\langle E \rangle_{\text{input}} = \langle E \rangle_{\text{output}}$$

and hence

$$\text{dB reduction} \left| \begin{array}{l} \text{Hard walled} \\ \text{Inlet} \end{array} \right. = 0 \quad (\text{C-33})$$

APPENDIX D

GEOMETRICAL AND MEAN FLOW DATA FOR THE QCSEE AND
BELLMOUTH INLETS

The quadratic triangulization scheme is used for predicting the attenuation of sound due to liners on the inlets' upper walls (see Figures 4a and 4b). As one may observe the total number of nodes equals 289 and the total number of elements equals 126 for both the QCSEE and Bellmouth inlet triangulization schemes. The total number of corner nodes equals 82 and the total number of mid-side nodes equals 207. The geometry of the inlets is specified in terms of the corner node number, IL and its Z- and r- coordinates, Z(IL) and R(IL) respectively. The "compressible" two dimensional axisymmetric mean flow at the corner node number, IL in terms of the axial and radial velocity components, $\bar{\phi}_z(IL)$ and $\bar{\phi}_r(IL)$ correspond to an average exit Mach number of 0.52. The free stream Mach number, M_∞ equals 0.12 for the QCSEE inlet and M is 0.0 for the Bellmouth inlet.

Table D-1. Geometrical and Mean Flow Data for
the QCSEE Inlet

($M_\infty = 0.12$, $M_e = 0.52$; See Figure 4-a)

l_L	Z(IL)	R(IL)	ϕ_z (IL)	ϕ_r (IL)
1	0.0	1.0500	0.0000	-0.5387
3	0.0	0.7875	0.4364	-0.2204
5	0.0	0.5250	0.4401	-0.0958
7	0.0	0.2625	0.4330	-0.0276
9	0.0	0.0000	0.4315	0.0000
20	0.1	0.9182	0.6271	-0.3934
22	0.1	0.8034	0.5993	-0.3026
24	0.1	0.5739	0.5166	-0.1129
26	0.1	0.3443	0.4850	-0.0415
28	0.1	0.1148	0.4766	0.0057
30	0.1	0.0000	0.4752	0.0000
41	0.2	0.8768	0.7618	-0.2545
43	0.2	0.6576	0.6283	-0.1264
45	0.2	0.4384	0.5484	-0.0577
47	0.2	0.2192	0.5232	-0.0011
49	0.2	0.0000	0.5146	0.0000
60	0.3	0.8564	0.8215	-0.1358
62	0.3	0.7494	0.7196	-0.0868
64	0.3	0.5353	0.6047	-0.0502
66	0.3	0.3212	0.5646	-0.0101
68	0.3	0.1071	0.5600	0.0400
70	0.3	0.0000	0.5590	0.0000
81	0.4	0.8500	0.7894	-0.0205
83	0.4	0.6375	0.6930	-0.0353
85	0.4	0.4250	0.6146	-0.0234
87	0.4	0.2125	0.5845	0.0115
89	0.4	0.0000	0.5759	0.0000

Table D-1. (Continued)

l_L	Z(IL)	R(IL)	ϕ_z (IL)	ϕ_r (IL)
100	0.5	0.8516	0.7395	0.0188
102	0.5	0.7452	0.7059	0.0037
104	0.5	0.5323	0.6355	-0.0086
106	0.5	0.3194	0.6131	-0.0042
108	0.5	0.1065	0.5948	0.0505
110	0.5	0.0000	0.5942	0.0000
121	0.7	0.8638	0.6648	0.0550
123	0.7	0.6479	0.6340	0.0291
125	0.7	0.6319	0.6067	0.0185
127	0.7	0.2160	0.5892	0.0196
129	0.7	0.0000	0.5865	0.0000
140	0.9	0.8847	0.5969	0.0710
142	0.9	0.7741	0.5970	0.0603
144	0.9	0.5529	0.5746	0.0408
146	0.9	0.3318	0.5621	0.0346
148	0.9	0.1106	0.5472	0.0625
150	0.9	0.0000	0.5449	0.0000
161	1.1	0.9109	0.5401	0.0751
163	1.1	0.6832	0.5425	0.0616
165	1.1	0.6555	0.5246	0.0559
167	1.1	0.2277	0.4953	0.0491
169	1.1	0.0000	0.4608	0.0000
180	1.3	0.9389	0.5023	0.0699
182	1.3	0.8215	0.5131	0.0680
184	1.3	0.5868	0.5005	0.0773
186	1.3	0.3521	0.4734	0.0900
188	1.3	0.1174	0.3461	0.1180
190	1.3	0.0000	0.2284	0.0000

Table D-1. (Continued)

I_L	$Z(IL)$	$R(IL)$	$\bar{\phi}_z(IL)$	$\bar{\phi}_r(IL)$
201	1.4	0.9525	0.4876	0.0647
203	1.4	0.7144	0.5042	0.0719
205	1.4	0.4763	0.4880	0.0988
207	1.4	0.2381	0.3829	0.1657
209	1.4	0.0000	0.0000	0.0000
220	1.5	0.9652	0.4817	0.0593
222	1.5	0.8722	0.4985	0.0595
224	1.5	0.6862	0.5067	0.0691
226	1.5	0.5002	0.5036	0.0981
228	1.5	0.3142	0.4433	0.2121
230	1.5	0.2212	0.3765	0.3361
241	1.6	0.9765	0.4748	0.0524
243	1.6	0.8069	0.4999	0.0540
245	1.6	0.6373	0.5142	0.0763
247	1.6	0.4676	0.5192	0.1474
249	1.6	0.2980	0.4970	0.2980
260	1.8	0.9935	0.4750	0.0316
262	1.8	0.9165	0.4853	0.0305
264	1.8	0.7624	0.5127	0.0391
266	1.8	0.6083	0.5408	0.0626
268	1.8	0.4542	0.5977	0.1282
270	1.8	0.3771	0.6177	0.1583
281	2.0	1.000	0.5053	0.0000
283	2.0	0.8500	0.5124	0.0108
285	2.0	0.7000	0.5316	0.0205
287	2.0	0.5500	0.5634	0.0251
289	2.0	0.4000	0.5887	0.0000

Table D-2. Geometrical and Mean Flow Data for
the Bellmouth Inlet

($M_\infty = 0.0$, $M_e = 0.52$; See Figure 4-b)

l_L	$Z(IL)$	$R(IL)$	$\bar{\phi}_z(IL)$	$\bar{\phi}_r(IL)$
1	0.0000	1.0000	0.0000	-0.2020
3	0.0000	0.7500	0.2239	-0.1860
5	0.0000	0.5000	0.2460	-0.0885
7	0.0000	0.2500	0.2459	-0.0381
9	0.0000	0.0000	0.2457	0.0000
20	0.0690	0.8147	0.1770	-0.2932
22	0.0690	0.7129	0.2891	-0.1684
24	0.0690	0.5092	0.2764	-0.0898
26	0.0690	0.3055	0.2690	-0.0466
28	0.0690	0.1018	0.2655	-0.0146
30	0.0690	0.0000	0.2620	0.0000
41	0.1379	0.7716	0.3492	-0.1856
43	0.1379	0.5787	0.3144	-0.1033
45	0.1379	0.3858	0.2956	-0.0581
47	0.1379	0.1929	0.2868	-0.0265
49	0.1379	0.0000	0.2781	0.0000
60	0.2759	0.7198	0.3908	-0.0978
62	0.2759	0.6298	0.3820	-0.0856
64	0.2759	0.4499	0.3452	-0.0546
66	0.2759	0.2699	0.3267	-0.0306
68	0.2759	0.0900	0.3191	-0.0099
70	0.2759	0.0000	0.3115	0.0000
81	0.4138	0.6897	0.4306	-0.0537
83	0.4138	0.5173	0.3853	-0.0361
85	0.4138	0.3449	0.3597	-0.0261
87	0.4138	0.1724	0.3478	-0.0134
89	0.4138	0.0000	0.3358	0.0000

Table D-2. (Continued)

l_L	$Z(l_L)$	$R(l_L)$	$\bar{\phi}_z(l_L)$	$\bar{\phi}_r(l_L)$
100	0.5517	0.6897	0.3818	0.0000
102	0.5517	0.6035	0.3984	-0.0057
104	0.5517	0.4311	0.3808	-0.0150
106	0.5517	0.2586	0.3682	-0.0113
108	0.5517	0.0862	0.3621	-0.0040
110	0.5517	0.0000	0.3559	0.0000
121	0.8276	0.6897	0.3640	0.0000
123	0.8276	0.5173	0.3858	-0.0011
125	0.8276	0.3449	0.3811	-0.0011
127	0.8276	0.1724	0.3762	-0.0005
129	0.8276	0.0000	0.3714	0.0000
140	1.1034	0.6897	0.3661	0.0000
142	1.1034	0.6035	0.3903	0.0018
144	1.1034	0.4311	0.3852	0.0075
146	1.1034	0.2586	0.3743	0.0110
148	1.1034	0.0862	0.3618	0.0061
150	1.1034	0.0000	0.3492	0.0000
161	1.2414	0.6897	0.3810	0.0000
163	1.2414	0.5173	0.3942	0.0090
165	1.2414	0.3449	0.3803	0.0225
167	1.2414	0.1724	0.3485	0.0295
169	1.2414	0.0000	0.3167	0.0000
180	1.3793	0.6897	0.3986	0.0000
182	1.3793	0.6035	0.4089	0.0075
184	1.3793	0.4311	0.3976	0.0290
186	1.3793	0.2586	0.3633	0.0655
188	1.3793	0.0862	0.2123	0.1121
190	1.3793	0.0000	0.0000	0.0000

Table D-2. (Continued)

l_L	$Z(IL)$	$R(IL)$	$\bar{\phi}_Z(IL)$	$\phi_r(IL)$
201	1.4483	0.6897	0.4046	0.0000
203	1.4483	0.5485	0.4134	0.0168
205	1.4483	0.4074	0.4020	0.0413
207	1.4483	0.2662	0.3731	0.0867
209	1.4483	0.1250	0.1880	0.2350
220	1.5172	0.6897	0.4121	0.0000
222	1.5172	0.6250	0.4240	0.0084
224	1.5172	0.4957	0.4188	0.0294
226	1.5172	0.3664	0.4060	0.0616
228	1.5172	0.2371	0.3794	0.1282
230	1.5172	0.1724	0.3480	0.2067
241	1.6552	0.6897	0.4304	0.0000
243	1.6552	0.5755	0.4426	0.0194
245	1.6552	0.4613	0.4385	0.0460
247	1.6552	0.3470	0.4283	0.0871
249	1.6552	0.2328	0.4107	0.1540
260	1.7931	0.6897	0.4514	0.0000
262	1.7931	0.6897	0.4514	0.0000
264	1.7931	0.5378	0.4657	0.0269
266	1.7931	0.4365	0.4664	0.0589
268	1.7931	0.3352	0.4656	0.1068
270	1.7931	0.2845	0.4587	0.1434
281	2.0000	0.6897	0.4745	0.0000
283	2.0000	0.6013	0.4940	0.0110
285	2.0000	0.5130	0.5006	0.0213
287	2.0000	0.4246	0.5183	0.0352
289	2.0000	0.3362	0.5513	0.0421

BIBLIOGRAPHY

1. Nayfeh, A. H., Kaiser, J. E., and Tellonis, D. P., "The Acoustics of Aircraft Engine-Duct Systems," AIAA Paper No. 73-1153, 1973.
2. Baumeister, K. J., "Finite Difference Theory for Sound Propagation in a Lined Duct with Uniform Flow Using the Wave Envelope Concept," NASA Technical Paper 1001, August 1977.
3. Bell, W. A., Meyer, W. L. and Zinn, B. T., "Predicting the Acoustic Properties of Arbitrarily Shaped Bodies by Use of an Integral Approach," AIAA Paper No. 76-494 (1976).
4. Hogge, H. D. and Ritzi, E. W., "Theoretical Studies of Sound Emission from Aircraft Ducts," Presented to AIAA-Aero-Acoustics Conference, Seattle, Washington, 1973.
5. Tam, C. K. W., "Transmission of Spinning Acoustic Modes in a Slightly Non-Uniform Duct," Journal of Sound and Vibration, Vol. 18, 1971, pp. 339-351.
6. Nayfeh, A. H., Kaiser, J. E., and Tellonis, D. P., "Transmission of Sound through Annular Ducts of Varying Cross Section," AIAA Journal, Vol. 13, Jan. 1975, pp. 60-65.
7. Unruh, J. F. and Eversman, W., "The Utility of the Galerkin Method for the Acoustic Transmission in an Attenuating Duct," Journal of Sound and Vibration, Vol. 23, pp. 187-197 (1972).
8. Arlett, P. L., Bahrani, A. K., and Zienkiewicz, O. C., "Application of Finite Elements to the Solution of Helmholtz's Equation," Proceedings of Institute of Electrical Engineers, Vol. 115, 1762-1766 (1968).
9. Miller, B. A., Dastoli, B. J. and Wesoky, H. L., "Effect of Entry-Lip Design on Aerodynamics and Acoustics of High-Throat-Mach-Number Inlets for the Quiet, Clean, Short-Haul Experimental Engine," NASA TM X-3222, 1975.
10. QF-1 8" Bearing Housing Assembly Drawing, Engine Fan and Jet Noise Facility, NASA Lewis Research Center, Cleveland, Ohio, Drawing No. CR 501994.
11. Huebner, K. H., The Finite Element Method for Engineers, John Wiley and Sons, Inc., New York, 1975.

12. Bisplinghoff, R. L., Ashley, H., and Halfman, R. L., Aeroelasticity, Addison-Wesley Publishing Company, Inc., Reading, 1955.
13. Tyler, J. M. and Sofrin, T. G., "Axial Flow Compressor Noise Studies," SAE Transactions, Vol. 70, 1962, pp. 303-332.
14. Eversman, W. and Beckemeyer, R. J., "Transmission of Sound in Ducts with Thin Shear Layers-Convergence to the Uniform Flow Case," The Journal of the Acoustical Society of America, Vol. 52, No. 1, Pt. 2, July 1972, pp. 216-220.
15. Tester, B. J., "Some Aspects of "Sound" Attenuation in Lined Ducts Containing Inviscid Mean Flows with Boundary Layers," Journal of Sound and Vibration, Vol. 28, No. 2, May 1973, pp. 217-245.
16. Nayfeh, A. H., Kaiser, J. E., and Shaker, B. S., "Effect of Mean-Velocity Profile Shapes on Sound Transmission Through Rectangular Ducts," Journal of Sound and Vibration, Vol. 34, No. 3, June 1974, pp. 413-423.
17. Rice, E. J., "Attenuation of Sound in Soft-Walled Circular Ducts " Aerodynamic Noise, H. S. Ribner, ed., Univ. of Toronto Press, 1969, pp. 229-249.
18. Wu, J. C., Sigman, R. K., Hubbarth, J. E. and McMahon, H. M., "Potential Flow Studies of Lift-Fan Inflow Interference Phenomena," Aerospace Research Labs ARL 73-0132, Oct. 1973.
19. Lieblin, S. and Stockman, N. O., "Compressibility Corrections for Internal Flow Solutions," Journal of Aircraft, Vol. 9, No. 4, April 1, 1972, pp. 312-313.
20. Hess, J. L. and Smith, A. M. O., "Calculation of Potential Flow about Arbitrary Bodies," Progress in Aeronautical Sciences, Vol. 8, Pergamon Press, 1967, pp. 1-138.
21. Kellogg, D. D., Foundations of Potential Theory, Dover Publications, New York, 1953.
22. Smith, A. M. O. and Pierce, J., "Exact Solution of the Neumann Problem. Calculations of Non-Circular Plane and Axially Symmetric Flows About or Within Arbitrary Boundaries," Douglas Aircraft Co., Report ES-26988, April, 1958.
23. Liepmann, H. W. and Roshko, A., Elements of Gasdynamics, John Wiley and Sons, Inc., New York, 1957.
24. Pipes, L. A. and Harvill, L. R., Applied Mathematics for Engineers and Physicists, McGraw-Hill Book Company, New York, 1970.

25. Math Science Library, Published by Control Data Corporation, Vol. VI, 1973.
26. Morfey, C. L., "Acoustic Energy in Non-Uniform Flows," Journal of Sound and Vibration, Vol. 4, pp. 159-170 (1971).
27. Rice, E. J., "Spinning Mode Propagation in Ducts with Acoustic Treatment," NASA TN D-7913, NASA Lewis Research Center, Cleveland, Ohio, February 1975.
28. Baumeister, K. J., "Generalized Wave Envelope Analysis of Sound Propagation in Ducts with Stepped Noise Source Profiles and Variable Axial Impedance," NASA TM X-71674.
29. Levine, H. and Schwinger, J., "Radiation of Sound from Circular Pipe," Physical Review, Vol. 73, 1948, pp. 383-406.
30. Tack, D. H. and Lambert, R. F., "Influence of Shear Flow on Sound Attenuation in a Lined Duct," The Journal of the Acoustical Society of America, Vol. 38, 39-45 (1951).
31. Rice, E. J., "Propagation of Waves in an Acoustically Lined Duct with a Mean Flow," Basic Aerodynamic Noise Research, I.R. Schwartz, ed., NASA SP-207, 1969, pp. 345-355.
32. Abrahamson, A. L., "A Finite Element Algorithm for Sound Propagation in Axisymmetric Ducts Containing Compressible Mean Flow," AIAA Paper No. 77-1301, October 1977.
33. Mungur, P., and Gladwell, G. M. L., "Acoustic Wave Propagation in a Sheared Fluid Contained in a Duct." Journal of Sound and Vibration, Vol. 9, No. 1, January 1969, pp. 28-48.
34. Goldstein, M., and Rice, E. J., "Effect of Shear on Duct Wall Impedance," Journal of Sound and Vibration, Vol. 30, No. 1, 1973, pp. 79-84.
35. CRC Math Tables, Published by CRC, pp. 454, 17th Ed. (1964).
36. Zinn, B. T., "Longitudinal Mode Acoustic Losses in Short Nozzles." Journal of Sound and Vibration, Vol. 22, No. 1, 1972, pp. 93-105.
37. Denbigh, K., The Principles of Chemical Equilibrium, Cambridge University Press, London, 1971.

END DATE FILMED : MAY 31, 1979